Influence of hydrodynamics and correlation of metal contents with settling velocities on contamination distribution in a stormwater detention basin

Xiaoxiao Zhu

N°d'ordre NNT : 2019LYSEI035

THESE de DOCTORAT DE L'UNIVERSITE DE LYON
opérée au sein de
INSTITUT NATIONAL DES SCIENCES APPLIQUEES DE LYON

Ecole Doctorale ED162
MECANIQUE, ENERGETIQUE, GENIE CIVIL, ACOUSTIQUE

Spécialité/ discipline de doctorat : GENIE CIVIL

Soutenue publiquement le 26/06/2019, par :
Xiaoxiao ZHU

INFLUENCE OF HYDRODYNAMICS AND CORRELATION OF METAL CONTENTS WITH SETTLING VELOCITIES ON CONTAMINATION DISTRIBUTION IN A STORMWATER DETENTION BASIN

Devant le jury composé de :

DEWALS, Benjamin	Professeur à Université de Liège	Président
RUBAN, Véronique	Directrice de recherche à IFSTTAR	Rapporteure
SECHET, Philippe	Maître de Conférences HDR à Grenoble INP	Rapporteur
BERTRAND-KRAJEWSKI, Jean-Luc	Professeur à INSA de Lyon	Examinateur
BLANC-BISCARAT, Denise	Maître de Conférences à INSA de Lyon	Examinatrice
LE COZ, Jérôme	Chargé de recherche – HDR à IRSTEA	Examinateur
CLEMENS, Francois	Professeur à TU Delft	Examinateur
DEWALS, Benjamin	Professeur à Université de Liège	Examinateur
LIPEME KOUYI, Gislain	Maître de Conférences HDR à INSA de Lyon	Directeur de thèse
GIBELLO, Claire	Responsable Service Exploitation Métropole de Lyon	Invitée

Département FEDORA – INSA Lyon - Ecoles Doctorales – Quinquennal 2016-2020

SIGLE	ÉCOLE DOCTORALE	NOM ET COORDONNEES DU RESPONSABLE
CHIMIE	**CHIMIE DE LYON** http://www.edchimie-lyon.fr Sec. : Renée EL MELHEM Bât. Blaise PASCAL, 3e étage secretariat@edchimie-lyon.fr INSA : R. GOURDON	M. Stéphane DANIELE Institut de recherches sur la catalyse et l'environnement de Lyon IRCELYON-UMR 5256 Équipe CDFA 2 Avenue Albert EINSTEIN 69 626 Villeurbanne CEDEX directeur@edchimie-lyon.fr
E.E.A.	**ÉLECTRONIQUE, ÉLECTROTECHNIQUE, AUTOMATIQUE** http://edeea.ec-lyon.fr Sec. : M.C. HAVGOUDOUKIAN ecole-doctorale.eea@ec-lyon.fr	M. Gérard SCORLETTI École Centrale de Lyon 36 Avenue Guy DE COLLONGUE 69 134 Écully Tél : 04.72.18.60.97 Fax 04.78.43.37.17 gerard.scorletti@ec-lyon.fr
E2M2	**ÉVOLUTION, ÉCOSYSTÈME, MICROBIOLOGIE, MODÉLISATION** http://e2m2.universite-lyon.fr Sec. : Sylvie ROBERJOT Bât. Atrium, UCB Lyon 1 Tél : 04.72.44.83.62 INSA : H. CHARLES secretariat.e2m2@univ-lyon1.fr	M. Fabrice CORDEY CNRS UMR 5276 Lab. de géologie de Lyon Université Claude Bernard Lyon 1 Bât. Géode 2 Rue Raphaël DUBOIS 69 622 Villeurbanne CEDEX Tél : 06.07.53.89.13 cordey@univ-lyon1.fr
EDISS	**INTERDISCIPLINAIRE SCIENCES-SANTÉ** http://www.ediss-lyon.fr Sec. : Sylvie ROBERJOT Bât. Atrium, UCB Lyon 1 Tél : 04.72.44.83.62 INSA : M. LAGARDE secretariat.ediss@univ-lyon1.fr	Mme Emmanuelle CANET-SOULAS INSERM U1060, CarMeN lab, Univ. Lyon 1 Bâtiment IMBL 11 Avenue Jean CAPELLE INSA de Lyon 69 621 Villeurbanne Tél : 04.72.68.49.09 Fax : 04.72.68.49.16 emmanuelle.canet@univ-lyon1.fr
INFOMATHS	**INFORMATIQUE ET MATHÉMATIQUES** http://edinfomaths.universite-lyon.fr Sec. : Renée EL MELHEM Bât. Blaise PASCAL, 3e étage Tél : 04.72.43.80.46 Fax : 04.72.43.16.87 infomaths@univ-lyon1.fr	M. Luca ZAMBONI Bât. Braconnier 43 Boulevard du 11 novembre 1918 69 622 Villeurbanne CEDEX Tél : 04.26.23.45.52 zamboni@maths.univ-lyon1.fr
Matériaux	**MATÉRIAUX DE LYON** http://ed34.universite-lyon.fr Sec. : Marion COMBE Tél : 04.72.43.71.70 Fax : 04.72.43.87.12 Bât. Direction ed.materiaux@insa-lyon.fr	M. Jean-Yves BUFFIÈRE INSA de Lyon MATEIS - Bât. Saint-Exupéry 7 Avenue Jean CAPELLE 69 621 Villeurbanne CEDEX Tél : 04.72.43.71.70 Fax : 04.72.43.85.28 jean-yves.buffiere@insa-lyon.fr
MEGA	**MÉCANIQUE, ÉNERGÉTIQUE, GÉNIE CIVIL, ACOUSTIQUE** http://edmega.universite-lyon.fr Sec. : Marion COMBE Tél : 04.72.43.71.70 Fax : 04.72.43.87.12 Bât. Direction mega@insa-lyon.fr	M. Philippe BOISSE INSA de Lyon Laboratoire LAMCOS Bâtiment Jacquard 25 bis Avenue Jean CAPELLE 69 621 Villeurbanne CEDEX Tél : 04.72.43.71.70 Fax : 04.72.43.72.37 philippe.boisse@insa-lyon.fr
ScSo	ScSo* http://ed483.univ-lyon2.fr Sec. : Viviane POLSINELLI Brigitte DUBOIS INSA : J.Y. TOUSSAINT Tél : 04.78.69.72.76 viviane.polsinelli@univ-lyon2.fr	M. Christian MONTES Université Lyon 2 86 Rue Pasteur 69 365 Lyon CEDEX 07 christian.montes@univ-lyon2.fr

*ScSo : Histoire, Géographie, Aménagement, Urbanisme, Archéologie, Science politique, Sociologie, Anthropologie

Acknowledgements

I would like to acknowledge all peoples and institutions who have contributed to the accomplishments of this thesis.

First of all, I would like to express my great gratitude to my supervisor, Gislain Lipeme Kouyi, for his continuous guidance and support of my PhD work, for his availability, motivation, enthusiasm and immense knowledge.

I am grateful to all the members of jury: Véronique Ruban and Philippe Sechet to report this thesis and their constructive comments; Benjamin Dewals as president and all other jury members Jean-Luc Bertrand-Krajewski, Francois Clements, Denise Blanc-Biscarat, Jérôme Le Coz to evaluate my PhD work and their constructive comments.

I would like to especially thank Jean-Luc Bertrand-Krajewski for welcoming me at DEEP and scientific guidance; Vincent Chatain, Mathieu Gauthier, Denise Blanc-Biscarat, Cécile Delolme and Jean-Baptiste Aubin for their bio-chemical and statistic knowledge and scientific guidance; Stéphane Vacherie, Nicolas Walcker, Serge Naltchayan, Dominique Babaud, Richard Poncet and Hervé Perier-Camby for all technical and data supports; Nathalie Dumont and David Lebouil for ICP analyse supports; Nathalie Goubet, Valérie Boiron, Frédérique Dutel and Agnès Brunella for all the administrative help.

I would also like to show my gratitude to Francois Clemens, Jérôme Le Coz and Joe Marner for their scientific suggestions on LSPIV. I appreciate the discussions on image treatment with Serge Miguet, Mihaela Scuturici, Catherine Pothier and Thomas Léglantier. Thanks to Laëtitia Bacot, for all the exchanges.

I would like to thank all the members of Laboratory DEEP, especially Coulomb team: Sylvie Barraud, Hélène Castebrunet, Pascal Le Gauffre, Frédéric Cherqui. Thanks to all Ph.D (past, present and future) and post-doc, especially Ainhoa and Alejandro, for all the exchanges (CFD group, conferences, daily discussions, etc), Hexiang for all scientific discussions and Robin, Céline, Christel, Santiago, Jérémie, Kamilia, Tanguy, Khiem, Luis, Rémy, Lucie, Ola, Manon, Quifang, Bomin, Valentine, Helen, Julie, Janett, Camille, Amin, Kévin, Ruben, Corrado, Bruno, for all types of happy discussions.

I would like to acknowledge OTHU, Métropole de Lyon, ANR CABRRES program, CSC for the scientific and financial supports.

Finally, I am very grateful to my family and friends, especially my parents, for their selfless support and love. Special thanks to my future husband Bonan, who not only shares my life, my happiness, my depression but also gives me scientific support all along of my thesis.

Abstract

Stormwater detention basins have three main functions: storing rainwater to prevent flooding, promoting settling of particulate pollutants, avoiding resuspension and remobilization of settled pollutants to the downstream. The design and the management of such facilities requires the knowledge of hydrodynamic and sediment characteristics, as well as the ability to predict areas where deposits are highly contaminated.

The main objective of this PhD work is to identify the areas where pollutant levels in sediments are high in detention and settling basin. The studied site is the stormwater detention basin (Django Reinhardt basin or DRB), which is an extended and dry basin at the outlet of an industrial watershed. This basin has been the subject of numerous investigations within the framework of the Field Observatory for Urban Water Management (or observatoire de terrain en hydrologie urbaine - OTHU in French).

First of all, the measurements of surface velocities by Large-Scale Particle Image Velocimetry (LSPIV) permits to better understand the hydrodynamic behaviour in the basin. These measurements were used to evaluate CFD (Computational Fluid Dynamics) models. This is the first time, to the author's knowledge, this measurement technique has been applied in the case of stormwater management facilities. The results show that CFD models identify the main recirculation zone that promotes settling. These evaluated models were then used to simulate the transport of particulate pollutants, including sedimentation and resuspension. The exploitation of these simulations results enables to (i) identify the preferential areas where resuspended contaminated sediments may be conveyed to the downstream infiltration basin and (ii) predict the accumulation zones of some metals. Results also demonstrate that iron contents in sediments are strongly correlated to settling velocities and can be considered as a good indicator of the level of trace metal contamination of sediments.

The results obtained in this thesis contribute to improve the design of stormwater detention and settling basins and the management of contaminated sediments.

Keywords: Hydrodynamics, metal, resuspension, sediment, sedimentation, settling velocity, stormwater

Résumé

Les bassins de retenue-décantation ont trois fonctions principales : stocker les eaux pluviales pour éviter les inondations, favoriser la décantation des polluants particulaires, éviter la remise en suspension et la remobilisation des polluants décantés vers l'aval. La conception et la gestion de telles installations nécessitent de connaître les caractéristiques hydrodynamiques, celles des sédiments et de pouvoir prédire les zones où les dépôts sont fortement contaminés.

L'objectif principal de la thèse est d'identifier les zones où les teneurs en polluants sont élevées au niveau des sédiments des bassins de retenue-décantation. Le site d'étude est le bassin de rétention des eaux pluviales de Django Reinhardt (BDR), qui est un bassin sec à l'exutoire d'un bassin versant industriel. Ce bassin a fait l'objet de plusieurs études dans le cadre de de l'Observatoire de Terrain en Hydrologie Urbaine (OTHU).

Dans un premier temps, les mesures de vitesses de surface par LSPIV (Large-Scale Particle Image Velocimetry) ont permis de mieux comprendre l'hydrodynamique au sein de l'ouvrage. Ces mesures ont été exploitées pour évaluer les modèles CFD (Computational Fluid Dynamics). A notre connaissance, c'est la première fois que cette technique de mesure est appliquée au cas des ouvrages de gestion des eaux pluviales. Les résultats montrent que les modèles CFD identifient la principale zone de recirculation qui favorise la décantation. Ces modèles évalués ont ensuite été employés pour simuler le transport de polluants particulaires, leur sédimentation et leur remise en suspension. L'exploitation des résultats de ces simulations a permis d'indiquer les points où les sédiments sont remis en suspension et transférés vers le bassin d'infiltration à l'aval et de prédire les zones d'accumulation en métaux. Les résultats obtenus montrent également que les teneurs en fer dans les sédiments sont fortement corrélées aux vitesses de chute. Le fer pourrait être un bon indicateur du niveau de contamination des sédiments en certains métaux lourds.

Les résultats de cette thèse contribuent à améliorer les règles de conception des bassins de retenue-décantation des eaux pluviales et les stratégies de gestion des sédiments associés.

Mots-clés : Décantation, eaux pluviales, sédiments, métaux, remise en suspension, vitesse de chute, hydrodynamique

Table of contents

List of Figures

List of Tables

List of Acronyms / Abbreviations

ADV	Acoustic Doppler Velocimeter
APEO	Alkylphenol ethoxylates
BSS	Bed Shield Stress
BTKE	Bed Turbulent Kinetic Energy
CFD	Computational Fluid Dynamics
CLAHE	Contrast Limited Adaptive Histogram Equalization
DCC	Direct Cross Correlation
DFT	Discrete Fourier transform
DRB	Django Reinhart Basin
DSM-flux	Device for Stormwater and combined sewer flows Monitoring and the control of pollutant fluxes
EDF	Electricité de France – electricity of France company
GCPs	Ground Control Points
HTS	Hydrocyclone Trapping System
LOD	Limit of detection
LOQ	Limit of quantification
LW-HTS	Leaping-Weir and Hydrocyclone Trapping System
IA	Interrogative Area
Irstea	National Research Institute of Science and Technology for Environment and Agriculture
LSPIV	Large-Scale Particle Image Velocimetry
LWS	Leaping-Weir System
NRMSD	Normalized Root-Mean-Square Deviations

PAH	Polycyclic aromatic hydrocarbon
PBDE	Polybrominated diphenyl ethers
PIV	Particle Image Velocimetry
PSVD	Particle Settling Velocity Distribution
SA	Searching Area
S_{inlet}	Sediments sampled from inlet
S_{basin}	Sediments sampled from the bottom of basin
UVP	Ultrasonic Velocity Profiler
VPPs	Vertical Projection Points

List of Variables

ADWP	Antecedent dry weather period
ART	Average residence time
C	Concentration
C_L	Lagrangian time scale constant
CV	Coefficient of variation
D^*	Dimensionless particle diameter
d	Particle diameter
H_{total}	Total Depth
F	Forces
F_D	Drag coefficient depending on different particle's and fluid's characteristics
G	Specific gravity
g	Gravity acceleration
h_{max}	Max water level
I_{max}	Max intensity
I_{mean}	Mean Intensity
k	Turbulent kinetic energy
[M]	Metals concentrations
Q	Inflow rate of DRB
Q_{max}	Max inflow rate of DRB
Q_{mean}	Mean inflow rate of DRB
Q_1	Inflow rate of LW-HTS
Q_2	Flow rate between LWS and HTS

R	Correlation coefficient
RD	Rain Duration
RT	Reference Time
T	Integral time scale
T_L	Fluid Lagrangian integral time
TSS	TSS concentration
Turb	Turbidity
u	Velocity of the fluid
u_p	Velocity of the particle
$u',\ v',\ w'$	Velocity fluctuation
Vs	Settling velocity
ε	Turbulent dissipation rate
ζ	Normal distributed random number
ξ	Coefficient
ρ	Density of fluid
ρ_p	Density of particle
ϑ_m	Kinematic viscosity of water (m^2/s)

Introduction

Impervious surfaces expand along with urbanization, which in turn leads to increasing quantities of urban runoff during wet weather, as well as deteriorating quality of receiving waters. On the one hand, urban runoff could be overloaded and cause flood to the downstream, which endangers human life and damages infrastructure. On the other hand, urban runoff waters are contaminated by many chemical compounds including trace metals, polycyclic aromatic hydrocarbons and endocrine disruptive chemicals (e.g. Barbosa et al., 2012; Gasperi et al., 2014; Zgheib et al., 2012). The overloaded and untreated runoff water contaminates streams, rivers and coastal water, and harms the health of aquatic habitats.

Under such circumstances, the undesirable impacts of stormwater runoff should be controlled by discreet management efforts and the concept of best management practice (BMP) is brought forward (Field and Tafuri, 2006). Stormwater detention basins are one of the most adopted BMPs in developed countries (Urbonas, 1994; Lawrence et al., 1996) and are effective to intercept and trap particulate pollutants (Maniquiz-Redillas et al., 2014). For example, they are found in most cities in France, Canada, US and other European countries (Urbonas, 1994). Their effectiveness has already been proven to prevent flooding and trap pollutants by sedimentation, such as suspended solids, trace metals, particulate nutrients and hydrocarbons (e.g. Marsalek and Marsalek, 1997; Maniquiz-Redillas et al., 2014).

The design and management of stormwater detention basins are then important to control stormwater quantity and quality. On the one hand, the volume of such basins should be large enough to receive stormwater coming from the watershed area. On the other hand, the geometry should be well designed to increase sediment removal performance by settling. For example, Persson (2000) found that length-to-width ratio, locations and numbers of inlets and outlets, and subsurface berm are key elements for basin design. A subsurface berm or island in front of the inlet is recommended for a better hydraulic performance concerning short-circuiting, effective volume and amount of mixing. In order to better design and manage such facilities, it is of great significance to understand the hydrodynamic behaviour and sediments transport mechanisms. Hence, this PhD research is carried out in this context and in the framework of ANR CABRRES national program (on physical, chemical, microbiological, ecotoxicological characterization of sediments and the role of hydrodynamics on the variability of their characteristics, Lipeme Kouyi et al., 2014a).

This introduction is organized in 5 sections. The first section introduces stormwater detention basins and their main roles for urban stormwater management. The second one reveals their functions and related challenges. The third section summarizes the scientific investigations on

Django Reinhardt Basin (DRB) and other similar basins and points out potential improvements. The main objectives of this PhD work and the general strategy to achieve them are then presented. Finally, the general structure of this document is explained.

Role of stormwater detention basin for urban stormwater management

Stormwater detention basins are key components of BMPs, which allow to reduce runoff peak flows and control flow rate to the downstream. These basins continue to evacuate stormwater after rain events and remain dry during dry weather. They are initially designed to avoid flooding, and are later proved to be efficient to trap sediments and their associated pollutants by means of settling (Grizzard et al., 1986; Loganathan et al., 1994; Randall et al.1982). Stormwater detention basins now have three main functions:

- storing rainwater to prevent flooding,
- trapping particulate pollutants thanks to settling processes
- avoiding resuspension and remobilization of settled pollutants to the downstream.

Thanks to the basin dimensions and the limitation of outflow, the runoff peaks can be reduced. As most of the pollutants, such as trace metals, Polycyclic Aromatic Hydrocarbons (PAHs) and some pathogenic bacteria, in urban stormwater are conveyed in particulate phase (e.g. Ashley et al., 2004; Barbosa et al., 2012; Gasperi et al., 2014; Zgheib et al., 2012), the decontamination procedure by stormwater detention basins through settling processes is appropriate. The removal percentage of total suspended solids (TSS) is found to be mainly between 50% and 91% (see e.g. Bardin, 1999; Chebbo, 1992; Torres, 2008). Meanwhile, they are nature-based solutions, which do not require extra energy.

Functions of stormwater detention basins and related challenges and scientific questions

Stormwater detention basins are prone to accumulating large quantities of sediments that must be removed regularly in order to ensure their optimal trapping efficiency and guarantee their storage capacities. In addition, accumulated deposits in stormwater detention basins are ecosystems with a very rich fauna habitat, which could be resuspended by incoming water and represent a risk of contamination for surrounding superficial or underground aquatic environments. The dissemination in surrounding air of the bacterial contaminants adsorbed on really fine sediments (bacterial aerosol) could be a microbiological risk, e.g. through an inhalation of aerosols during maintenance (Bernardin-Souibgui et al., 2018). It is then essential to predict deposition zones and to mitigate the remobilization of particulate contaminants. Sustainable management of accumulated and contaminated sediments is also a big challenge as few reliable treatment or reuse method can be applied (e.g. Petavy et al., 2009).

Geochemical characterization can help to identify contamination zones, but requires large amounts of sampling procedures and laboratory measurements, which are complex, expensive and time-consuming. For example, Sébastian (2013) characterized sediments at twelve representative locations at the bottom, as well as at inlet and outlet of DRB. However, the analyses were limited to certain locations and the contamination distribution could not be drawn. On the other hand, computational fluid dynamic (CFD) or other modelling approaches could provide a convenient and low-cost way to determine contaminated deposition zones. Indeed, the knowledge of the velocity field (e.g. recirculation zones) is of great importance to predict sedimentation zones (Dufresne et al., 2009; Yan et al., 2014). For these purposes, their hydrodynamic behaviour (velocity fields, turbulence and shear stresses) and the mechanisms of the transport and transformations of sediments (sedimentation, resuspension, aggregation, collision and uptake of contaminants) have to be mastered. The use of an appropriate measurement technique to get a deep picture of velocity field seems useful.

Figure 1 shows a simplified sketch of a detention-settling basin and highlights the key mechanisms inside. It also demonstrates the interaction between hydrodynamics and biophysico-chemical processes. Sediment transport process in flow includes advection by flow velocity, sedimentation and erosion (Julien, 2010). Deposits occur at the bottom of basin thanks to the gravity of sediments, while the settled sediments may also resuspend by the incoming flow when the forces from the flow (e.g. shear stress and turbulence) exceed the resistance forces (e.g. gravity and frictional force from the boundary). Scientists proposed two boundary thresholds for deposition and resuspension movements, i.e. the shear stress (e.g. Julien, 2010; Stovin and Saul; 1994; Vanoni, 1975) and the turbulent kinetic energy (e.g. Dufresne, 2008; Yan et al, 2014). In addition, sediment transformations, including agglomeration, disintegration and other biological and chemical processes (e.g. oxidation-reduction reaction, biodegradation, uptake of contaminants) often occur and their spatial variability is strongly impacted by the hydrodynamics of the basin (e.g. Becouze-Lareure et al., 2018; Bernardin-Souibgui et al., 2018).

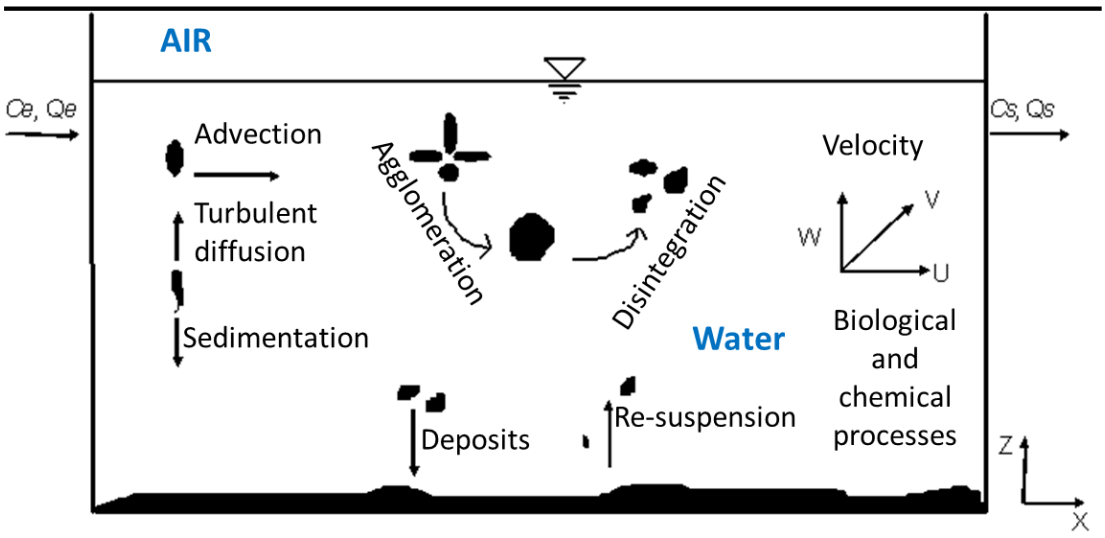

Figure 1. Hydrodynamic parameters and biophysico-chemical processes in detention-settling basins (Qe and Qs represent, respectively, the inlet and outlet flow rates, while Ce and Cs, represent respectively, the inlet and outlet concentrations of particles) (Lipeme Kouyi et al., 2014a)

Following scientific questions related to above matters can be pointed out:

- How does hydrodynamics (turbulence, shear flows, velocity field) interact with sediments and how this interaction affects sediments transport and transformations in settling-detention basins? What are their relationships?
- Which indicator(s) can be enhanced from the interaction between hydrodynamics and sediments physico-chemical characteristics? How these indicators can help for the management of the accumulated contaminated sediments?

Scientific investigations on DRB or other facilities and flow, and Research needs

Different researches have been carried out about the evolution of microbiological, physical, chemical and ecotoxicological characteristics of accumulated sediments in DRB located at Chassieu, France. The hydrodynamic behaviour and mechanisms of the transport and transformations of sediments have also been studied in this facility.

Torres (2008) characterized sediments collected from twelve points at the bottom of DRB and studied especially settling velocity distributions and their uncertainty. Both spatial and temporal variability on settling velocity distribution have been found (Torres et al., 2007). A 2D numerical model (Torres et al., 2008) for hydrodynamic and sediment transport simulation has been established accounting for inflow rate, water height, concentrations of TSS.

Sébastian (2013) investigated micropollutants in urban stormwater (from inlet and outlet of DRB) and in sediments. 100 substances have been analysed in dissolved and particulate phases in water at the inlet and outlet and 67% micropollutants have been detected. The removal efficiency of DRB has been proved regarding the majority of trace metals and PAH, as well as Polybrominated diphenyl ethers (PBDE) and Alkylphenol ethoxylates (APEO) for some rain events. High concentrations of micropollutants are observed in accumulated sediments, especially for trace metals and PAH. Negative removal efficiencies were also observed due to the resuspension of already settled micropollutants.

Yan (2013) established a 3D CFD model for the simulation of hydrodynamic behaviour and mechanism of sediment transport. A new boundary condition based on the comparison between Bed Turbulent Kinetic Energy (BTKE) and particles settling energy computed using their settling velocities has been proposed to determine sediment sedimentation and resuspension condition (Yan et al., 2014). The removal efficiencies and deposition zones are predicted and correspond to the observations.

Several investigations have also been realised in other stormwater basins and tanks. Dufresne (2008) carried out experiments and numerical modelling on a rectangular physical model. Flow pattern and sediment transports (efficiency, spatial distribution of deposits) have been performed. Particle tracking using a threshold value of BTKE boundary condition has been applied and compared with experimental results, and finally extended to a real large basin. El-Mufleh et al. (2013) characterized the trace metal fractionation in sediments from runoff water infiltration basins. For example, trace metals were observed to be very stable in small aggregates (10-50 μm). The study pointed out the role of the mobile trace metals fraction for stormwater sediments management. Isenmann (2016) developed an evaluation tool for stormwater decantation facility. The Euler-Lagrange method was used for flow and particle transport simulation in three basin models. New boundary conditions accounting for Bed Shear Stress (BSS) and BTKE have been proposed to determine the particle mobilization threshold. Vallet et al. (2016) developed a dynamic stormwater model for water quality simulation based on settling velocity distribution. Vezzaro et al. (2010) simulated the removal of micropollutants using a model based on relevant removal processes, such as settling, volatilization, sorption, biodegradation, and abiotic degradation.

Based on this research background, one can observe several studies on hydrodynamic behaviour through (i) experiments at laboratory scale or (ii) numerical modelling at laboratory pilots or field scales. But little is known on experimental measurements of hydrodynamic and sediments characteristics in a large-scale field basin. Indeed, the hydrodynamic behaviour strongly impacts mechanism of the transport and transformations of sediments, and is one of

the key reasons of spatio-temporal variability of sediments chemical, physical and microbiological characteristics (e.g. Bernardin- Souibgui et al., 2018; Lipeme Kouyi et al., 2018). The hydrodynamic behaviour and turbulence effects are not considered in numerous existent models for the fate of particulate pollutants in detention and settling basins. Besides, the current sampling strategy permits only sediments sampling from the bottom of basin, without an adapted inlet sediments sampling devices or techniques. In addition, the focus is not often placed on the role of both hydrodynamic and sediment characterizations in the determination of highly contaminated zones in spite of current sediment characterization researches. Hence, it is interesting to measure free surface velocity field in DRB and evaluate the numerical model, which has only be evaluated with observed deposition zone. The knowledge of priority cleansing or treatment zones accounting for sediments resuspension mechanism and contamination distribution could also help for the management of stormwater detention basin.

Table 1 indicates additional investigations regarding (i) use of CFD and PIV (Particle Image Velocimetry) for the understanding of hydrodynamic and sediment transport mechanisms and the design and management of stormwater facilities or structures; (ii) sediment characterization techniques and tracking indicators to assess contamination level; (iii) interactions and correlations between hydrodynamics and sediments' physical and chemical characteristics, and points out key results and the way that these results may support this PhD work.

Table 1. Literature reviews and their relations to this PhD work

Literature works	Objectives	Studied facilities/flows	Key results and perspectives	Relations to this PhD work
He and Marsalek., 2014	Enhancing sedimentation and trapping sediment with a bottom grid structure	Settling tank	Retained percentage of particles increased with the help of CFD	CFD model for hydraulic condition assessment and facility design
Park et al., 2008	Evaluation of settling performance and hydrodynamic behaviour	Sedimentation basins	Removal efficiency improved with remodelled basins	CFD simulation for basin remodelling
MoayeriKashani et al., 2017	Experimental investigation of fine sediment deposition using PIV	Sediment basin	2D collecting efficiency of fine particles were evaluated by PIV	PIV for fine sediment deposition investigation
Vonk et al., 2015	Spatial variations in sediment sources and sedimentation patterns	Mackenzie river	Spatial variations in geochemical characteristics	Geochemical techniques for sediment characterization
Meyer et al., 2018	Real-time monitoring of water quality	Small and middle scale river	Advantage of real-time monitoring, identification of pollutions sources by interpreting the correlation between different parameters	Water quality monitoring, correlation between different chemical parameters
Bishop et al., 2000	Contamination and biological effects of contamination	Stormwater ponds and natural wetland	Stormwater ponds are not clean ecosystems for wildlife and need contaminant monitoring	Sediment characterization
Jang et al.,2010	Residuals characterization for reuse and disposal options	Roadway stormwater system	Residuals are not a significant threat to environment concerning concentrations of metals and metalloids and trace organics	Chemical characterization of sediments
Rosenkrantz et al., 2008	Use of *Hydra hexactinella* for the assessment of the toxicity of stormwater and sediment samples	Retarding basins	*H. hexactinella* tended to avoid the sediment–water interface when exposed to sediment from all retarding basins	Tracking indicator for contamination assessment

Literature works	Objectives	Studied facilities/flows	Key results and perspectives	Relations to this PhD work
Wik et al., 2008	Sediment quality assessment (physico-chemical parameters and contaminants)	Road runoff detention systems (ponds, manholes and basins)	Low biological quality, extractable organic Zn is used as a tire wear marker, the maintenance is crucial to prevent contamination	Tracking extractable organic Zn as metal indicator for contaminant
Abarca et al., 2016	Response of particle size distributions to changes in water chemistry	Andean mountain stream confluence	Response of particle size distributions to changes in water chemistry	Chemical and hydrodynamic interactions
Molinaroli et al., 2009	Relationship between hydrodynamic parameters and grain size	Contrasting transitional environment, shallow water	Significant correlations were revealed, use of hydrodynamic energies for the understanding of sediment transport mechanism	Relationship between hydrodynamic and sedimentological parameters
Schwab et al., 2008	Hydrodynamic approach to modelling phosphorus distribution	Lake Erie	Spatial and temporal distribution of phosphorus was obtained.	Relationship between hydrodynamic and biochemical contamination distribution
Bartholoma and Flemming., 2007	Progressive grain-size sorting along an intertidal energy gradient	German Wadden Sea	Progressive grain-size sorting along an intertidal energy gradient	Relationship between hydrodynamic energy gradient and sediment size
Andral et al., 1999	Particle size distribution and hydrodynamic characteristics	Runoff from motoways	Sedimentation velocities on different particle size fractions were revealed	Relationship between particle size distribution and sedimentation velocity
Coppola et al., 2007	Quantitative investigations on the relationship on the particle size and organic carbon sorption	Washington Margin and Cascadia basin	Ultrafine particle fraction hosted the majority of organic carbon	Relation between sediments' physical and chemical characteristics

Objectives and research strategy

The design and management of such facility are of great interest, which lead to the main objectives of this PhD work, including:

- Analysis and understanding of hydrodynamic behaviour through Large-Scale Particle Image Velocimetry (LSPIV) technique, and evaluation of numerical models;
- Investigation of resuspension and remobilization of already settled sediments and determination of zones where sediments can be easily washed away by incoming stormwater and escape DRB;
- Prediction of the distribution of trace metal contamination by coupling the correlation of metal contents and settling velocity with sediment transport model.

The field site used for this PhD work is DRB, which has been under monitoring and investigating for at least 20 years, and is designed with multi-elements reminded below to promote sediments settling:

- Multi-inlets
- Large surface area compared to depth to trap sediments (long residence time)
- A gutter which drives water during dry weather
- A small tank at the centre of basin to trap hydrocarbon
- An overflow and three orifices towards outlet

In addition to current knowledge, this PhD work aims to bring new insights to the research community. The overall research strategy is illustrated in Figure 2.

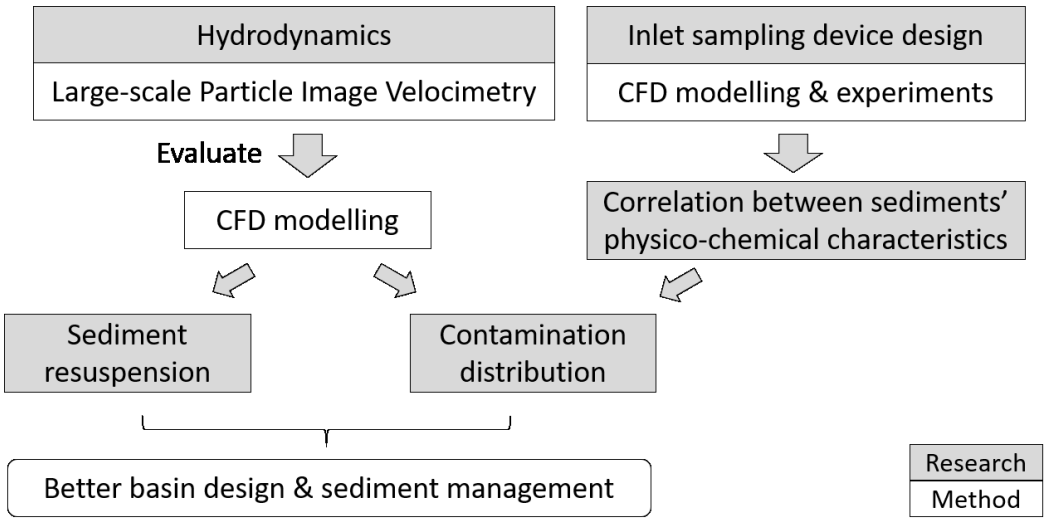

Figure 2. Overall research strategy

First of all, a new device is necessary and important to collect sediments from the inlet. A Hydrocyclone Trapping System (HTS) is considered thanks to its function to separate solids from liquid by centrifugal force. The HTS is connected to the Leaping-Weir System (LWS) and they serve together as a sediment sampling system.

Hydrodynamic behaviour strongly impacts mechanisms of the transport and transformations of sediments. LSPIV is an image-based, efficient, low-cost and convenient technique for experimental free surface velocity field measurement, which has been widely used in riverine environments. The application of LSPIV in DRB helps to understand the hydrodynamic behaviour and evaluate the numerical model, which is a base for sediment transport simulation.

The resuspension and remobilization of settled sediments could contaminate the downstream by carrying the associated pollutants. The investigations on sediment resuspension and remobilization mechanisms help to determine the priority cleansing zones where pollutants could be easily washed away and escape the basin.

A major part of pollutants are transported in a predominantly particulate phase in urban stormwater, while certain metals are relatively stable in the nature and could be used as indicators of contamination. The study of correlation between metal contents in sediments and settling velocity helps to connect sediments' physical and chemical characteristics. The combination of such correlation with particle transport model enables to simulate chemical transport through physical aspects and predict contamination zone where specific treatment could be comprehensively applied.

The final results help to better design and manage stormwater detention basins by taking into considerations multiple aspects, i.e. hydrodynamic behaviour, sediment sedimentation and resuspension, and distribution of trace metal contamination.

Document structure

In addition to the introduction, conclusions and perspectives, this document is organized in four chapters:

Chapter 1 introduces the experimental site and sampling strategy. The chapter proposes then a new designed sampling device for inlet sediments characterizations. The design procedure and trapping efficiency of this new sampling equipment are also revealed in this chapter.

Chapter 2 presents the hydrodynamic behaviour in DRB thanks to the Large-Scale Particle Image Velocimetry (LSPIV) technique. The results are used as a support for numerical model evaluation and particle deposits prediction.

Chapter 3 describes the sediment resuspension behaviour in DRB using CFD models, which is based on the hydrodynamic model evaluated in Chapter 2.

Chapter 4 shows the research methodology and results on particulate pollutant transport and the distribution of trace metal contamination in DRB. The contamination distribution is obtained by analysing the correlation between metal contents and settling velocity and coupling such correlation with solid transport models.

General conclusions and the perspectives are given at the end of the document.

Chapter 1. Presentation of experimental site and sampling strategy

This chapter aims to present the experimental site, i.e. Django Reinhart stormwater detention Basin (DRB) and sediment sampling strategy. In addition to the traps for sediment sampling at the bottom of the basin proposed by Torres (2008), a new sampling device is designed in this PhD work for the interception of sediments from the inlet of DRB. Section 1.1 introduces DRB and its characteristics. A detailed presentation of sediment sampling strategy is then given in Section 1.2. Finally, Section 1.3 shows a method for the design of inlet sampling device and its trapping performance.

1.1. Experimental site

The thesis is carried out under the framework of the field observatory for urban water management (http://www.graie.org/othu/) or OTHU in French (standing for observatoire de terrain en hydrologie urbaine). OTHU is an observation-based partnership launched in Lyon (France) in 1999 and supported by the Greater Lyon Metropolis (La Métropole de Lyon, direction Eau et déchets) and the Rhone Mediterranean Corsica Water Agency (Agence de l'eau Rhône Mediterranée et Corse). OTHU aims to improve knowledge and develop new technology in the field of Urban Water Management. It promotes the cooperation among researchers from different scientific fields, as well as the collaboration between researchers and end-users. The observatory provides reliable data (climate parameters, water quantity and quality) obtained from (i) continuous field measurements and (ii) campaigns of field sampling and laboratory analysis, on five main experimental sites and more than 20 other sites and laboratory prototypes with flow monitoring activity (Figure 1.1a).

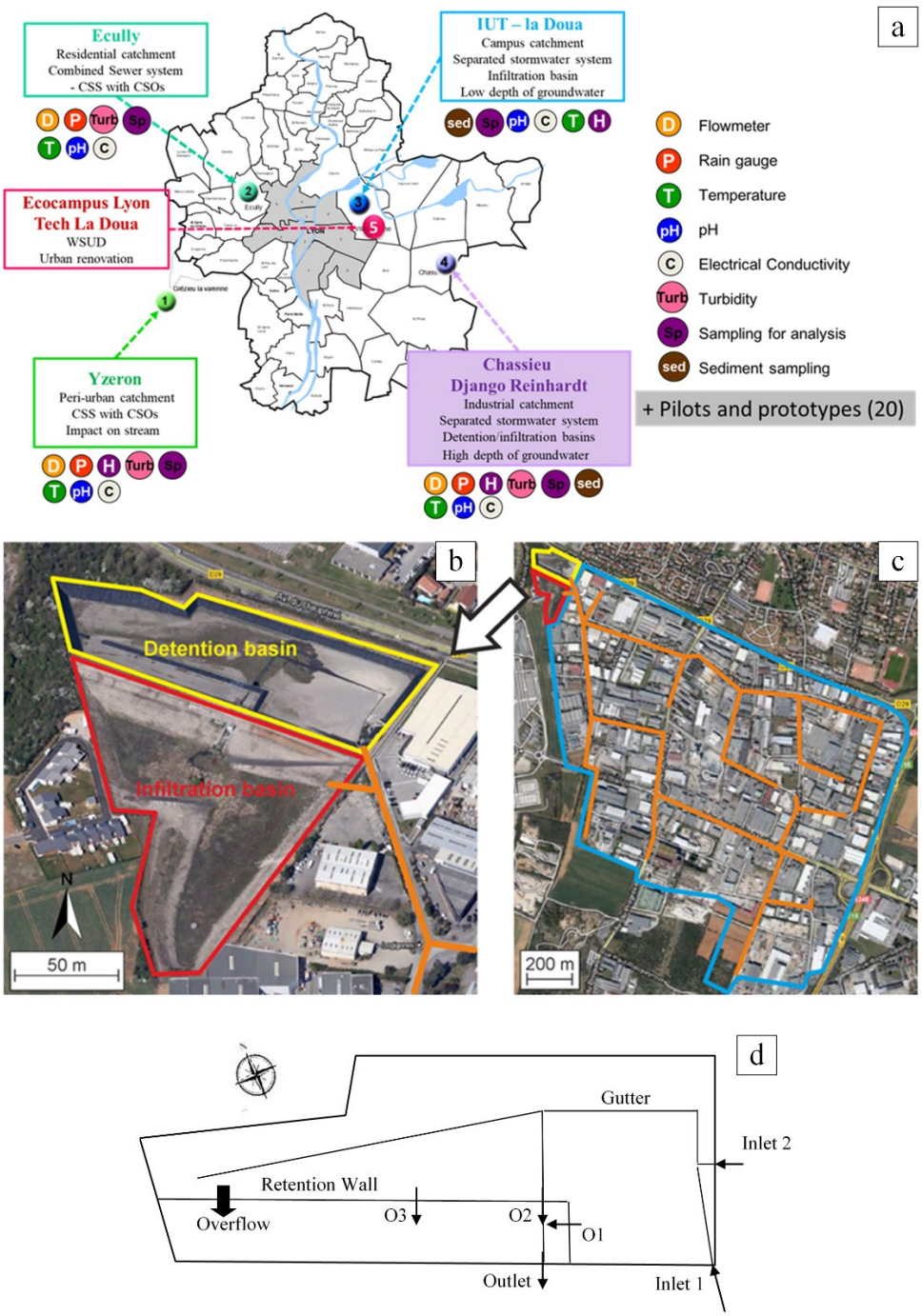

Figure 1.1. (a) Location of OTHU experimental sites in Lyon sewer system (adapted from OTHU website - http://www.graie.org/othu/): CSS = combined sewer system, CSOs = combined sewer overflow structures, WSUD = water sensitive urban design. (b) Django Reinhardt Basin (DRB) composed of a detention basin and infiltration basin. (c) Presentation of Chassieu catchment (Lipeme Kouyi et al., 2014b): blue lines surround the industrial watershed from which DRB receives water, orange lines represent the stormwater network. (d) Sketch of DRB.

The experimental and modelling investigations of this thesis are carried out in one of these sites, which is a stormwater detention basin, called Django Reinhart basin (DRB). The basin characteristics are presented in Table 1.1.

Table 1.1. Characteristics of Django Reinhardt Basin (DRB)

Type of characteristics	Characteristics
Location	Chassieu, France (in the east part of the metropolis of Lyon – Figure 1.1a)
Type of storm drainage system	Separated stormwater drainage system
Function	Dry basin designed to hold storm water to reduce local and downstream flooding and to allow sediment settling
Watershed type	Industrial watershed of 185 ha, illustrated in Figure 1.1c
Impervious rate	75%
Bottom surface area	11 000 m²
Storage capacity	32 000 m^3
Max outlet flow rate limit	0.35 m^3/s (Bardin and Barraud, 2004)
Materials	Bottom in bitumen and banks covered with plastic lining
Compositions	2 inlets (mainly inlet 1 operates), an outlet, a gutter guiding the flow to 3 orifices during dry periods and an overflow when the water height exceeds the retention wall (presented in Figure 1.1d).
Construction and maintenance	Built in 1975, rehabilitated in 2002, cleaned in 2006 & total sediment removal in 2013.
Monitoring	Continuous inflow and outflow rates, water levels in the basin, and inlet and outlet water quality measurements (pH, temperature, conductivity, turbidity). Inlet water quality is measured in a measurement station shown in Figure 1.2.

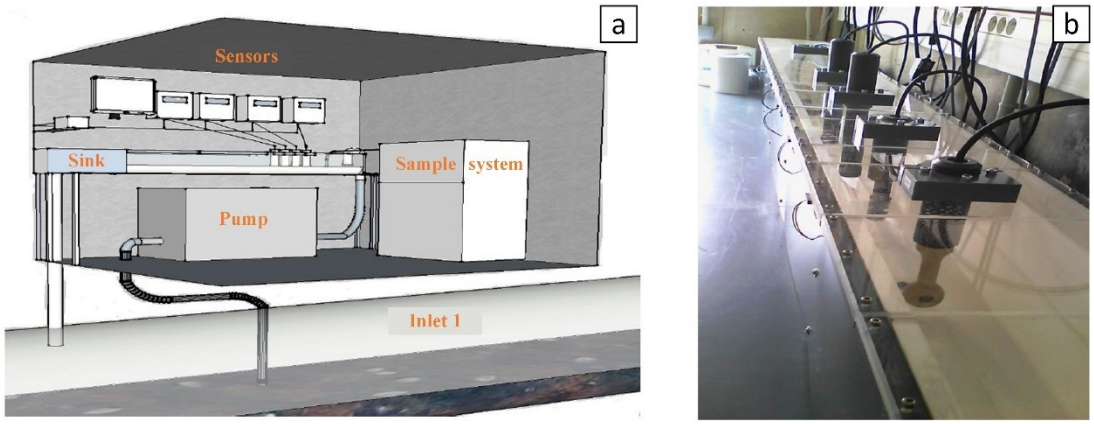

Figure 1.2. (a) Scheme of measurement station for inlet water quality measurement, (b) photo of measurement flume. (Source: Nicolas Walcker)

1.2. Strategy of sediment sampling

Five sampling points at the bottom of DRB (P01, P02, P04, P07, P12bis, illustrated in Figure 1.3a) are selected according to sediment accumulation zones and previous studies in order to better represent sediment characteristics in the basin (Sébastian et al., 2014b; Torres et al., 2007; Yan et al. 2014). Honeycomb-like sampling traps are installed before each rain event and collect settled sediments at each location during the rain event. As illustrated in Figure 1.4, P01 and P02 represent locations with medium particles (median size D50 of 40 - 200 µm) given their location near the inlet of basin and at the middle of flow pathway, respectively. P04 and P07 situate at the end of flow pathway and accumulate relatively fine sediments (median size D50 of 25 - 70 µm). P12bis is a special sampling point near a small tank designed to trap hydrocarbon and relatively medium and coarse sediments (median size D50 of 200 µm) are found at this point. For each point, 3 honeycomb-like traps (shown in Figure 1.3b) were placed in order to trap as many sediments as possible.

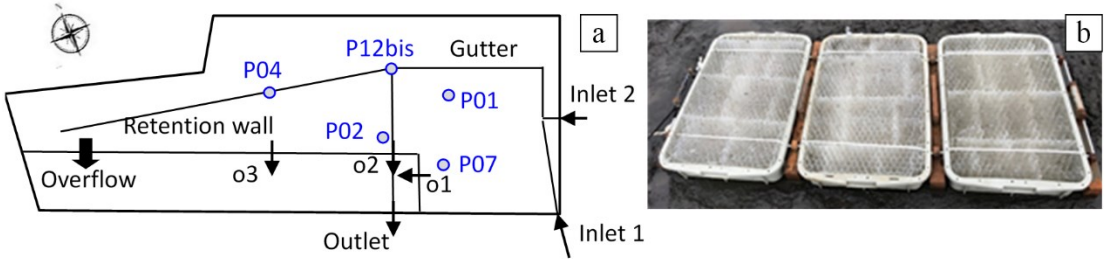

Figure 1.3. (a) Sketch of DRB and sampling points, (b) Honeycomb-like sampling traps.

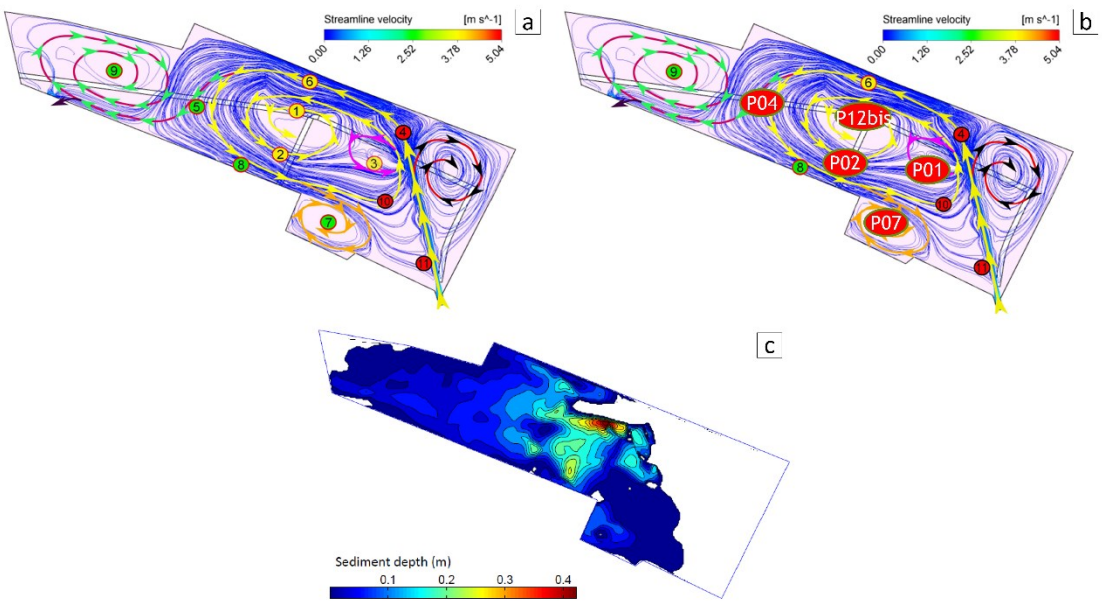

Figure 1.4. (a) Streamline of the fluid flow obtained by computational fluid dynamic (Q = 0.35 m^3/s, main flow rate from inlet 1) and sediment characteristics, where locations of sediments of different sizes are represented in different colours: red circles for coarse particles, yellow for median, and green for fine. (b) Streamline of fluid flow and location of different sampling points (P01, P02, P04, P07, P12bis). (c) Sediment depth distribution measurement in Django Reinhardt basin. (adapted from Yan, 2013).

The knowledge of the physical and chemical characteristics of incoming and existent sediments is important for the understanding of sediment transport mechanisms in DRB. It is not sure that properties of sediments collected in honeycomb-like sampling traps correspond to the incoming ones or the mixture with the existent settled particles. An appropriate sampling device is then required to collect sufficient and representative sediments from the inlet. The physical and chemical characteristics of incoming sediments can be used as input data of solid transport models. During this thesis, a new sampling device based on a Leaping-Weir connected to Hydrocyclone Trapping System (LW-HTS) was designed and installed to collect incoming sediments from the inlet of DRB, which will be presented in the next section.

1.3. Design and installation of LW-HTS for sediments sampling at the inlet of DRB

1.3.1. Preliminary sediment sampling from measurement flume

In order to analyse the sediment characteristics from the inlet, preliminary sampling experiments were realised thanks to the measurement flume (Figure 1.2), where sediment and rainwater samples were collected from the main inlet pipe (inlet 1 in Figure 1.1d) during the rain event of 16 January 2017. Sediments from P01 and P07 were also collected during the

same campaign. The particle-size distribution and settling velocity distribution of sediments were analysed and compared (illustrated in Figure 1.5 and Table 1.2). The measurements were performed using Mastersizer 2000 laser diffraction granulometer and VICAS protocol (Chebbo et al, 2009) for particle-size distribution and settling velocity, respectively (details on these methods are also presented in Chapter 4). Results show that particle-size distribution of samples from P01 and P07 peaks at around 55 µm and 950 µm and that of samples from inlet peaks at around 105 µm and 800 µm. In general, both particle size and settling velocity of sediments from inlet are higher than those in the basin. Indeed, the sediments collected from measurement flume originate from the inlet 1 pipe, close to the bottom (by means of a peristaltic pump suction, see Figure 1.2a) and aggregate in the experimental flume. We assume that the peristaltic pump suction brings a mixture of all type of sediments (fine and coarse particles) in the measurement flume, no grain size fractionation is done to collect only particle which may settle in the basin, even if median particles size D50 (Table 1.2) have same order of magnitude as those observed in DRB by Lipeme Kouyi et al. (2018). Hence, a trapping system to collect more representative sediments from the inlet of DRB is required.

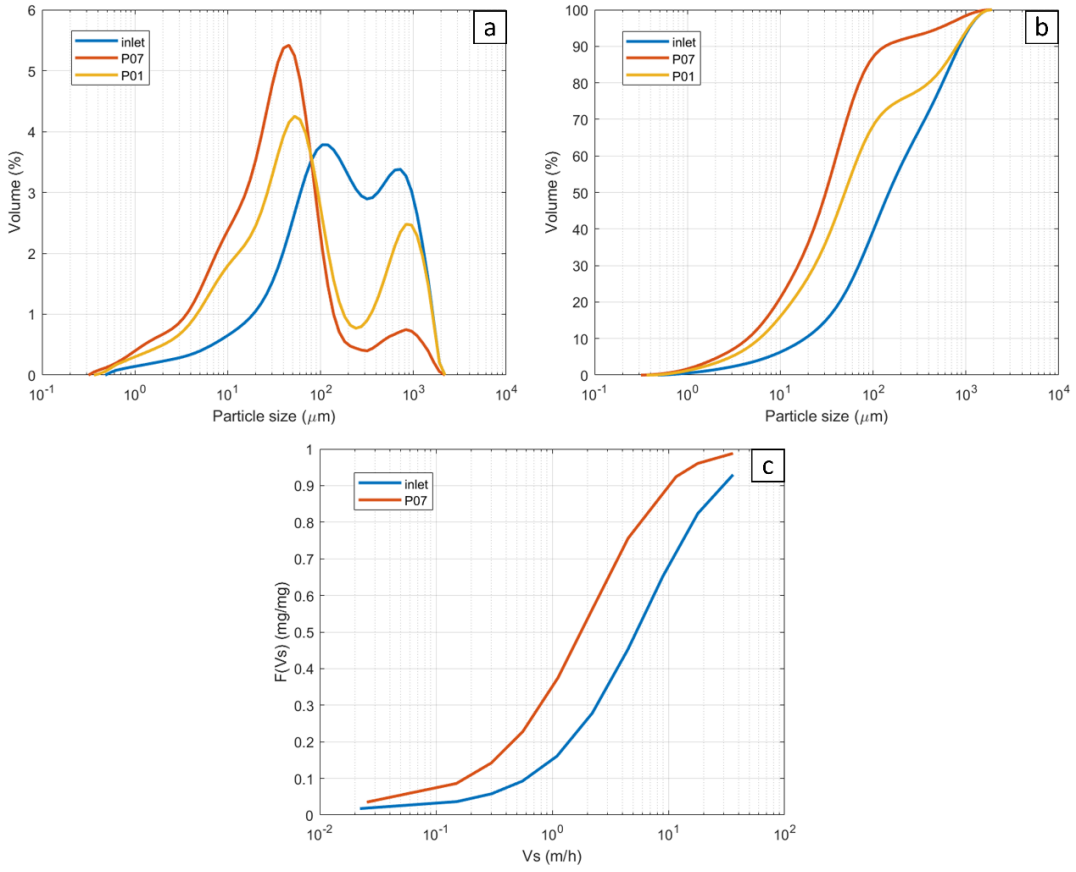

Figure 1.5. Comparison of physical characteristics of sediments collected from inlet flume and traps at P01, P07: (a) particle-size distribution, (b) cumulative particle-size distribution, (c) settling velocity distribution (except P01).

Table 1.2. Comparison of physical characteristics of sediments collected from inlet flume and traps at P01 and P07

Sampling location	Particle-size distribution (μm)			Settling velocity (m/h)		
	D10	D50	D90	V20	V50	V80
Inlet flume	21.1	170.1	973.3	1.47	5.54	16.66
P01	6.844	57.08	914.3	nm	nm	nm
P07	5.118	35.53	154.7	0.47	1.86	6.37

nm: not measured

D10: sieving size with 10% of particle mass passing through.

V10: 10% of particle volume has a settling velocity inferior to V10.

1.3.2. Design of Hydrocyclone Trapping System (HTS)

A Leaping-Weir System (LWS) was designed and constructed at the inlet of DRB, aiming to (i) measure low flow rates during the beginning and ending of storm events and (ii) intercept some fraction of the incoming sediments (Claro Barreto et al., 2015). In order to achieve the second purpose, two trapping systems, a hydrocyclone (HTS) and a lamella settler, were tested numerically and the HTS was chosen thanks to its higher trapping performances (Zhu et al., 2016). The HTS is composed of a hydrocyclone part, a trapping box and pipes, as shown in Figure 1.6c. The hydrocyclone part, which contains an inlet nozzle, a vortex finder, a cylinder and a cone section, is designed to separate solid particles from liquid media by means of a centrifugal force generated in the system. The cylinder and cone section are the main centrifugal separation parts. The vortex finder helps to drive a “clean” flow to the upward direction and prevent the sediments’ escape. The solid particles settle to the bottom of the cone section, and then slide to the trapping box through the pipes. The system was designed according to the different in-situ limits (e.g. maximum site dimensions and maximum weight of the HTS) and the design principles of literature (e.g. Silva et al., 2014). Generally, the design of hydrocyclone is based on the optimized ratios between the different dimensions and the cylinder diameter (Silva et al., 2014, Kim et al., 2015). Finally, HTS with optimized dimensions (shown in Table 1.3) were installed at the downstream of LWS. A combination of LWS and HTS was then used as a new sampling device to collect sediments from the inlet of DRB (illustrated in Figure 1.6b). Continuous measurements of velocity and water level are realized at the entrance of LWS. An electromagnetic flowmeter is also installed between LWS and HTS (Walcker et al., 2018).

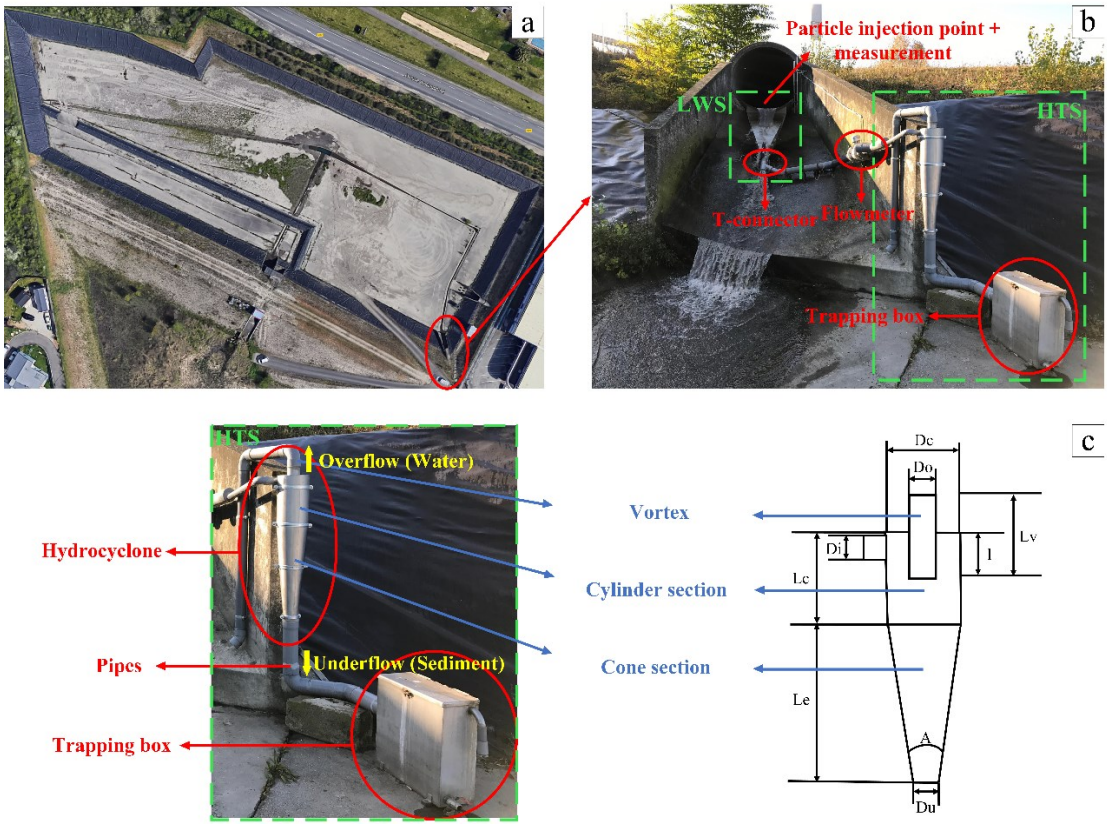

Figure 1.6. (a) Aerial view of basin (DRB), (b) Leaping-Weir and Hydrocyclone Trapping System (location shown in (a)), (c) Compositions of hydrocyclone.

Table 1.3. Dimensions of hydrocyclone

Parameter	Dc (mm)	Di (mm)	Do (mm)	l (mm)	Lv (mm)	Lc (mm)	Le (mm)	Du (mm)	A (°)
Value	200	50	80	200	300	320	635	100	9

Note: The symbols correspond to the symbols in Figure 1.6c.

1.3.3. CFD modelling of LW-HTS

Multiphase flows in the combination of LWS and HTS have been simulated using computational fluid dynamic approach (CFD) to understand its hydrodynamic behaviour and evaluate its trapping efficiency. A mesh with 3.25 million hexahedral cells is established for the whole LW-HTS. Figure 1.7 shows the geometry of LW-HTS and some mesh details of HTS and the connection between LWS and HTS. Multiple O-Grid blockings are applied in the cases of cylinder geometry. The detailed mesh information of LWS can be found in Claro Barreto (2014). The flow was simulated in steady state condition and the turbulence was simulated with the Re-Normalization Group (RNG) k-epsilon model (Orszag, 1993). The volume of fluid (VOF) method (firstly proposed by Hirt and Nichols, 1981) was used for free surface modelling.

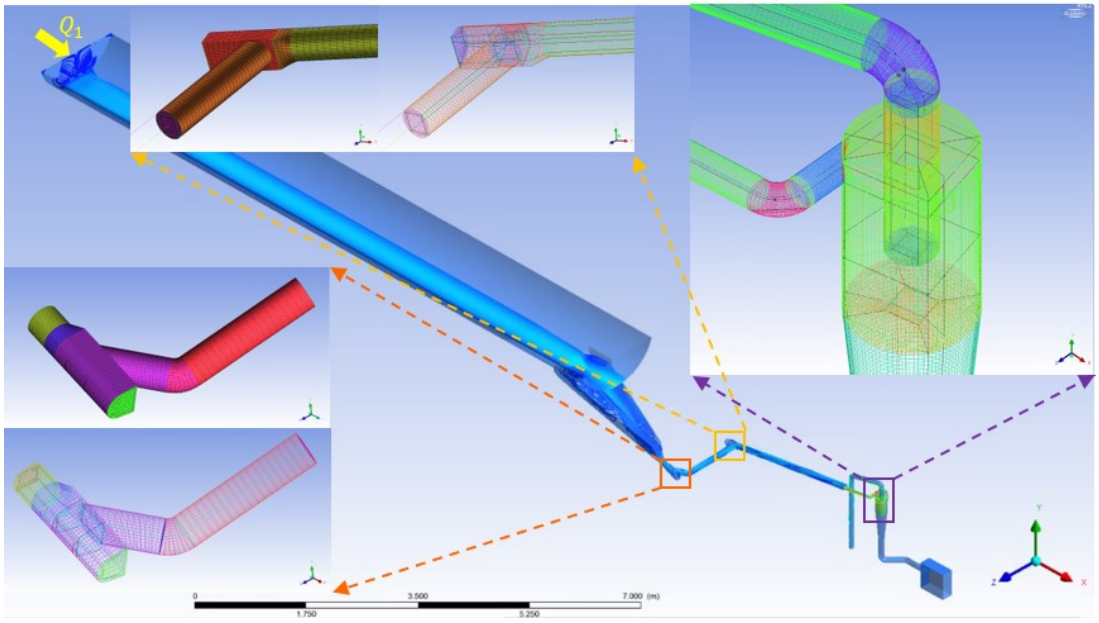

Figure 1.7. Geometry of LW-HTS and some mesh details

1.3.4. Hydrodynamic behaviour

Simulations with several inflow rates (Q_1 = 3, 6.5, 13, 13.65, 30, 60, 100, 250, 350 l/s) were performed for LW-HTS and the streamline is illustrated in Figure 1.8. The simulated hydrodynamic characteristics are presented in Figure 1.8. The averaged inlet velocity ($\overline{v_{1M}}$) and water height (h_1) are calculated at the cross section (indicated in yellow in Figure 1.8) 1 m upstream to the bottom opening of LWS. The flow rate between LWS and HTS Q_2 is also computed to be compared to measured data (marked in green in Figure 1.8).

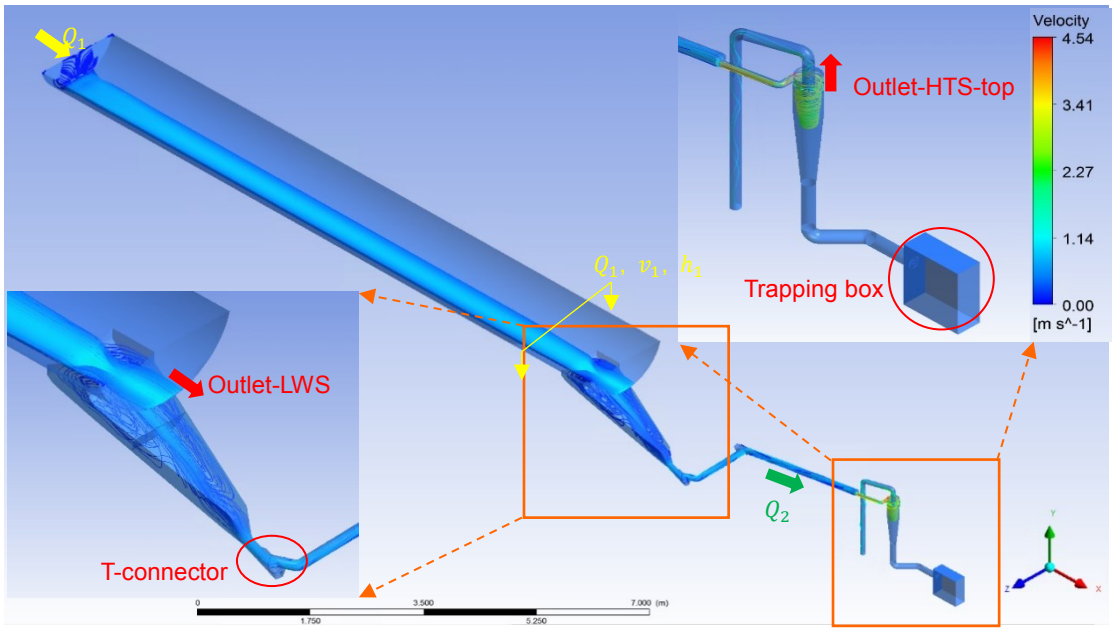

Figure 1.8. Streamline of LW-HTS colored by velocity magnitude

Continuous measurements of water quantity (velocity, water height and flow rate calculated by measured mean velocity and wet cross-section) are carried out at the inlet of LW-HTS. The averaged inlet velocity ($\overline{v_{1R}}$) and water height (h_{1R}) are the average of measured data with each corresponding inflow rate during the entire year of 2017. The measured and simulated water levels and mean velocities are compared (shown in Figure 1.9). It is observed that the difference between numerical results and measurements at the inlet of LW-HTS are relatively non-obvious when inflow rate (Q_1) is inferior to 13.65 l/s, where the relative deviations of average velocity ($\overline{v_1}$) and water height (h_1) are inferior to 8%. The overall relative deviations are less than 20%, which are related to different method for velocity calculations and VOF diffusion. In reality, surface velocity is measured by a radar and average velocity is then obtained by multiplying it by a coefficient. The difference might also be related to the diffusion at the surface caused by VOF model, which is larger with a higher inflow rate. Despite the differences, the measured and simulated water levels and mean velocities are consistent considering the uncertainties.

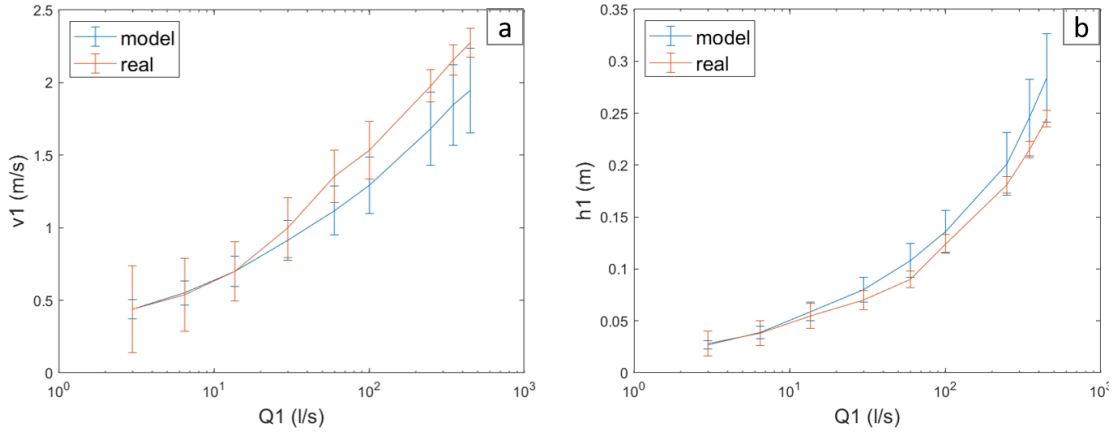

Figure 1.9. Comparison of measured and simulated water levels and mean velocities

The flow rate between LWS and HTS (Q_{2R}) is measured by an electromagnetic flowmeter and reaches its maximum at around 6 l/s once inflow rate Q_1 reaches 13.65 l/s. In fact, sediments could stay at T-connector, which cause a flow rate diminution. In the case of heavy rain, the high inflow rate could wash away the stored sediments and LW-HTS operates similarly as CFD model. In other cases, Q_2 could only reach around 3 l/s. As shown in Figure 1.10, Q_2 remains around 3 l/s even when Q_1 achieves 1.1 m^3/s. However, Q_2 arrives at around 4.5 l/s later as the earlier heavy rain washes away a part of sediments.

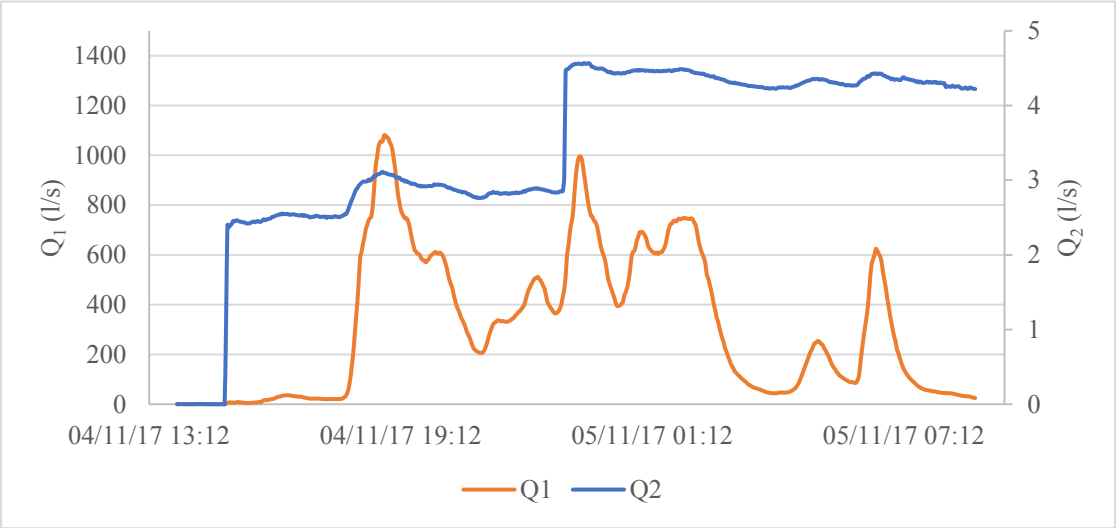

Figure 1.10. Example of Q_2 evolution due to trapped sediment at the T-connection of LW-HTS (rain event of 04-05 Nov 2017)

1.3.5. Particle tracking and trapping efficiency

Experiments *in situ* during dry weather were carried out in order to evaluate the trapping efficiency of LW-HTS. Fire hydrant water was used to simulate stormwater. Artificial particles (density: 1240 kg/m^3, particle-size distribution illustrated in Figure 1.11a) were chosen according to sediment characteristics *in situ* (Becouze-Lareure et al., 2014) and injected near the bottom opening of LWS (Flow rate Q_1 = 13.65 l/s). They were then collected at T-connector and trapping box (shown in Figure 1.6b). The total mass and particle-size distribution of injected and trapped particles are measured to evaluate the efficiency of LW-HTS. Results show that 19.25% of injected particles were trapped in the trapping box and 8.97% were blocked in the T-connector. The particle-size distribution and cumulative particle-size distribution of the injected and collected particles were analysed and illustrated in Figure 1.11. Particles collected at trapping box are similar to injected ones in terms of particle-size distribution as they peak both at around 210 µm. Blocked particles at T-connection are coarser than injected ones.

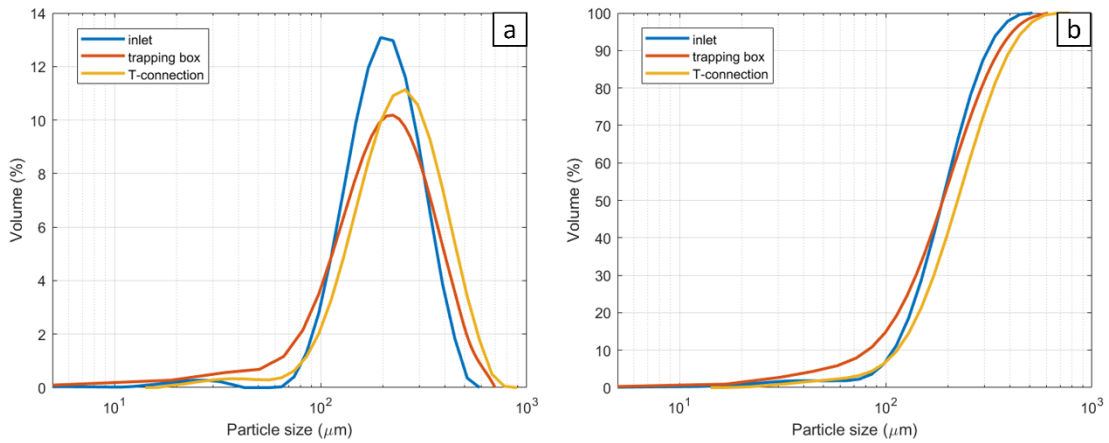

Figure 1.11. (a) Particle-size distribution, (b) cumulative particle-size distribution of injected and trapped artificial particles (obtained from experiments *in situ*)

In addition to *in situ* experiments, CFD modelling was also applied to simulate sediment transport. Particles with the same characteristics as those used in field experiments, as well as finer particles were injected in the system. The modelling parameters are shown in Table 1.4.

Table 1.4. Sediment transport modelling strategy

Lagrange approach	Discrete phase model (DPM)
Particle density	1 240 kg/m^3
Particle size	115, 140, 161, 180, 201, 222, 248, 280, 332 µm, representing D10-D90 (same as characteristics of the artificial sediments used during field experiments), as well as fine particles with sizes of 10, 20, 30, 40, 50, 60, 70, 80, 90, 100 µm
Injection	1 m upstream to the bottom opening of LWS
Maximum iterative steps	5e+06
Boundary condition for DPM	Inlet and outlet: escape. Side wall: reflect. Bed wall of trapping box: combination of trap and reflect with the developed user-defined function (UDF) using BSS and BTKE as criteria (see more details in Chapter 3).
Particle dispersion due to turbulence	Stochastic modelling: discrete random walk model (DRWM), Lagrangian constant time scale C_L = 0.15.

For injected particles of the same characteristics as *in situ* experiments, percentages of trapped, escaped and incomplete particles are represented in Figure 1.12. The trapping efficiency of LW-HTS augments from 40% to 73% as the particle size increases. In total, 54% of injected particles were intercepted, comparing to the trapping efficiency of 30% obtained by the experiments.

The difference could be explained by (i) wall effects on particles (Happel and Brenner, 1983): some particles stayed on the wall during experiments; (ii) loss of collected particles during the particles transfer given their fine size. In addition, the trajectories of fine particles with sizes of 10 - 100 µm were also simulated given that fine particles are often present in stormwater and associated with pollutants (e.g. Ashley et al., 2004). Results show that the trapping efficiency of LW-HTS augments from 30% to 40% as the particle size increases from 10 to 100 µm. In general, 100% of particles passing through LWS were trapped in HTS.

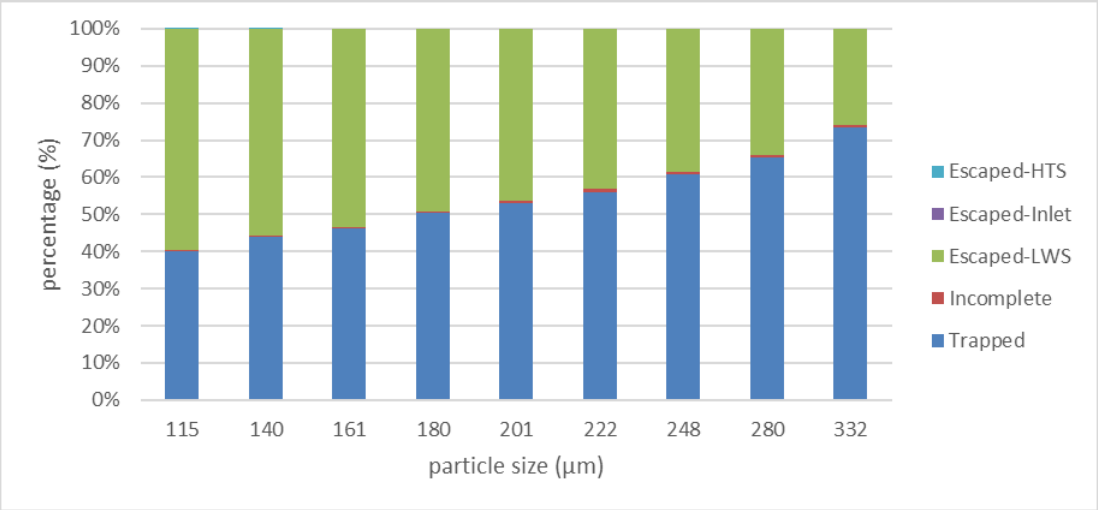

Figure 1.12. Trapping efficiency according to CFD modelling results (Q_1 = 13.65 l/s, particles of same characteristics of experiments)

In addition, particles (sizes of 10 - 332 µm) were injected in CFD model according to different inflow rates (Q_1 = 6.5 - 350 l/s). The trapping efficiencies and particles' residence time are illustrated in Figure 1.13. As already shown before, coarser particles are easier to be trapped and nearly 100% of particles passing through LWS were trapped in HTS. Even though the coarse particles (201-332 µm) in low flow rate condition (Q_1 = 6.5 l/s) stay incomplete at the end of calculation, their residence time is more than 15h (much longer than average residence time of DRB, which is around 4-5h). Hence, these particles tend to be trapped finally in real life. When comparing the trapping efficiency in different hydrodynamic conditions, more particles tend to follow the overflow of LWS upstream for higher inflow rate, and thus less are likely to be trapped in HTS. Overall, particles stay longer in the system in lower inflow rate conditions (maximum at around 33h when Q_1 equals 6.5 l/s). For Q_1 between 13 and 60 l/s, finer and coarser particles tend to stay longer in the system, while median particles (around 200 µm) are trapped firstly in the box. This is because particles of less than 200 µm in diameter firstly reach the hydrocyclone, while finer particles tend to settle more slowly with the centrifugal force. On the other hand, the coarser particles might firstly settle in the pipe or at T-

connector and be resuspended later by the incoming water. In the case of strong flows (e.g. Q_1 = 350 l/s), the coarser the particles are, the earlier they are trapped.

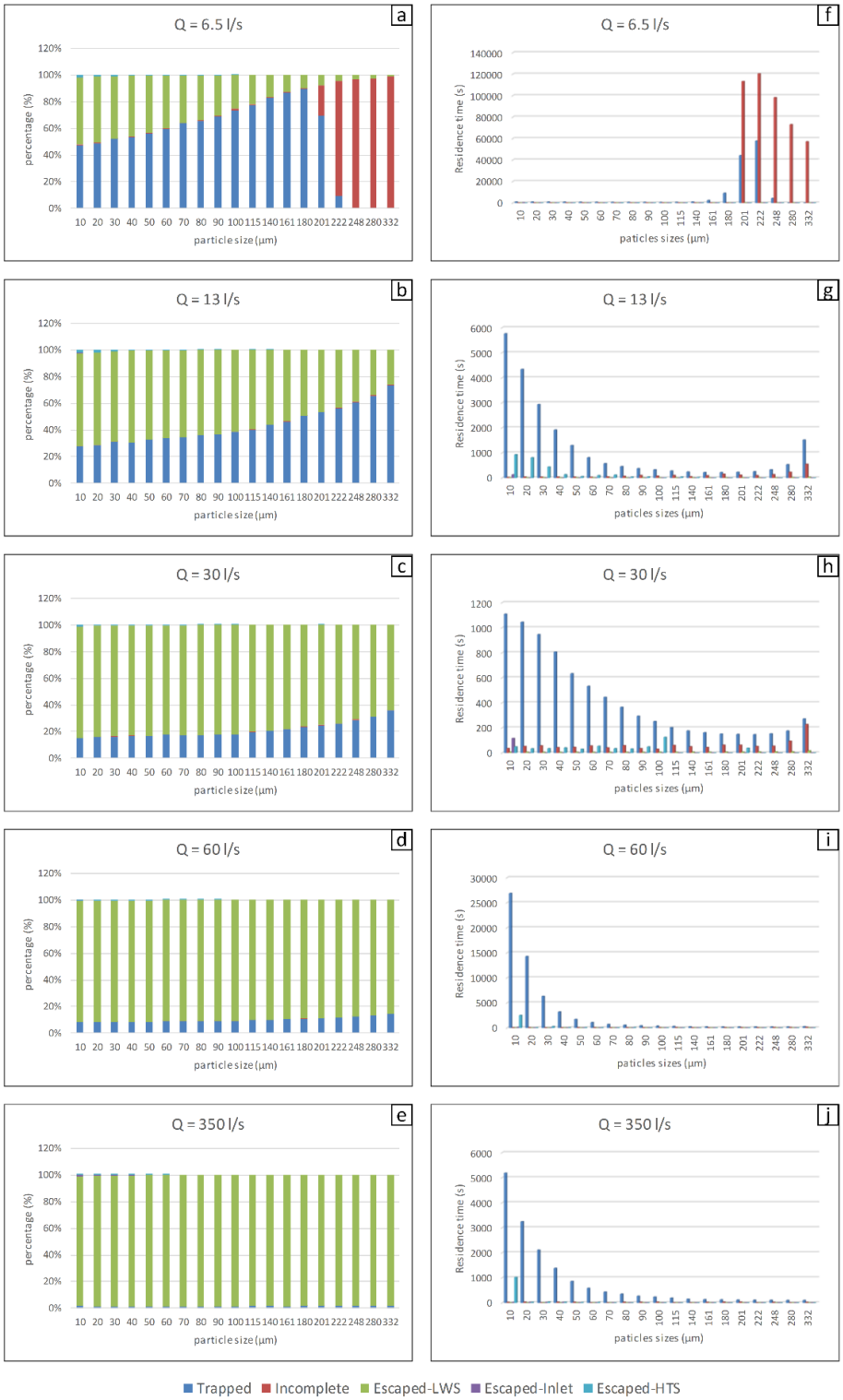

Figure 1.13. (a-e) Trapping efficiency of LW-HTS and (f-j) particles' residence time in LW-HTS

1.3.6. Comparison of sediment characteristics from inlet and from traps in DRB

Sediments were collected from both LW-HTS (inlet) and traps at the bottom of DRB during five rain events (illustrated in Figure 1.14). The characteristics of the sampled rain events are presented in Table 1.5. Additional details on campaigns can be found in Chapter 4.

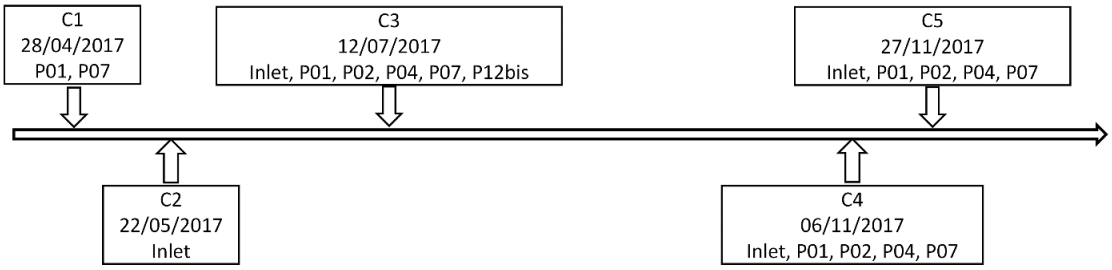

Figure 1.14. Campaign timeline and sampling points for each campaign

Table 1.5. Characteristics of the sampled rain events and corresponding hydraulic parameters in DRB

Campaign date of year 2017	C1 28/04	C2 22/05	C3 12/07	C4 06/11	C5 27/11
Rainfall characteristics					
Rain Duration (hour:min)	19:22	08:14	03:02	18:26	16:28
Total Depth (mm)	26.5	17.5	10.5	30.9	11.2
Mean Intensity ($mm \cdot h^{-1}$)	1.4	2.1	3.4	1.7	0.7
Max intensity ($mm \cdot h^{-1}$)	6	7.5	58.2	11.7	6.9
ADWP (days)	23	4	8	12	11
DRB hydraulic parameters					
Mean inflow rate (m^3/s)	0.21	0.31	0.24	0.31	0.11
Max inflow rate (m^3/s)	0.76	0.81	1.27	1.08	0.77
Max water level (m)	0.51	0.54	0.39	0.69	0.50

ADWP: antecedent dry weather period

The sediments' characteristics are illustrated in Figure 1.15, Figure 1.16 and Table 1.6. Results show that the properties of sediments from the basin are related to the sediments intercepted from LW-HTS at the inlet as their particle-size distributions peak at around the same size. The sediments from the inlet are coarser than those from the basin during C3 and C5. On the other hand, sediments collected from inlet are relatively fine during C2. In fact, C2 was carried out just after the installation of LW-HTS, while C3 and C5 were realised later when sediments

could aggregate and accumulate along with operation time before the campaigns. In addition, there is some leak from the trapping box, which might carry some fine particles. Settling velocities of sediments from inlet are variable from one campaign to another as already demonstrated by Torres (2008). Compared to sediments collected from basin, inlet sediments settle more quickly during C3 and settle slower during C4 and C5, except for P02 in the case of C5.

Table 1.6. Comparison of particle-size and settling velocity of sediments from inlet and basin

Sample		Particle size (µm)			Settling velocity (m/h)		
		D10	D50	D90	V20	V50	V80
C1	P01	9.9	69.2	501.9	1.9	7.0	21.7
	P07	9.5	54.5	206.4	1.9	6.6	20.0
C2	inlet	11.1	55.6	312.9	1.8	6.7	20.2
C3	inlet	24.2	313.5	1365.8	3.2	11.6	32.8
	P01	9.1	52.9	308.5	2.9	9.6	28.9
	P02	6.3	37.7	260.9	1.0	3.4	9.9
	P04	7.4	45.3	493.5	1.9	6.9	22.2
	P07	8.2	45.5	200.9	1.3	4.1	12.4
	P12bis	12.5	78.3	402.3	2.1	7.5	23.3
C4	inlet	nm	nm	nm	0.5	1.9	6.1
	P01	23.7	144.6	1077.0	1.6	5.9	16.9
	P02	20.0	199.3	1282.7	0.9	2.9	8.1
	P04	18.8	129.4	1224.0	0.8	2.6	7.7
	P07	17.3	79.8	641.5	1.9	6.7	20.8
C5	inlet	370.9	870.5	1473.1	0.9	4.3	14.7
	P01	16.5	78.5	520.2	1.7	6.0	17.3
	P02	18.8	100.2	944.4	0.6	2.1	6.9
	P04	28.6	433.3	1268.2	1.5	5.4	15.3
	P07	20.7	109.8	870.0	1.6	5.7	16.2

nm: not measured

D10: sieving size with 10% of particle mass passing through.

V10: 10% of particle volume has a settling velocity inferior to V10.

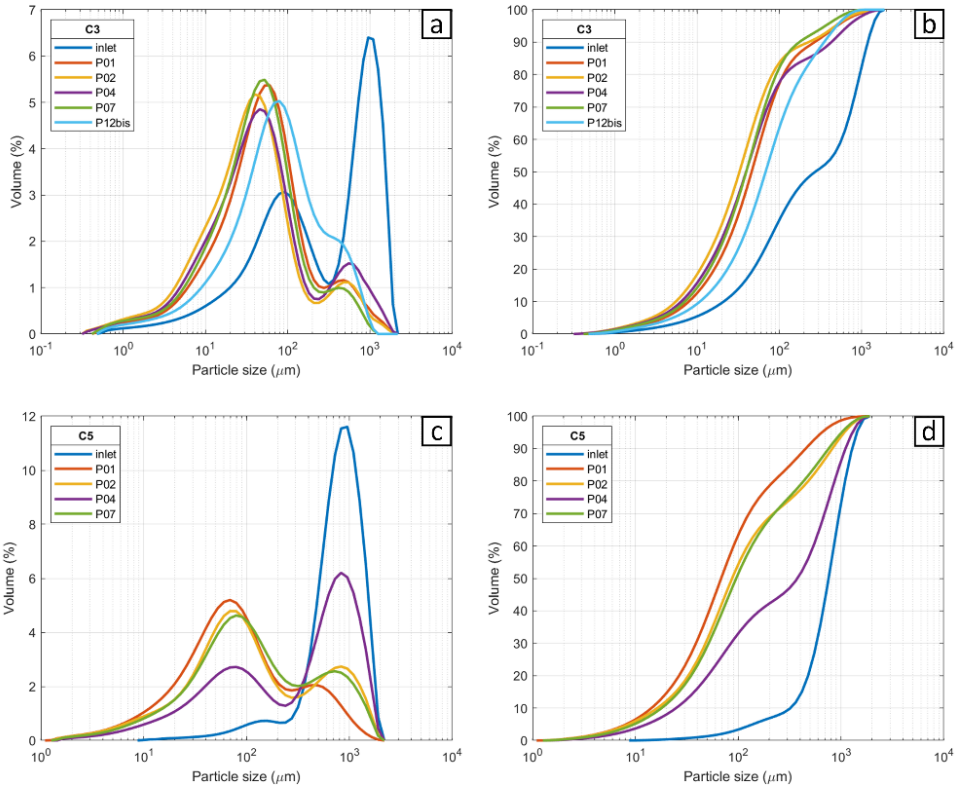

Figure 1.15. Comparison of (a) & (c): particle -size distribution, (b) & (d) cumulative particle-size distibution of sediments from inlet and basin (C3 and C5, respectively).

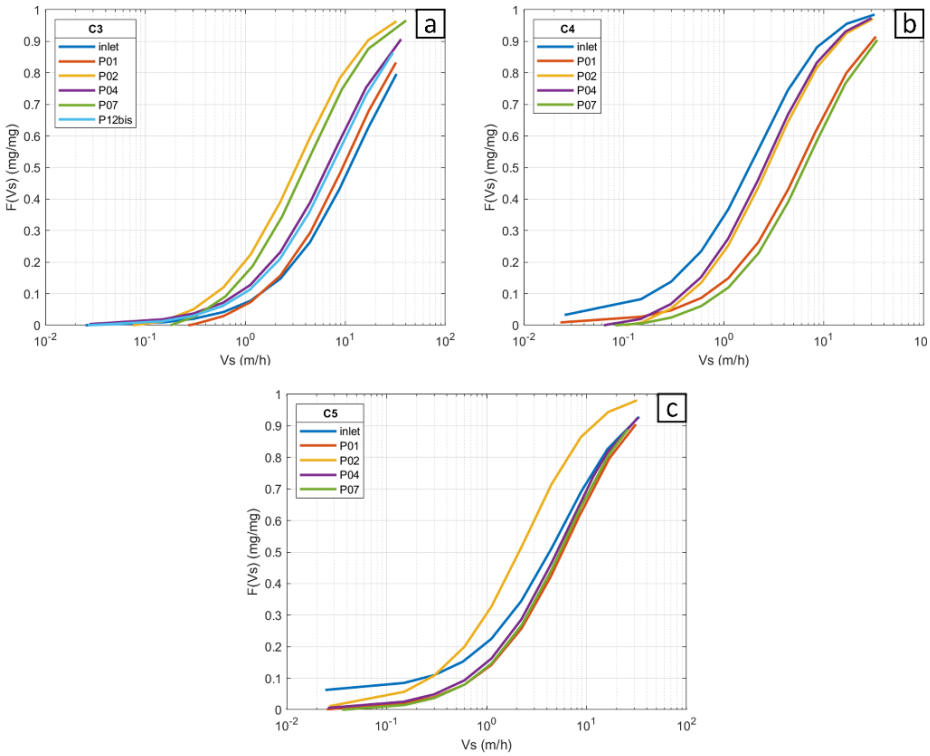

Figure 1.16. Comparison of settling velocity distribution of sediments from inlet and basin (C3-C5)

1.3.7. Section conclusions

Preliminary experiments in the inlet measurement flume showed higher values for sediments' sizes and settling velocities. This might be the result of sediment aggregation in the measurement flume. In addition, we assume that samples collected downstream of peristaltic pumping suction are not representative of likelihood settling particles in the basin. Hence, a HTS is designed to intercept particles that may settle in the basin and collect more representative samples. The experiments and numerical simulation of LW-HTS permit to understand and evaluate its hydrodynamic behaviour. Meanwhile, the trapping percentage of particles of different sizes in different flow conditions helps to evaluate the trapping efficiency. As expected, results show that LW-HTS has a better trapping performance for coarser particles and nearly 100% of particles passing through LWS are trapped in HTS. The LW-HTS are then used for sediment sampling at the inlet of DRB and the sediments characteristics are comparable to those trapped in the basin, particularly regarding settling velocity distribution and values. As for sediments' sizes, sediments collected from the inlet are relatively coarse comparing to those trapped in the basin for certain campaigns, due to the fact that sediments could aggregate and accumulate in LW-HTS along with the operation time before campaigns and some leak of fine particles from the trapping box of LW-HTS. It is then proposed to use more efficient cleaning equipment before each campaign and add a honeycomb-like trap in the trapping box to avoid resuspension of fine particles.

1.4. Chapter conclusions

This chapter presents the experimental site DRB and sediment sampling strategy. In addition to the honeycomb-like traps proposed by Torres (2008) for sediment sampling at the bottom of DRB, a new device LW-HTS is designed and proposed for sediment sampling at the inlet of DRB. The trapping efficiency and the representativeness of sediments intercepted by LW-HTS are proved by experiments and numerical modelling. It is shown that LW-HTS enables to trap all fractions of particles including the finer and coarser ones (10-300 μm). LW-HTS has a better trapping performance for coarser particles and nearly 100% of particles passing through LWS are trapped in HTS. To improve the trapping efficiency, it is proposed to use more efficient cleaning equipment before each campaign and add a honeycomb-like trap in the trapping box to avoid resuspension of fine particles. The LW-HTS is then used for sediment sampling at the inlet of DRB and the sediments characteristics are comparable to those trapped in the basin, particularly regarding settling velocity distribution and values. Based on this sampling strategy, an original research on the correlation between metal contents in sediments and settling velocity is carried out, which will be presented in Chapter 4.

Chapter 2. Application of LSPIV for free surface velocity measurement in DRB

This chapter aims to understand the hydrodynamic behaviour in DRB using Large-Scale Particle Image Velocimetry (LSPIV). The experimental free surface velocity field of DRB is obtained and supports the numerical model evaluation and particle deposits prediction. The prediction of particle and pollutant deposits will be discussed in Chapters 3 and 4. The published work related to this chapter is "Zhu, X., Lipeme Kouyi, G. (2019). An analysis of LSPIV□based surface velocity measurement techniques for stormwater detention basin management. Water Resources Research, 55(2), 888-903. https://doi.org/10.1029/2018WR023813".

2.1. Introduction

The hydrodynamic characteristics play an important role for the transport and sedimentation of particulate pollutants in DRB. The developed CFD model (Yan, 2013; Yan et al., 2014) enables to simulate its hydrodynamic behaviour and particle transport. However, the model needs to be evaluated by an experimental velocity field, while the complex field conditions make it impossible to access for spatial measurements without contact with the flow. Meanwhile, traditional velocimetry techniques, such as Acoustic Doppler Velocimeter (ADV), are limited for point velocity measurement at a given time, and thus are unable to obtain a global, spatio-temporal velocity field. The presence of the measurement equipment body could influence the reliability of collected velocity values. In addition, stormwater detention basins are often forbidden to access for security reasons. Accessing these basins is extremely dangerous during and at the end of storm events due to the water height and strong turbulences caused by the complex geometry. Hence, a no-contact measurement strategy such as image-based or radar-based techniques is required. Large-Scale Particle Image Velocimetry (LSPIV) is an image-based approach to measure large-scale water surface velocity (Muste et al., 2008). The installation of a camera combined to the use of the free surface velocity extraction tool is a low-cost, effective and convenient technique to get a broad and quick view of the key flow patterns within field stormwater detention basins. Furthermore, this may represent an innovative way to explain sedimentation processes in these basins, to check their design, sizing and performances, and to help for their retrofit and management.

LSPIV was derived from the PIV method (Particle Image Velocimetry) (Adrian, 1991), which was conceived for laboratory small-scale measurement. Various investigations have been carried out for LSPIV measurements in riverine environment for areas of 100 to 5000 m2

(Muste et al., 2008). The measurement and mapping of the flow distribution are widely applied (i) during floods (Fujita and Komura, 1994; Fujita et al., 2007) and (ii) near hydraulic structures (Fujita et al., 2003; Fleit et al., 2016), demonstrating LSPIV as a quick and safe method for the flow measurement with comprehensive and quantitative information in large-scale environments. The performance of LSPIV for the measurement in shallow flow has also been studied by Kantoush et al. (2011) and Muste et al. (2014), proving the flexibility and reliability of LSPIV to characterize shallow free surface flows.

LSPIV methods usually have three phases: camera recording, image orthorectification, and velocity field calculation. As an image-based approach, LSPIV needs a camera to record image sequences of high-quality flow movements under appropriate illumination. Flow patterns can be represented by natural tracers as foam, light debris, vegetation, wood, surface waves, or sometimes artificial particles (Muste et al., 2008). Image othorectification is often needed as many campaigns collect images from a bank or a bridge oblique to the free surface plane. In this phase, an appropriate image transformation scheme using at least 6 ground control points (GCPs) in real and image coordinates is required. Conventionally, it is better to have more than 10 GCPs, which are non-aligned and uniformly distributed within the camera viewshed, i.e. the entire region visible in the camera (Le Coz et al, 2014). Finally, LSPIV algorithms permit to estimate velocities by searching the most probable displacement of tracers between two consecutive frames. Many LSPIV algorithms based on the cross-correlation calculation were developed, including Fudaa-LSPIV (Le Coz et al, 2014) and PIVlab (Thielicke and Stamhuis, 2014).

The objectives of this chapter are to (i) investigate the hydrodynamic behaviour in stormwater detention basin by means of free surface velocity field measurements using LSPIV technique, and (ii) evaluate CFD simulation results and explain the spatial sediments distribution at the bottom of DRB.

2.2. Methods and materials

2.2.1. Camera recording

A camera (Axis P1347) has been installed at the south bank of the basin (see Figure 2.1a) since 2013, aiming to continuously record surface flow videos. The camera position and camera viewshed are illustrated in Figure 2.1b and c, respectively. The camera is placed at the summit of a pole with a tilt angle of 6º and at 3.49 m height from the platform, which is 4.44 m height compared to the base of DRB (shown in in Figure 2.1b). The camera has a CMOS sensor with size of 10.2 mm (1/2.5"). The lens aperture is f/1.6 with a focal length of 3.5-10 mm. Given the large size of interrogation zone, a combination of camera resolution of 2560 × 1920 pixels and

frame rate of 12 fps is chosen for better recognition of tracer paths. The camera is connected to a PC computer via RJ45 to record videos continuously. Recorded videos are split into 5-min-length image sequences for further processing.

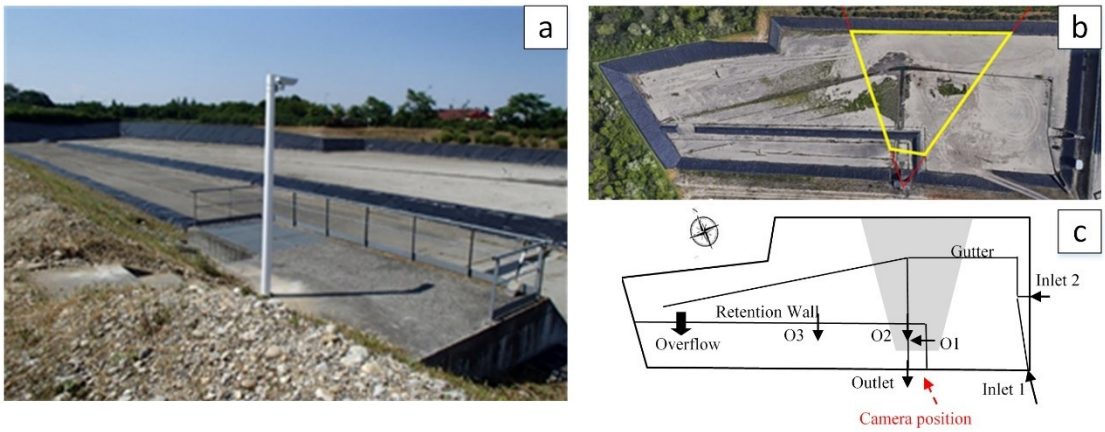

Figure 2.1. (a) Camera Axis P1347 in situ, (b) Top view of DRB with camera viewshed surrounded by yellow lines (photo from Google Map). (c) Sketch of DRB with camera viewshed emphasized with grey background.

2.2.2. LSPIV image treatment

The obtained image sequences are then treated by an LSPIV image treatment procedure. Fudaa-LSPIV and PIVlab, two commonly used LSPIV image treatment tools, are both applied in this study in order to strengthen results by redundancy.

Fudaa-LSPIV is a free software developed by EDF (Electricité de France – electricity of France company) and Irstea (National Research Institute of Science and Technology for Environment and Agriculture), and implemented by DeltaCAD (Le Coz et al, 2014). The software has been applied in riverine environment of different scales (laboratory and field) and periods (flood and normal) (Hauet et al., 2014; Le Boursicaud et al., 2016). PIVlab is an open-source toolbox based on Matlab environment, developed by Thielicke and Stamhuis (2014). PIVlab was firstly realized to analyse the flapping flight of birds (Thielicke, 2014) and then extended to various domains, such as biochemical analyses, wind measurements and velocity measurement in rivers (Dutta, 2015; Lewis et al., 2015; Lewis et al., 2018; Tauro et al., 2017; Yang, 2016). Whatever the tool is, there are four main image treatment steps: orthorectification, pre-treatment, image processing and post-treatment. As discussed above, the velocity field calculated from orthorectified images via the last three steps. A comparison between the two LSPIV tools is detailed in Table 2.1.

Table 2.1. Presentation of Fudaa-LSPIV and PIVlab tools for LSPIV image treatment

	Fudaa-LSPIV (Le Coz et al, 2014)	PIVlab (Thielicke and Stamhuis, 2014)
Orthorectification	Provide image orthorectification by giving Ground Control Points (GCPs) in real and image coordinates.	Need to import already orthorectified images.
Pre-treatment	No pre-treatment options.	Provide different pre-treatment options to enhance the images in order to emphasize tracer appearance, such as contrast limited adaptive histogram equalization (CLAHE) (Shavit et al., 2007), intensity highpass (Gonzalez & Wintz, 1987) and intensity capping (Shavit et al., 2007).
Image processing	Cross-correlation transformation.	Cross-correlation transformation could be solved by two approaches: Direct Cross Correlation (DCC) & Discrete Fourier transform (DFT).
Post-treatment	Eliminate extreme velocities by giving a threshold, possible to define correlation threshold.	Eliminate extreme velocities by choosing the limits manually through velocity distribution figure, or semi automatically by calculating the mean velocity and standard deviation.

Fudaa-LSPIV takes the image orthorectification into consideration, which could be realized by simply inputting different GCPs pairs in real and image coordinates. PIVlab enables different pre-treatment options to enhance the images, such as (i) CLAHE, to increase the readability of image data, (ii) intensity highpass, to remove low frequency background and (iii) intensity capping, to reduce the bias of results caused by bright particles (Thielicke and Stamhuis, 2014). The image processing is carried out by cross-correlation algorithm, which is the key element to extract 2D velocity field by searching the tracer pattern between different image areas. The discrete cross-correlation function C is defined as follows (Huang et al., 1997):

$$C(m,n) = \sum_i \sum_j A(i,j)B(i-m, j-n) \qquad \text{Equation 2.1}$$

Where A and B correspond to the interrogation area of two consecutive images. (m,n) represents the displacement of tracers within the time inter0val between consecutive images

related to A and B respectively. The location of the intensity peak in the matrix C gives the most probable tracer displacement.

However, Equation 2.1 is sensitive to intensity changes in A and B. Thus, an optimized algorithm is applied to compensate the drawback by normalization (shown in Equation 2.2) (Fincham and Spedding, 1997; Huang et al., 1997).

$$C(m,n) = \frac{\sum_i \sum_j (A(i,j) - \bar{A})(B(i-m, j-n) - \bar{B})}{\left(\sum_i \sum_j (A(i,j) - \bar{A})^2\right) \sum_i \sum_j \left((i-m, j-n) - \bar{B}\right)^2)^{1/2}} \quad \text{Equation 2.2}$$

Where, $\bar{A}$ and $\bar{B}$ represents the means of A and B. The optimized algorithm is applied in Fudaa-LSPIV, as well as for DCC approach in PIVlab (Le Coz et al, 2014; Thielicke and Stamhuis, 2014). In addition to DCC, which calculates directly in spatial domain, PIVlab provides also a less accurate but more efficient approach DFT, which computes in frequency domain after Fourier transform. The inaccuracy could be compensated by using passes of different kernels (Westerweel et al., 1997). More details of the mathematical background can be found elsewhere (e.g. Raffel et al., 2007).

Post-treatment of LSPIV data helps to filter extreme values of velocity. We can define the velocity threshold and correlation threshold manually to eliminate outliers in Fudaa-LSPIV. In PIVlab, it is possible to choose the limits manually through velocity distribution figure or semi automatically by calculating the mean velocity and standard deviation.

2.2.3. Methodology and data exploitation

DRB is a complex stormwater management facility, which includes many parts such as: (i) acceleration zone at the inlet, (ii) storage and stabilization zone at the centre of the basin and (iii) overflow weir at the outlet. Preliminary tests were firstly carried out in a small-scare laboratory pilot, where similar flow condition can be found and well mastered. These preliminary tries aim to evaluate the tools for free surface velocity measurements in small-scale physical model. In addition, orders of the free surface velocity magnitudes are assumed to be comparable to those exhibiting at the field scale. Afterward, the LSPIV technique is applied to DRB under field flow conditions in order to catch the key flow patterns and potential sedimentation zones. Finally, the measured flow velocity is used to evaluate broadly the representativeness of DRB CFD models.

2.2.3.1. Preliminary tests on laboratory scale

Experiments in the laboratory were realized in DSM-flux (Device for Stormwater and combined sewer flows Monitoring and the control of pollutant fluxes) (Maté Marín et al., 2018). As illustrated on the right hand of Figure 2.2, DSM-flux is a rectangular open channel composed of four main zones. The velocity measurements were performed in the stabilization (green) and overflow (blue) zones because of their stable hydrodynamic characteristics. In this study, inflow rate of 0.009 m^3/s was injected from inlet.

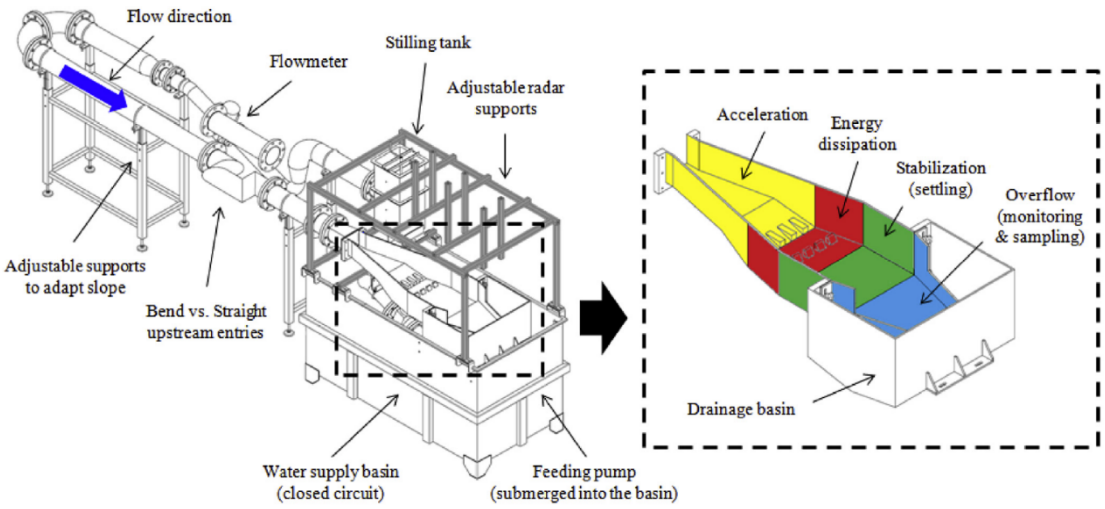

Figure 2.2. Schematic of DSM-flux in laboratory (Maté Marín et al., 2018)

A camera (Olympus Tough TG-820) with resolution of 1920 × 1080 pixels and frame rate of 30 fps was placed at the top of DSM-flux device to record flow information for PIV treatments. Biodegradable particles (corn starch) were injected from the inlet (stilling tank, shown in Figure 2.2), aiming to increase the readability of tracers during PIV treatments.

Furthermore, ADV measurements were also carried out using Nortek Vectrino Velocimeter (Nortek, 2004), which help to evaluate the PIV results. The measuring parameters are illustrated in Table 2.2. In this study, ADV measurements were realized at 2 cm under the free water surface in order to (i) be as near as possible to the water surface, and (ii) meet the requirement that all the receivers are submerged in water for 3D velocity measurement. An ADV device was placed at different measuring points using a specially constructed moving and support system. Twenty-five points were measured within the camera viewshed.

Table 2.2. ADV measuring parameters using Nortek Vectrino Velocimeter (Nortek, 2004)

ADV parameters	
Distance from probe	5 cm
Sampling volume diameter	6 mm
Sampling volume height (selected)	7 mm
Acquisition frequency	50 Hz
Probe type	Side-looking probe
Measure time	5 min
Despiking method	Phase-Space Threshold despiking algorithm (Goring and Nikora, 2002) with the modifications introduced by Wahl (2002)

The relative differences of the velocity magnitudes obtained by ADV and PIV were calculated as below:

$$Relative\ \ difference\ \ (v_{ADV}, v_{PIV}) = \frac{|v_{ADV} - v_{PIV}|}{v_{ADV}} \qquad \text{Equation 2.3}$$

2.2.3.2. Application for the DRB free surface velocity measurements

As for DRB, its surface movements are continuously recorded by a field camera. The videos were firstly pre-selected according to their content quality including: (i) illumination: Glare and shadow were avoided to maintain appropriate illumination; (ii) wind: Permanent wind should be excluded as it could influence the surface flow velocity and thus bias the analysis of the hydrodynamic behavior of the DRB, (iii) rain: Raindrops could deform the natural tracers (water wavelets and floating items), and therefore, only the videos at the end of rain event were kept. At the same time, the inflow rate is measured ceaselessly in the field every 2 min. Once the video is chosen, we can obtain the corresponding inflow rate by removing the estimated residence time of flow from inlet to the camera viewshed at the basis of video record time step.

Two rain events were monitored during 2013 and 2014 and several video clips (2 hours in total) meet the requirements for LSPIV analysis mentioned above (appropriate illumination, without raindrops and without wind when the trees remain immobile). Nine representative videos with inflow rates of 0.002, 0.012, 0.015, 0.02, 0.025, 0.03, 0.815 and 1.984 m^3/s were analyzed. Averaged velocity fields were then computed using the chosen image sequences in order to remove random and temporary wind effects (Lewis et al., 2018; Muste et al., 2011).

The raw images were firstly orthorectified with Fudaa-LSPIV thanks to 19 well-chosen GCPs. These points were at different heights and scattered all over the camera viewshed, in order to accurately project the entire 3D real space into 2D image. Their 3D real coordinates were measured in two steps: (i) GPS (Global Positioning Systems) measurements of their vertical projection points (VPPs) at the bottom of DRB using D-GPS (Differential-GPS) Trimble. The D-GPS Trimble is composed of two receivers: mobile receiver (shown in Figure 2.3b) to get its location, as well as, base receiver to corrects the errors and improve the accuracy (illustrated in Figure 2.3a). The red point illustrated in Figure 2.3b, corresponding to VPP, was measured. (ii) Determination of relative heights between GCPs and their corresponding VPPs. A pole with uniformly distributed markers (every 50 cm), serving as height measurement tool, was vertically placed (shown in Figure 2.3c) at each VPPs and recorded by the camera. These relative heights were randomly chosen and GCPs coordinates were then obtained by adding the relative heights to the vertical (height) coordinate of VPPs. The raw and orthorectified images with GCPs are displayed in Figure 2.3d and Figure 2.3e.

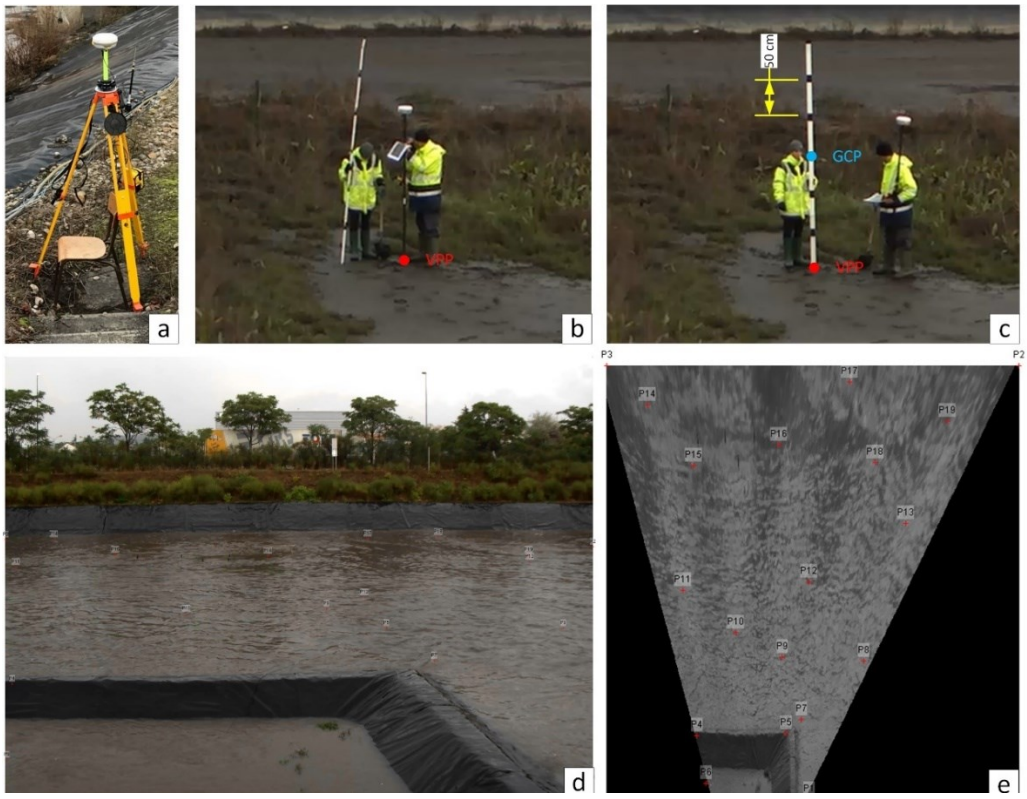

Figure 2.3. Image orthorectification: (a) GPS measurement: base receiver of D-GPS Trimble, (b) GPS measurement: mobile receiver of D-GPS Trimble, measured at red point, corresponding to the vertical projection point (VPP) of Ground Control Point (GCP), (c) height measurement tool, pole with uniformly distributed markers (every 50 cm), with an example showing the pair of GCP (in blue) and VPP (in red), (d) raw image with GCPs, (e) orthorectified image with GCPs.

After orthorectification, Fudaa-LSPIV and PIVlab were utilised to extract free surface velocity field by searching the most probable displacement of natural tracers (water wavelets and floating items). The extreme velocities were eliminated using two filters in PIVlab: (i) standard deviation filter, the velocities are limited in the scope of $\bar{u} \pm 7 \times \sigma_u$, where $\bar{u}$ represents mean velocity and σ_u represents standard deviation of u, (ii) local median filter through a normalized median test, which evaluates the velocity fluctuation with respect to the median in a 3 × 3 neighbourhood around a central vector (see more details in Thielicke and Stamhuis, 2014; Westerweel et al., 2005). The same velocity limits were then applied in Fudaa-LSPIV.

Sensitivity tests on the following parameters related to image treatments have been carried out: (i) lengths of image sequences, (ii) scales of orthorectification, (iii) sizes of interrogation area and searching areas (IA and SA) in Fudaa-LSPIV, (iv) numbers of passes of different IA kernels in PIVlab, and (v) pre-treatment methods in PIVlab. The variation of velocity magnitudes under different parameter sets is described by NRMSD (normalized root-mean-square deviations, Chai and Draxler, 2014).

$$RNRMSD = \frac{\sqrt{\sum_{i=1}^{n}(x_{1,n} - x_{2,n})^2 / n}}{(\overline{x_1} + \overline{x_2}) / 2} \qquad \text{Equation 2.4}$$

The optimal parameters were then applied for final LSPIV image treatments. The final results obtained by Fudaa-LSPIV and PIVlab have been compared and their velocity vector differences were calculated according to Equation 2.5.

$$\Delta\vec{v} = \vec{v}_{PIVlab} - \vec{v}_{Fudaa-LSPIV} \qquad \text{Equation 2.5}$$

2.3. Results

2.3.1. Preliminary experiments in a small-sized laboratory condition - DSM-flux

Figure 2.4a illustrates the surface velocity field obtained by PIV when the flow rate Q equals 0.009 m^3/s (measurement points are reduced for easier reading). Results show that water flows from upstream (left) to downstream (right) with velocity magnitudes ranging from 0.2 to 0.3 m/s. On the other hand, ADV measurement points are sparse. Therefore, the entire velocity field is obtained via linear interpolation of the measurement data (shown in Figure 2.4b). In both subfigures, velocity fields are illustrated by arrows showing directions and colors representing magnitudes.

In addition, a PIV calculation point (denoted by asterisk in Figure 2.4c) was selected near each ADV measurement point (denoted by filled circle). The velocity magnitudes obtained by PIV

and ADV were compared pairwise. Results demonstrate that their velocity magnitudes are mainly similar at the centre with relative differences less than 8% (illustrated in green, Figure 2.4c). On the other hand, significant deviations in velocity magnitudes are observed near the periphery (shown in red, Figure 2.4c) as foams along the wall are noises to visual tracers. It is also noticed that there is a line of low velocity (illustrated in Figure 2.4a), which is due to the junction between stabilization (green) and overflow (blue) zones (shown in Figure 2.2). Finally, PIVlab results are consistent with ADV measurement results, proving PIV capable of providing velocity measurements for complex stormwater management facilities at a small scale.

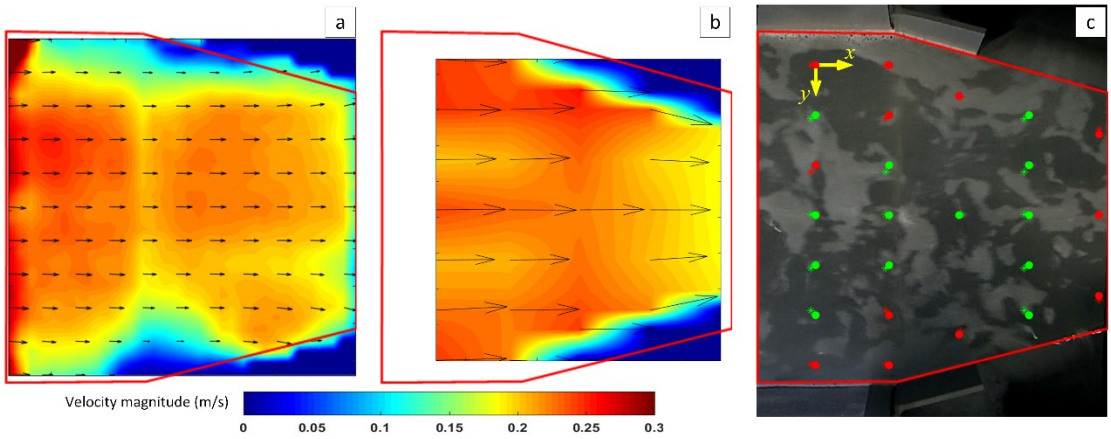

Figure 2.4. Comparison of PIV and ADV results (Q = 0.009 m^3/s, boundaries of the interrogation zone are marked as red lines): (a) Free surface velocity field with reduced measurement points obtained by PIV, (b) Velocity field at 2 cm under water surface obtained by ADV, (c) ADV measurement locations (•) and PIV calculations locations (*). Locations where relative differences of PIV and ADV results are less than 8% are represented in green, and in red when their relative differences range from 14% to 44%. Origin and x, y directions are marked in yellow.

2.3.2. Application for the DRB free surface velocity measurements

2.3.2.1. Sensitivity study of LSPIV parameters

In order to obtain the optimal parameters for LSPIV analysis, different sensitivity tests were firstly carried out upon the video of 8 August 2013, 16h04min 18-23s, with an inflow rate equal to 0.03 m^3/s. Effects of different parameters are discussed below:

Length of images sequences: Three video durations (5s, 10s and 18s) were tested aiming to determine an appropriate length of image sequences, which is (i) sufficient for wind effect suppression, while at the same time (ii) as less as possible in order to save computation time and avoid errors created by flow changes through time. The obtained velocity fields are shown in Figure 2.5, with NRMSD varying from 0.26 to 0.44. The differences are due to the varying

velocity field through time. Therefore, 5s is chosen for later calculations to minimize the effect of the unsteady state of the flow between consecutive frames.

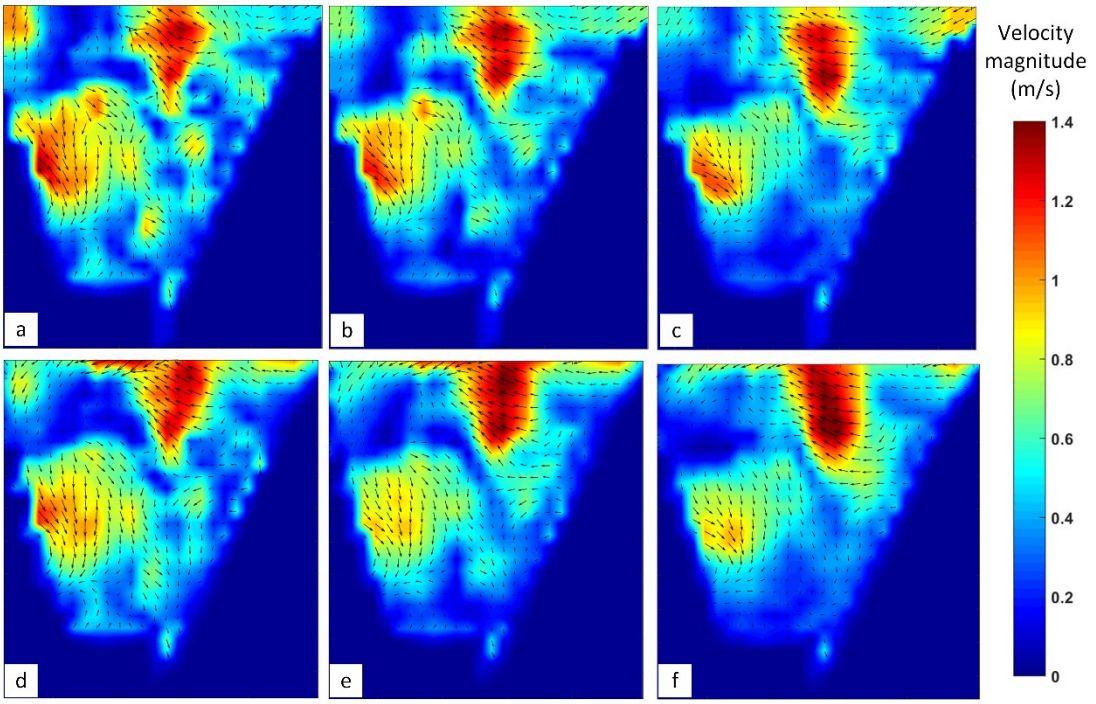

Figure 2.5. Sensitivity test on length of image sequences: (a) Fudaa – 5s, (b) Fudaa – 10s, (c) Fudaa – 18s, (d) PIVlab – 5s, (e) PIVlab – 10s, (f) PIVlab – 18s

Scales of orthorectification: According to the pinhole camera model, zones near the camera are present at the bottom of the image and occupy more pixels than remote zones. Therefore, after orthorectification, rectangular images are reshaped into trapeziums, as shown in Figure 2.6a-b. Resolutions of orthorectified images vary according to different transformation scales (possible scale choices are illustrated in Figure 2.6c-e). Downsampling of images usually suffers from image information loss, but can improve LSPIV analysis efficiency. Figure 2.6c represents the case when all the boundaries are downsampled (default in Fudaa-LSPIV), while Figure 2.6d-e account for the cases when the pixels in y and x_1 remain unchanged after orthorectification, respectively. The obtained free surface velocity fields for these three cases are consistent (illustrated in Figure 2.7). Hence, the resolution of 0.1118 m/pixel is applied for further calculations in order to save calculation time.

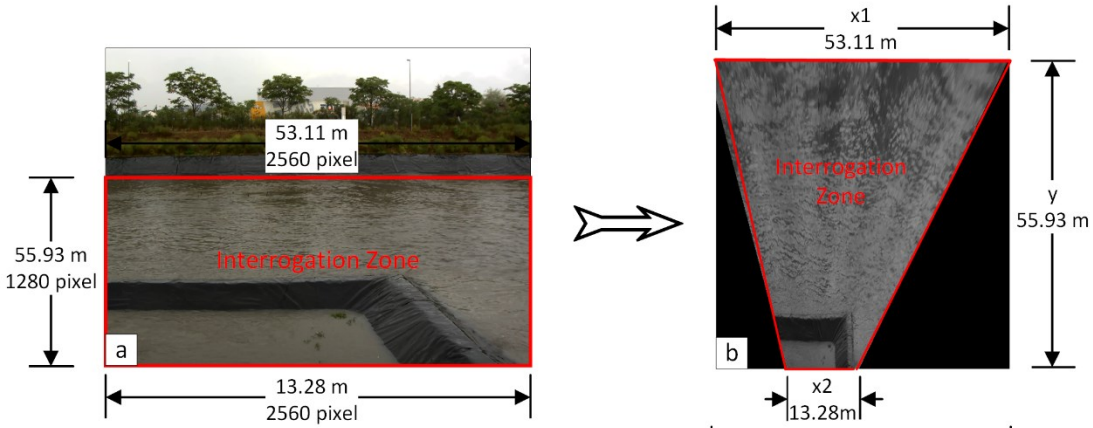

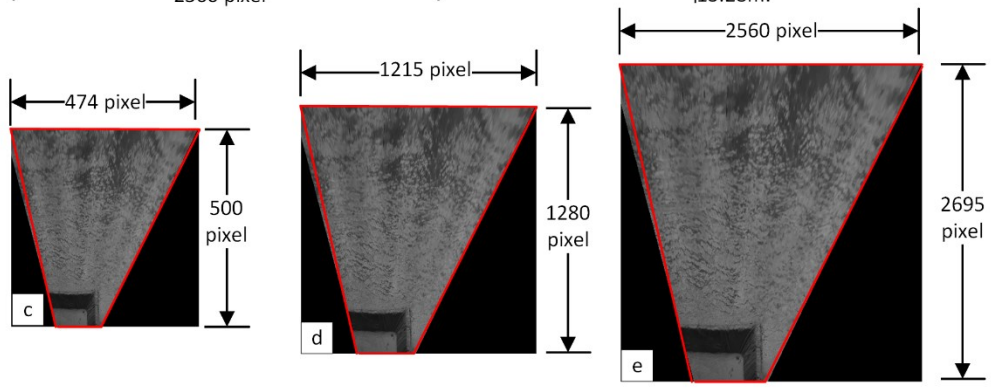

	Resolution (m/pixel)	x1	x2	y
c	0.1118	downsampled	downsampled	downsampled
d	0.0437	downsampled	downsampled	unchanged
e	0.0200	unchanged	downsampled	upsampled

Figure 2.6. Different scales of orthorectification: (a) original image (projective), (b) orthorectified image, (c) 0.1118 m/pixel, downsampling in x_1, x_2 and y, (d) 0.0437 m/pixel, resolution unchanged in y, (e) 0.02 m/pixel, resolution unchanged in x_1. x_1, x_2 and y are represented in (b).

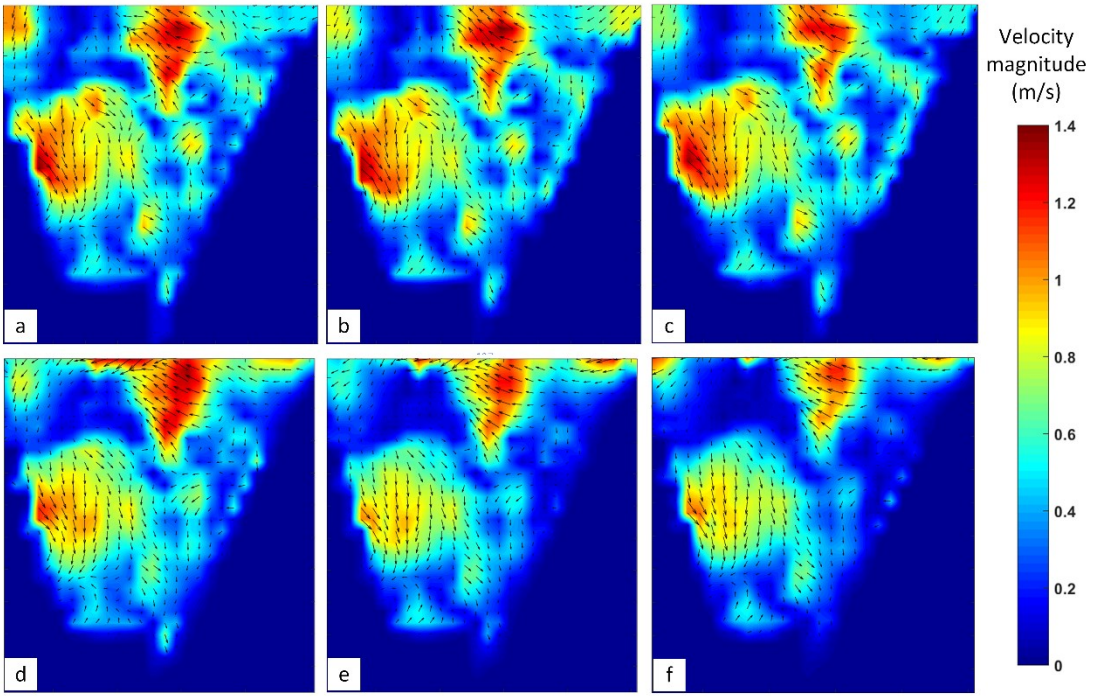

Figure 2.7. Sensitivity test on different scales of orthorectification: (a) Fudaa – 0.1118 m/pixel, (b) Fudaa – 0.0437 m/pixel, (c) Fudaa – 0.02 m/pixel, (d) PIVlab – 0.1118 m/pixel, (e) PIVlab – 0.0437 m/pixel, (f) PIVlab – 0.02 m/pixel

Sizes of IA and SA in Fudaa-LSPIV: The key element of LSPIV image processing is to search the most probable tracer path by comparing IA of two consecutive frames in the scope of SA. The sizes of IA and SA depend on the tracer size and determine the calculation time. Different sizes of IA and SA were then tested in Fudaa-LSPIV and the obtained results are illustrated in Figure 2.8. Images with IA of 16, 32 and 64 pixels were firstly analysed, and the obtained velocity field is more disturbed and not representative when IA equals to 16 (Figure 2.8a) and 64 pixels (Figure 2.8c), respectively. More analyses were conducted with SA of 8, 16, 32, 64 pixels while IA equals 32 pixels, of which the results with IA and SA both equal to 32 appears more appropriate (Figure 2.8b/d/e/f).

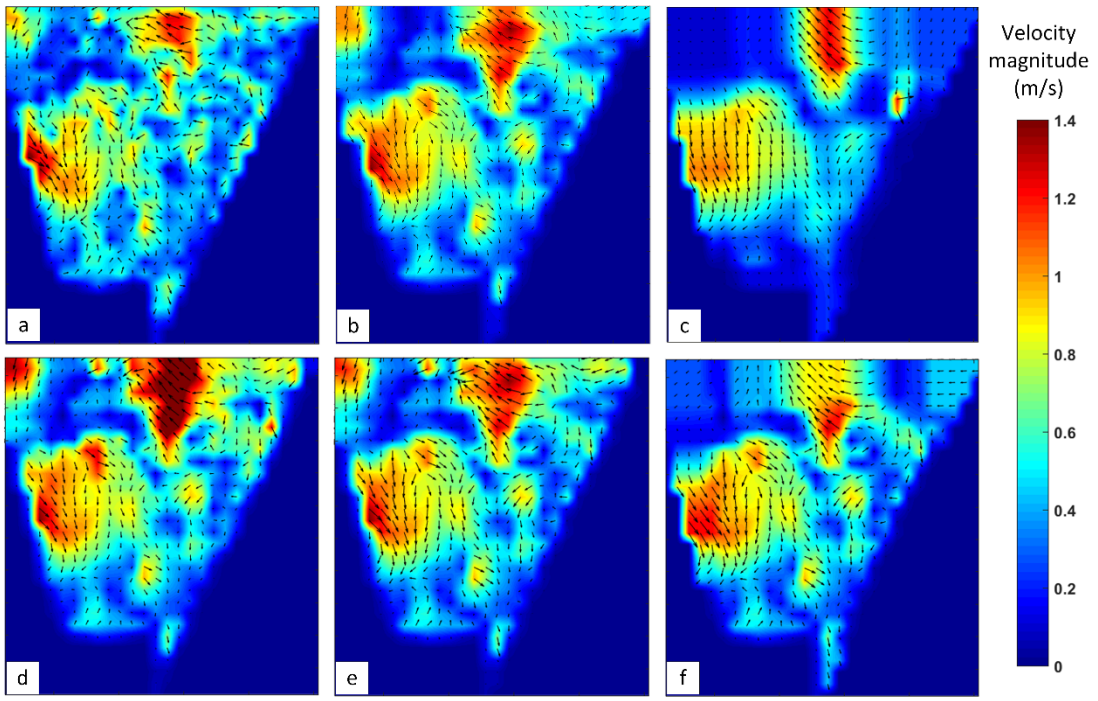

Unit: pixel	a	b	c	d	e	f
IA*	16	32	64	32	32	32
SA**	16	32	64	8	16	64

*IA: square interrogation area, where the number represents its side length

**SA: square search area, where the number represents the distance between the centre of IA and the edge of SA

Figure 2.8. Sensitivity test on the size of IA and SA in Fudaa-LSPIV

Numbers of passes of different IA kernels in PIVlab: In PIVlab, the pass of a larger kernel helps to calculate global velocities and the smaller one is used for local results with more accuracy. In this study, two passes with IA size of 64, 32 pixels and 3 passes with IA size of 64, 32, 16 pixels were applied in PIVlab, respectively (presented in Figure 2.9). Although, three-pass calculation gives slightly more accurate results, two passes are sufficient and more efficient to present the flow patterns and are thus utilised in the further calculations.

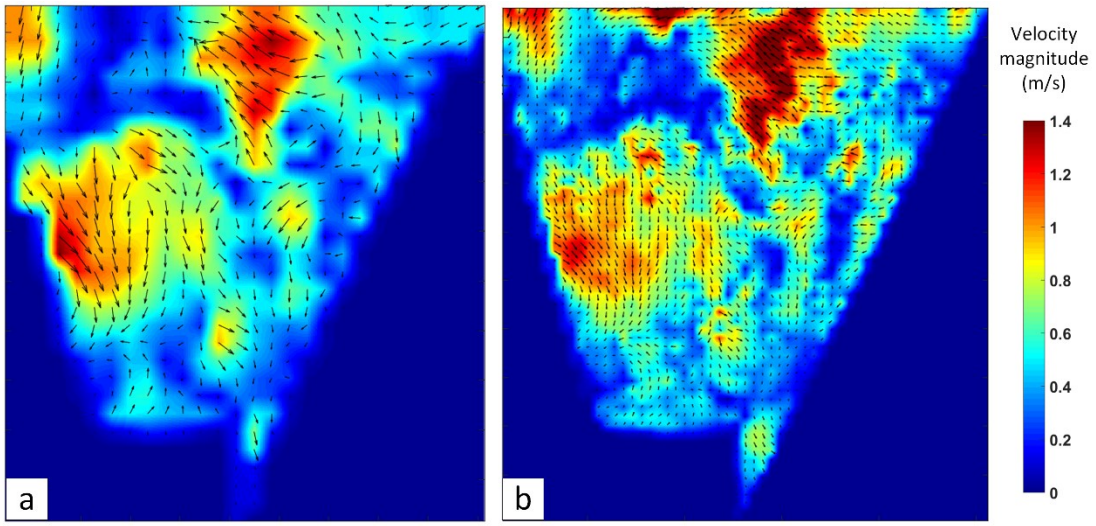

Figure 2.9. Sensitivity test on the number of passes of different IA size in PIVlab: (a) 2 passes with IA size of 64, 32 pixels, (b) 3 passes with IA size of 64, 32, 16 pixels

Pre-treatment methods in PIVlab: Finally, different PIVlab pre-treatment methods were applied in the analyses and the results show a great similarity with or without CLAHE, highpass and intensity capping treatments (illustrated in Figure 2.10). Thus, no pre-treatment is applied in the final calculations.

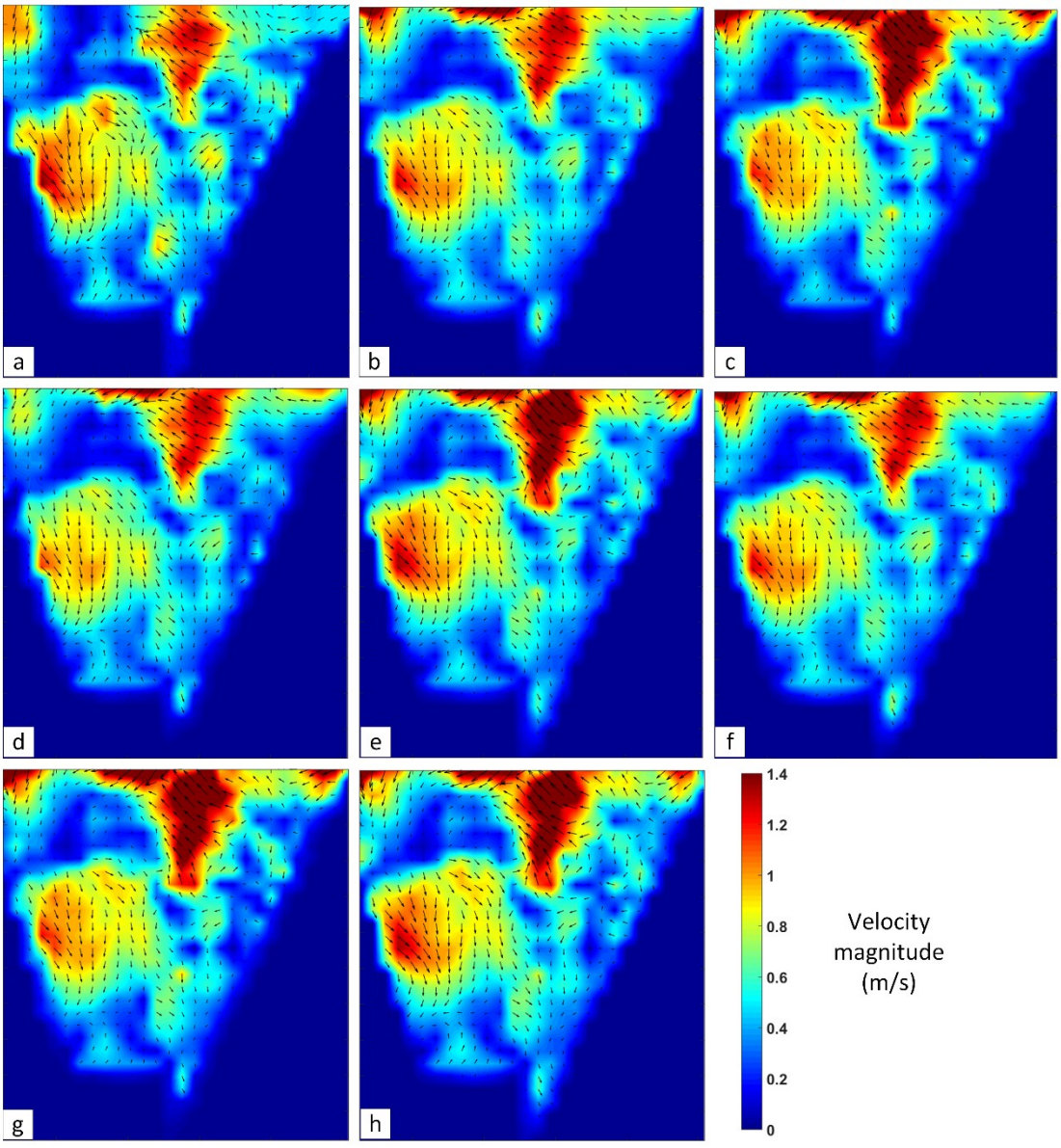

Figure 2.10. Sensitivity test on PIVlab pre-treatment: (a) without pre-treatment, (b) CLAHE, (c) highpass, (d) intensity capping, (e) CLAHE + highpass, (f) CLAHE + intensity capping, (g) highpass + intensity capping, (h) CLAHE + highpass + intensity capping

Overall, the optimal parameters of LSPIV applied in the future analyses are summarized in Table 2.3.

Table 2.3 Optimized parameters applied in the LSPIV analysis

Parameters	Value
Video duration	5 s
Scales of orthorectification	0.1118 m/pixel
Size of interrogation and searching areas in Fudaa-LSPIV	IA = 32 pixel, SA = 32 pixel
Size and numbers of passes of different IA kernels in PIVlab	2 passes of IA = 64 and 32 pixel
Pre-treatment methods in PIVlab	None

2.3.2.2. Free surface velocity field measurements in DRB

Figure 2.11 and Figure 2.12 illustrate the free surface velocity field extracted from nine different videos with LSPIV-Fudaa and PIVlab, respectively. Results show that the flow mainly runs from right to left in the camera viewshed, which corresponds to the fact that the basin inlet is located at the right. In general, an area with relatively low velocity is observed at the centre of the basin, which may promote deposition in this area. Two main flow patterns are observed: (i) Water comes from the upper-right corner of the camera viewshed and moves towards the lower-left part. In some cases, a swirl is created at the centre area (c, f and g), while in some other cases, flow continues to move to left side (a and h). (ii) Flow moves from lower-right corner towards upper-left part (b, d, e and i). It is also noticed that the flow patterns of two neighbouring time intervals are similar in spite of the difference of inflow rate (b and i).

The velocity fields extracted with Fudaa-LSPIV and PIVlab were then compared with each other and their velocity vector differences were calculated according to Equation 2.5 (illustrated in Figure 2.13, same colour bars as in Figure 2.11 and Figure 2.12). Results illustrate that the velocity magnitude deriving from the two tools is nearly identical in the majority of the interrogation zone, especially the centre part near the camera position. However, some velocity deviations are observed at the periphery of the camera viewshed (illustrated in Figure 2.13). In fact, Fudaa-LSPIV and PIVlab have different strategies dealing with velocities at image boundaries, which are often oblique after orthorectification (shown in Figure 2.14a). Rectangular interrogation areas near these boundaries do not fit the image areas. Errors may occur as wrong interrogation areas (non-image areas) are taken into calculation (e.g. long green arrows in Figure 2.14b). Therefore, some abnormal zones with extreme high velocities are observed at image boundaries in the PIVlab treatment results (Figure 2.12a/b/c/f/g/(i). Overall, both Fudaa-LSPIV and PIVlab demonstrate similar flow patterns, especially at centre zones, which is consistent with observations.

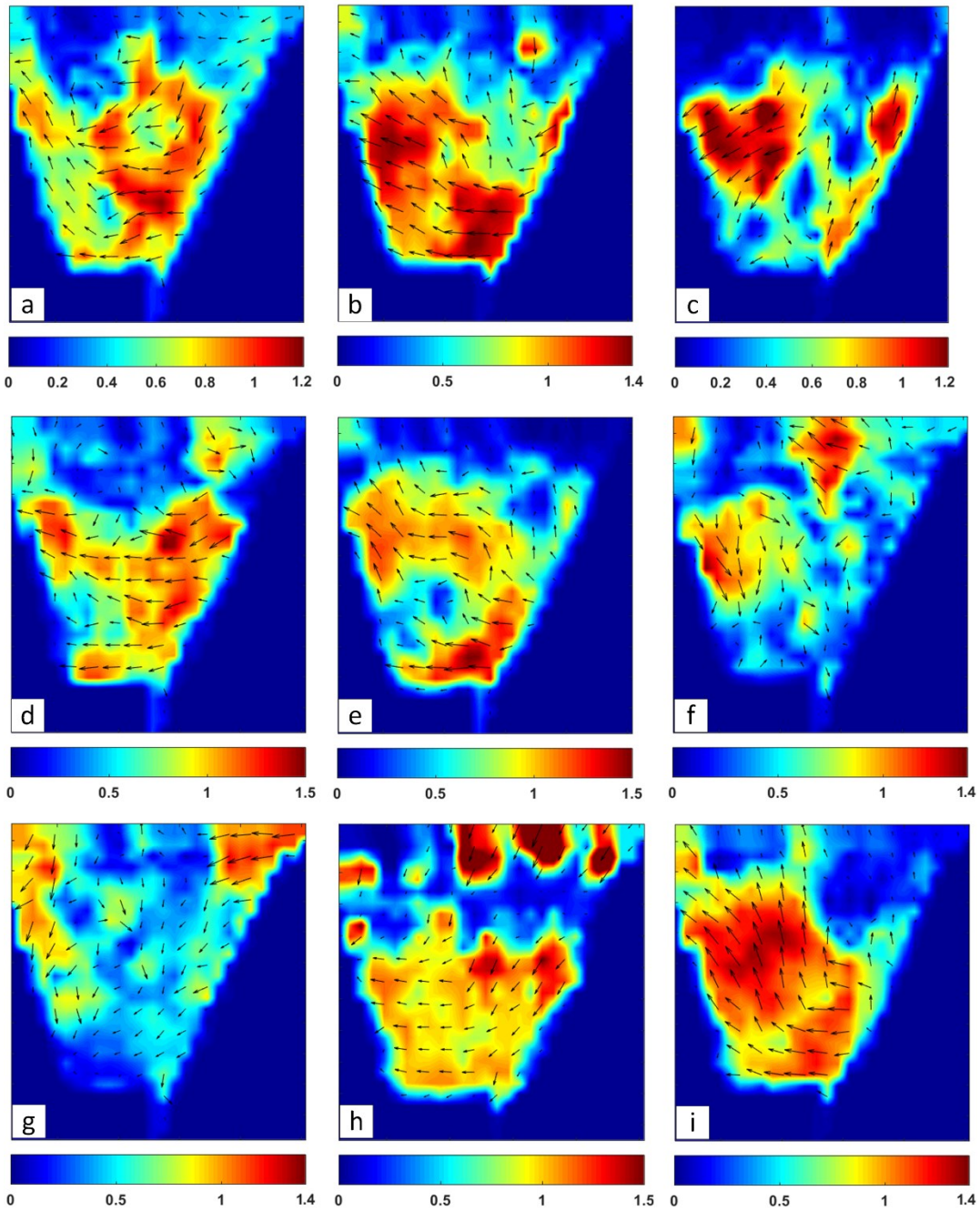

	Inlet flow rate (m^3/s)	Time
a	0.002	22 Mar 2014, 19h15min 0-5s
b	0.012	8 Aug 2013, 13h48min 0-5s
c	0.015	8 Aug 2013, 16h48min 0-5s
d	0.02	8 Aug 2013, 16h23min 5-10s
e	0.025	7 Aug 2013, 17h05min 0-5s
f	0.03	8 Aug 2013, 16h04min 18-23s
g	0.03	8 Aug 2013, 16h03min 0-5s
h	0.815	7 Aug 2013, 12h47min 0-5s
i	1.984	8 Aug 2013, 14h02min 0-5s

Figure 2.11. Free surface velocity field extracted from 9 different videos with Fudaa-LSPIV: color bars represent the velocity magnitude in m/s

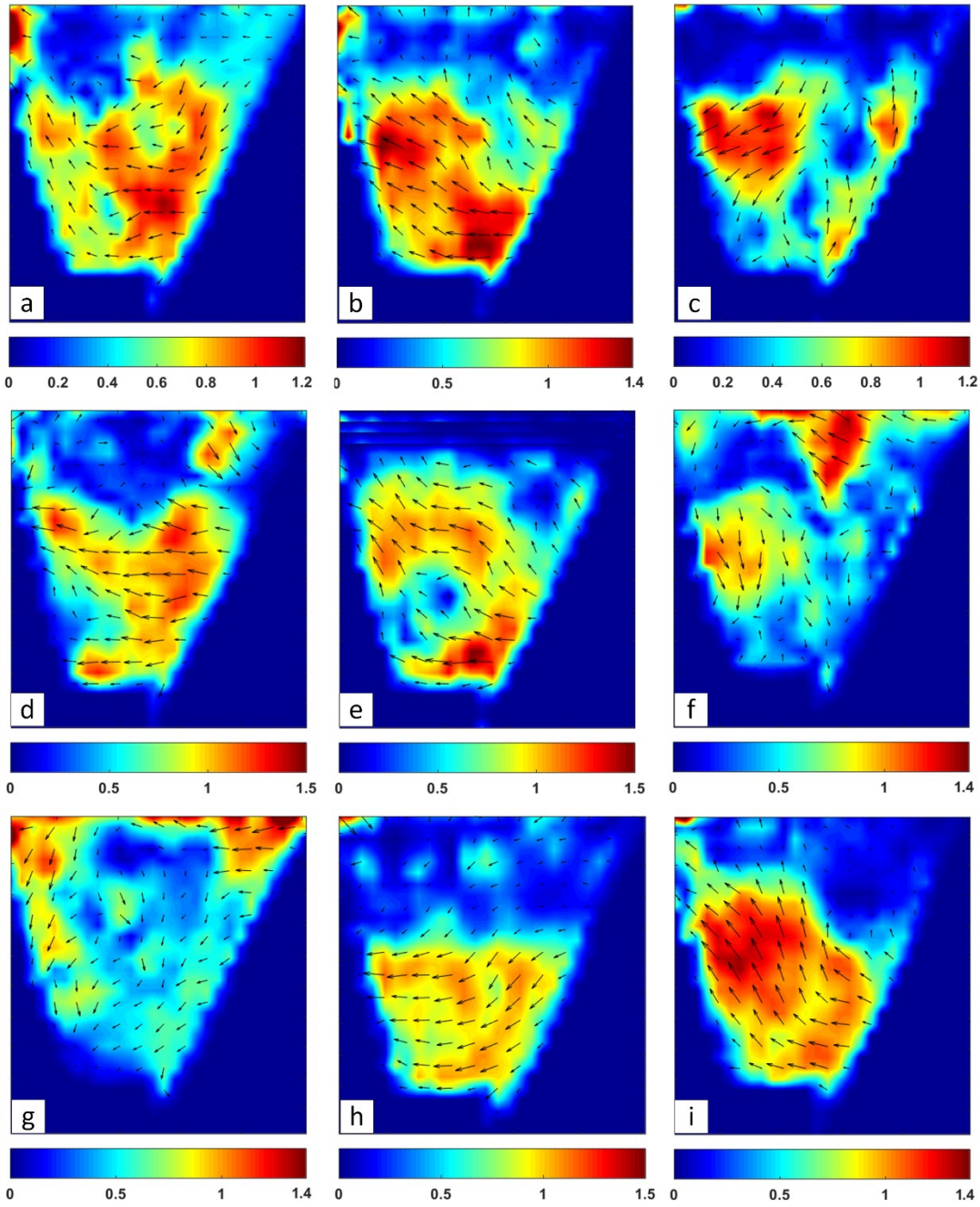

	Inlet flow rate (m^3/s)	Time
a	0.002	22 Mar 2014, 19h15min 0-5s
b	0.012	8 Aug 2013, 13h48min 0-5s
c	0.015	8 Aug 2013, 16h48min 0-5s
d	0.02	8 Aug 2013, 16h23min 5-10s
e	0.025	7 Aug 2013, 17h05min 0-5s
f	0.03	8 Aug 2013, 16h04min 18-23s
g	0.03	8 Aug 2013, 16h03min 0-5s
h	0.815	7 Aug 2013, 12h47min 0-5s
i	1.984	8 Aug 2013, 14h02min 0-5s

Figure 2.12. Free surface velocity field extracted from 9 different videos with PIVlab: color bars represent the velocity magnitude in m/s

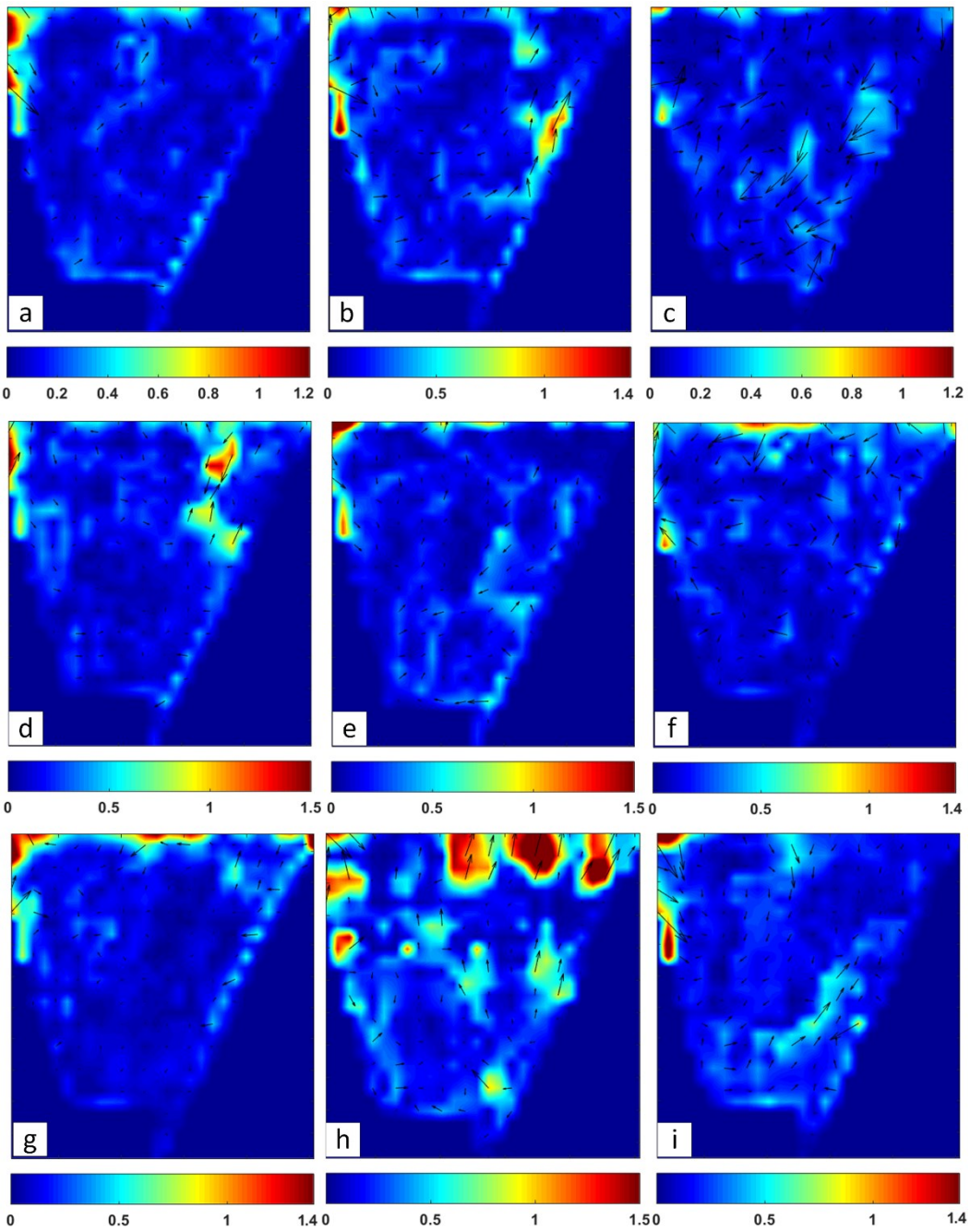

	Inlet flow rate (m^3/s)	Time
a	0.002	22 Mar 2014, 19h15min 0-5s
b	0.012	8 Aug 2013, 13h48min 0-5s
c	0.015	8 Aug 2013, 16h48min 0-5s
d	0.02	8 Aug 2013, 16h23min 5-10s
e	0.025	7 Aug 2013, 17h05min 0-5s
f	0.03	8 Aug 2013, 16h04min 18-23s
g	0.03	8 Aug 2013, 16h03min 0-5s
h	0.815	7 Aug 2013, 12h47min 0-5s
i	1.984	8 Aug 2013, 14h02min 0-5s

Figure 2.13. Difference of velocity vectors extracted with Fudaa-LSPIV and PIVlab: color bars represent the magnitude of velocity vector differences in m/s, arrows represent their directions.

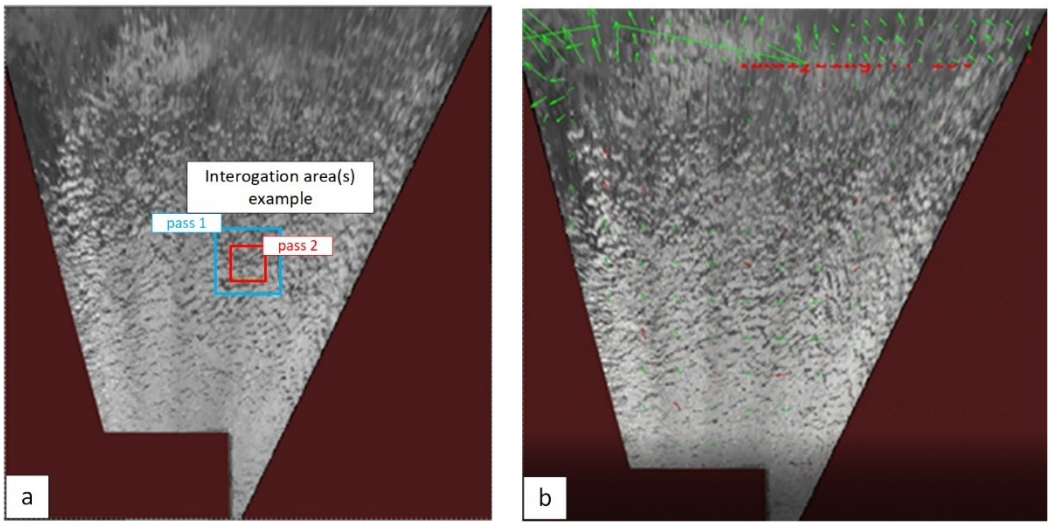

Figure 2.14. PIVlab treatment: (a) example of interrogation area(s), (b) treatment of velocities at image boundaries in PIVlab.

2.3.3. Evaluation of CFD modelling of DRB using LSPIV data

The hydrodynamic behaviour of the DRB has been simulated using CFD approach with mesh size of 850000 (Lipeme Kouyi et al. 2010; Yan et al., 2014). Three different inflow rates (Q = 0.025, 0.03 and 0.815 m^3/s) were applied for this preliminary comparison between CFD and LSPIV results. The flows were simulated in steady condition using ANSYS Fluent (version 14 and 16) software and the visible zone in the camera is illustrated in Figure 2.15. CFD results show that the flow mainly comes from the upper-right side in the camera viewshed, and then creates a swirl in the counterclockwise direction for all the three cases. However, the location and size of the swirl vary with different flow rates (e.g. only a partial swirl can be observed within the camera viewshed in Figure 2.15f). When comparing with LSPIV results, similar swirl can be observed at the centre of basin for some cases (c, f and g). Low velocities (c, e and g) and swirls that probably lead to sediment settling are observed at the centre of the basin, which corresponds to the fact that the centre accumulates the majority of sediments (illustrated in Figure 2.16).

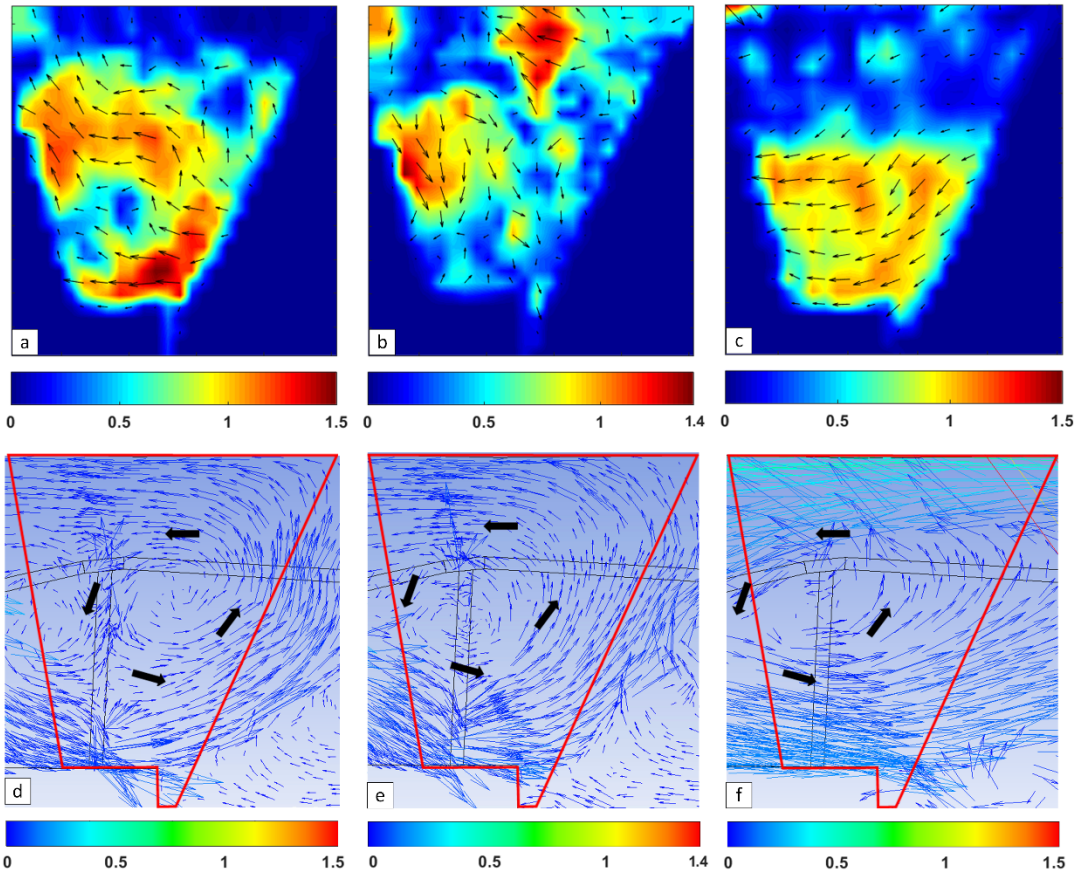

	Inlet flow rate (m^3/s)	Time
a/d	0.025	7 Aug 2013, 17h05min 0-5s
b/e	0.03	8 Aug 2013, 16h04min 18-23s
c/f	0.815	7 Aug 2013, 12h47min 0-5s

Figure 2.15. Free surface velocity field obtained by LSPIV and CFD modelling (color bars represent the velocity magnitude in m/s): (a-c) LSPIV, (d-f) CFD modelling. Black arrows indicate the recirculation direction, areas with red border represent camera viewshed.

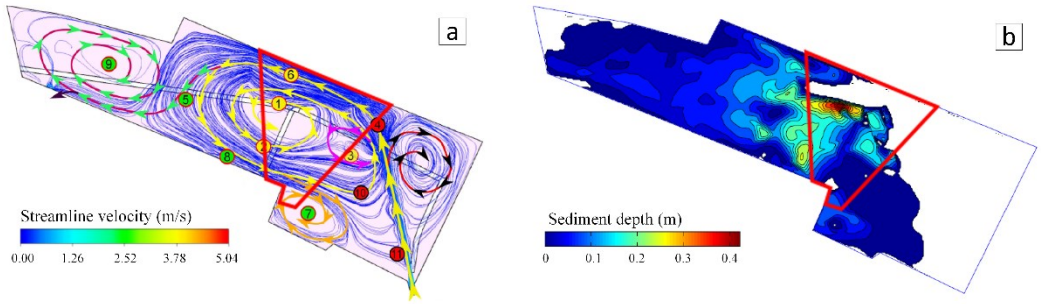

Figure 2.16. (a) Streamline of the fluid flow obtained by CFD (Q = 0.35 m3/s, main flow rate). Locations of sediments of different sizes are represented in different colours: red circles for coarse particles, yellow for median and green for fine. (b) Sediment depth distribution measurement in DRB. Red borders represent the camera viewshed. (Adapted from Yan, 2013)

Several differences are observed and different hypotheses have been investigated. First of all, CFD models were simulated in steady conditions, and the dynamic situation of the flow were not accounted in the models, which may be one of the key reasons for the differences. In addition, the current CFD model applied a symmetrical boundary condition at the top of computational domain to simulate free surface, new simulations with VOF model (see e.g. Hirt and Nichols, 1981) were then performed to see if this might be the reason for the difference. Figure 2.17 shows the comparison of CFD results using symmetrical boundary condition and VOF model with mesh size of 3 million. Results show that flow comes from inlet and then creates a counter-clockwise swirl at the centre of DRB with symmetrical boundary. A small swirl is then created near orifice 1. On the other case, three swirls are observed with VOF model. Bed shear stress (BSS) and bed turbulent kinetic energy (BTKE) at the bottom of DRB are also calculated and results show that BSS and BTKE at inlet are higher than at the other parts of DRB, which lead to the fact that few sediments are accumulated near the inlet (shown in Figure 1.4c). A slight difference is observed at the centre of basin where BSS and BTKE are relatively low using symmetrical boundary, which is more consistent with the measurement results. Indeed, the centre of DRB accumulates large amount of sediments (shown in Figure 1.4c).

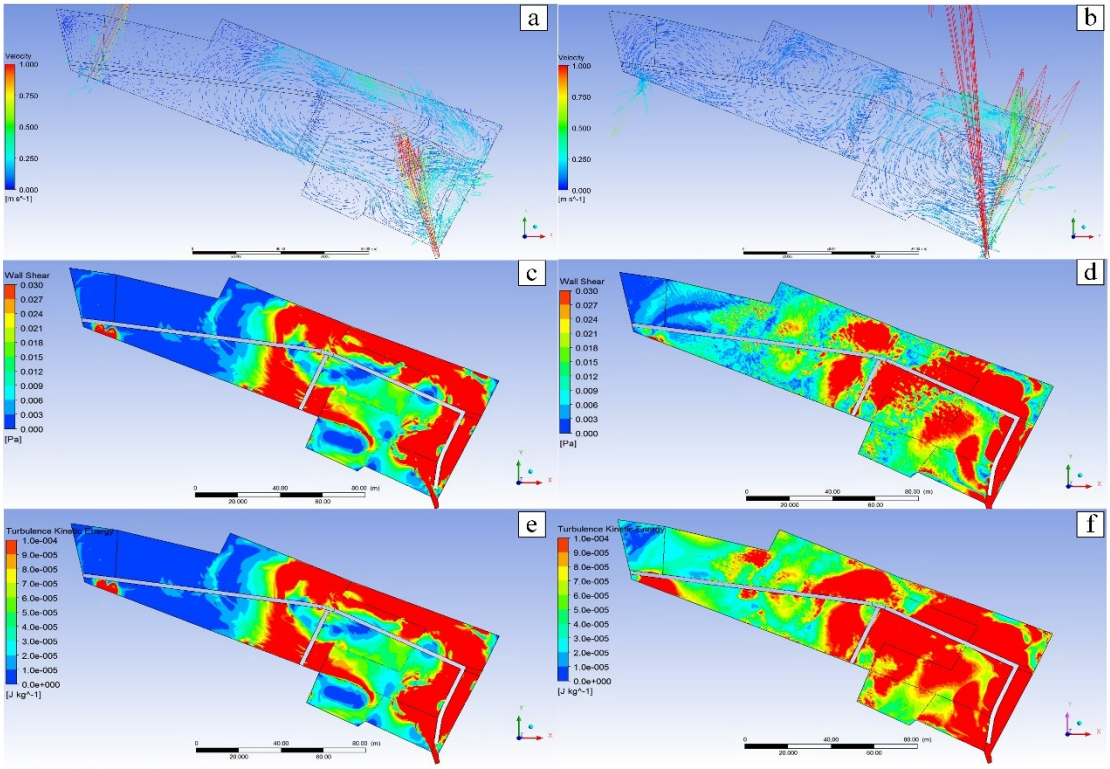

Figure 2.17. Comparison of CFD results obtained with symmetrical boundary (a/c/e) and VOF model (b/d/f) for free water simulation: (a&b) flow vector at free surface (limited at 1 m/s), (c&d) bed shear stress at the bottom, (e&f) bed turbulent kinetic energy at the bottom of DRB.

The effect of inlet number was also tested as the current CFD model simulates only flow from

the main inlet (inlet 1 in Figure 1.1d). Indeed, DRB operates mainly with inlet 1, but flow might also come from inlet 2 when the flow rate is high. Figure 2.18 illustrates the flow vector in the case of 2 inlets. The similar swirls are observed, thus the model is not improved with 2 inlets.

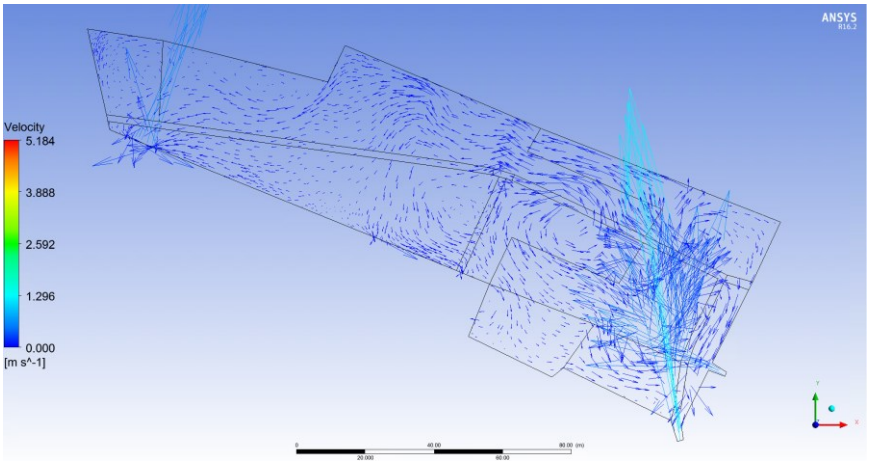

Figure 2.18. CFD modelling with 2 inlets (Q_1 = 0.35 m^3/s, Q_2 = 0.175 m^3/s)

Another hypothesis for the difference between LSPIV measurements and CFD modelling results is the wind effect. Indeed, wind effect could affect the free surface velocity field and the current CFD model doesn't take this into consideration. At the time of experiments, there was no wind measurements *in situ*. Thus, approximate wind information was collected from the weather measurement station of Meteo France nearby (at Bron, 45°43'30"N, 4°56'12"E). The measurements were carried out at 10 m height from earth surface. For example, wind direction and velocity are (270º, 3.0 m/s) and (140º, 2.5 m/s) at 12h and 13h of 07 Aug 2013, respectively (see wind direction illustration in Figure 2.19, the orientations of DRB are illustrated in Figure 2.1c). This might be the reason that flow comes from the upper-right side without swirl (measured by LSPIV at 12h47 of 07 Aug 2013, illustrated in Figure 2.15c) as water flow might be influenced by the wind from northeast. Further wind measurements *in situ* are now available and will be used to prove the hypothesis and eliminate wind effects. The wind measurements could be combined with LSPIV results to obtain the real water velocity field or be used in CFD model to simulate surface flow with wind effects.

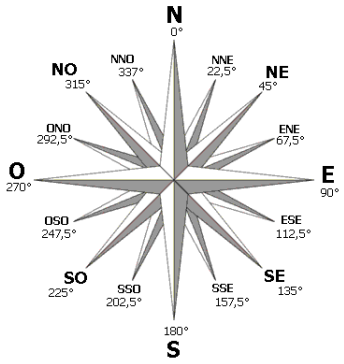

Figure 2.19. Wind direction illustration

2.4. Discussions

2.4.1. Application of LSPIV in field stormwater detention basin

Flows in stormwater detention basins are often classified as shallow flows given the large surface areas compared to their depths. For instance, DRB occupies a large bottom surface area (11 000m^2) with a depth only up to 1.5 m. Under such circumstance, a 2D surface free velocity field measurement is capable of representing the main flow pattern. In the literature, most LSPIV measurements of such shallow flow are limited to small rectangular basins in laboratory (Kantoush et al., 2011; Muste et al., 2014). However, hydrodynamic behaviours in field stormwater detention basins can be far more complicated given their complex geometrical structures designed to achieve their functions (mitigation of flood risks and pollution) (Persson, 2000). The investigation in this thesis assesses the use of LSPIV measurement in such complex field condition and provides a new LSPIV application.

In general, field stormwater detention basins are often installed and managed by practitioners and/or scientists. It is feasible to install an uninterrupted camera with Internet connection for remote control in the field. Once the camera is installed, the orthorectification procedure presented in this study can be applied in any stormwater detention basin. LSPIV analyses can then be realized after collection and selection of appropriate videos. Overall, with representative videos (e.g. under respectively low, mean and high inflow rate circumstances), LSPIV can be applied in any basin for the understanding of its hydrodynamic behaviour.

In addition to velocity measurement, LSPIV method can also be used for sediment deposition prediction. In our case, results obtained from LSPIV measurement of DRB illustrate an area with relatively low velocities, where sediment settling is more likely to happen. Meanwhile, LSPIV velocity measurements help to evaluate the hydrodynamic behaviour obtained by CFD modelling. The validated model can then be used for sediment transport simulation in the basin. Overall, the application of LSPIV velocity field measurement results for sedimentation zones prediction can be promoted to any stormwater detention basin.

2.4.2. LSPIV benefits compared to other methods

Stormwater detention basins are often forbidden to access for security reasons, which makes velocity measurements complicated or even impossible. Accessing these basins is extremely dangerous during and at the end of storm events due to the water height and strong turbulences caused by the complex geometry (e.g. presence of acceleration and stabilization zones, several outlets parallel and/or vertical to inlet, presence of obstacles and/or pits, etc.). That is why no wide experience in field measurement in stormwater detention basin has been found. CFD modelling may be an alternative solution. It proves to be a safe and convenient approach to get

the overall hydrodynamic behaviour and sedimentation distribution (see e.g. Adamsson et al., 2003; Yan et al., 2014). However, like all the models, the obtained results need to be evaluated by measurement data. Meanwhile, CFD simulation that accounts for unsteady condition and varying inflow rate through time (as often encountered in field facility during and at the end of storm events) is time-consuming and need huge computer capacities.

As far as field measurement is concerned, few have been conducted in stormwater facilities (e.g. stormwater detention basin). Two methods were applied for the velocity measurement of small-scale shallow flow: UVP and LSPIV (Choufi et al., 2014, Kantoush et al., 2011, Klepiszewski et al., 2011). UVP measures velocity profile in water using Acoustic Doppler technology, which refers only to sparse point measurements and has field condition limits, such as access to the field measurement domain. LSPIV, on the other hand, shows the advantage as low-cost, safe and convenient. Such advantages reveal the significance of LSPIV measurement in a real stormwater detention basin.

2.4.3. Improvements for LSPIV application

This study proves LSPIV's capability for free surface velocity field measurement in stormwater detention basin, while several improvements may be considered for future application. Our current work uses a single camera to investigate key flow patterns at the centre of basin. More cameras may be needed in the field to cover more areas for the study of hydrodynamic behaviour elsewhere. For instance, a camera can be installed at the inlet as it represents an acceleration zone compared to the stabilization zone at the centre of basin. Moreover, remote zones have a lower resolution and thus less accurate LSPIV results compared to the zones near the camera. Another camera at the north bank of the basin can compensate this drawback. In general, given the large size of stormwater detention basin, several cameras are necessary to cover the entire basin for a thorough flow pattern study. Researchers can decide numbers and locations of the cameras according to the specific flow pattern and the field requirements in each basin.

The identification of tracers is often discussed in the LSPIV study (Muste et al., 2008). In addition to the current natural particles (water wavelet and floating items), artificial particles (e.g. the biodegradable particles used in DSM-flux experiments) can be added to increase the readability of tracers and increase the accuracy. Finally, wind measurements and analyses in the field can be useful to eliminate wind effects on surface velocity by combining with LSPIV results to obtain the real water velocity field or simulating wind velocity in CFD model. Vertical profile can be further measured by UVP (Klepiszewski et al., 2011) and compared with CFD results to investigate the effect of bed form.

2.5. Chapter conclusions

The knowledge of hydrodynamic characteristics in a stormwater detention basin is a key element to better predict sedimentation zone and better deal with its management or retrofit if required. This chapter presents LSPIV, a safe, convenient and efficient image-based method, for the free surface velocity field measurement in a stormwater detention basin. The methodology was firstly evaluated in DSM-flux at laboratory scale against ADV measurements and results prove their consistence. The sensitivity of different image processing parameters was tested to obtain more robust results when applying LSPIV to DRB. Final results show two main flow patterns: (i) Water comes from the upper-right corner and moves towards the lower-left part. In some cases, a swirl is created at the centre, while in some other cases, flow continues to move leftward; (ii) Flow moves from lower-right corner towards upper-left part. Meanwhile, low velocities and swirls that probably lead to sediment settling are observed at the centre of the basin. Overall, the velocity fields obtained by Fudaa-LSPIV and PIVlab, two developed and mostly used LSPIV tools are similar at the centre of the basin. LSPIV data are also used to evaluate CFD models. The simulated and measured velocity field are similar at the centre of the basin (the main recirculation and low velocity values at the centre of DRB). Several differences are observed and different hypotheses have been investigated. Additional CFD tests, including the boundary condition for the free surface (VOF approach or symmetrical wall) and 2 inlets, have been performed without significant improvements. Finally, it should be pointed out that wind condition can be important and should be further investigated.

Derived findings show that LSPIV is capable of measuring the free surface velocity field in a stormwater detention basin and is a safer, more convenient, more efficient method comparing to traditional field measurement techniques. The obtained velocity field can support numerical model evaluation and particle deposits prediction. Furthermore, the investigation results of the hydrodynamic behaviour and particle deposits thanks to the LSPIV methodology could help to better manage or retrofit some stormwater facilities. Further investigations with more cameras, artificial tracers and wind measurements could help to improve the accuracy of LSPIV measurements.

Chapter 3. Modelling of sediment resuspension and remobilization

The hydrodynamic behaviour has been experimentally and numerically studied in Chapter 2 and by Yan et al. (2014), respectively. The transport mechanism of sediments from inlet has been discussed by Yan et al. (2014), but the resuspension and remobilization of already settled sediments *in situ* have been left behind. Evaluated models (in Chapter 2) are used in this chapter to analyse the particle resuspension and transfer in order to identify the priority cleansing zone where sediments are easily to be washed away and escape the basin. Related published work is shown in "Zhu, X., Lipeme Kouyi, G., Becouze-Lareure C, Barraud, S, Bertrand-Krajewski, J.-L. (2017). 3D numerical modelling of resuspension and remobilization of sediments in a stormwater detention basin. Aquaconsoil, Lyon, 26-30 june 2017".

3.1. Introduction

Stormwater detention basins remain dry during dry weather. Settled sediments in these basins may be resuspended depending on hydrodynamic conditions and transported elsewhere within the basin or towards the outlet. Mechanisms involved in particles resuspension and remobilization are still not well known in actual detention basins. CFD offers an alternative to investigate the hydrodynamic characteristics and the solid transport mechanisms in detention basins. It is less expensive and more flexible than *in situ* measurements of all key parameters related to resuspension (turbulence, velocity field, shear stresses).

During storm events, the resuspension and the remobilization of accumulated sediments on which pollutants are often attached may explain the variability of physical, chemical, biological and ecotoxicological characteristics of sediments as well as the low and sometimes negative (Sébastian, 2013) settling efficiency in detention basins, particularly after a long period without cleansing. Although previous CFD modelling (Torres, 2008; Yan et al., 2014, Zhu et al., 2019) allowed analysing hydrodynamic behaviour and sediment distribution in the DRB, the resuspension and remobilization phenomena have not been well investigated. In this chapter, the trajectories of settled sediments after their resuspension and remobilization are simulated. The objective is to quantify the rate of resuspension and the amount of sediments that escape from the DRB.

3.2. Methods and materials

3.2.1. CFD modelling

The CFD approach was applied for numerical modelling using Ansys Fluent software. The flow simulation is based on the basic equations governing fluid flow, which are mass conservation and the momentum conservation (i.e. Navier-Stokes equations) (Ferziger and Peric, 2002). The flow was simulated for steady state conditions and the turbulence was modelled by the Re-Normalization Group (RNG) k-epsilon model (Launder and Spalding, 1974, Orszag et al., 1993).

The sediment transport was simulated based on the hydrodynamic model outputs and on the Lagrange approach DPM (Discrete Phase Model). DPM applies the Newton's second Law to each particle, as shown by Equation 3.1.

$$\frac{du_p}{dt} = F_D(u - u_p) + \frac{g(\rho_p - \rho)}{\rho_p} + F \qquad \text{Equation 3.1}$$

where u_p is the velocity of the particle; u is the velocity of the fluid; g is the gravity acceleration; ρ and ρ_p are the densities of the fluid and the particle, respectively; F is all additional forces; and F_D is a drag coefficient depending on different particle's and fluid's characteristics, which was computed according to Morsi and Alexander (1972).

Several simulations with different inflow rates (0.25, 0.35 and 0.45 m^3/s) were performed simulated under steady state condition (mesh : 3 million cells). Independent mesh test was carried out with three different scale meshes (650 000, 850 000, and 1 million) (Lipeme Kouyi et al. 2010; Yan et al., 2014). In this PhD work, more meshes (3 million and 12 million) were tested and results are quite similar. The steady state condition was chosen due to limited calculation capacity given the mesh size. The inlet flow rate was set to 0.35 m^3/s (corresponds to the maximum outlet flow rate), which is considered to be a reference discharge often reached at DRB inlet/outlet for the majority of rain events. Lower and higher inflow rates around this reference value (0.25 and 0.45 m^3/s, respectively) were also simulated to take into consideration the flow variation. The free surface is approximated by a symmetry wall boundary condition and the water depth is set to be 0.55 m, which is the maximum depth when the basin is filled (see e.g. rain event of 19-20 Mai 2017 in Figure 3.1). It is also noticed that this water depth corresponds to multiple inflow rates (e.g. 0.2 - 0.8 m^3/s in Figure 3.1).

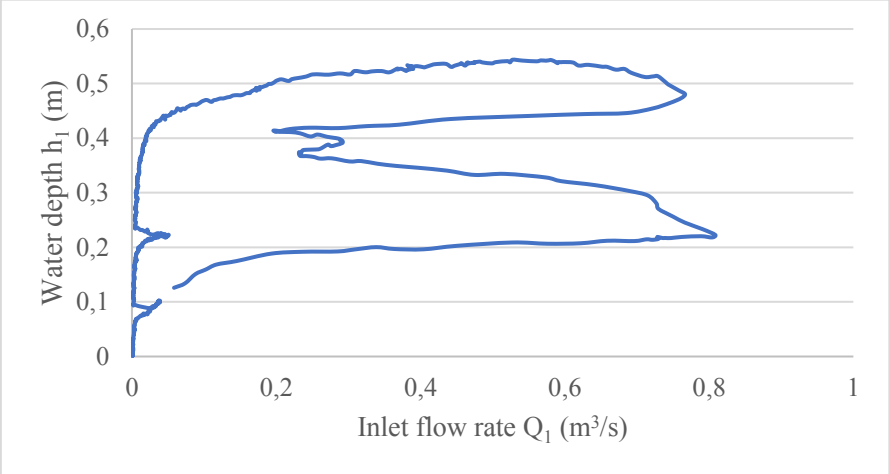

Figure 3.1. Inlet flow rate against water depth for the rain event of 19-20 May 2017

The particles were injected from 5 sampling points (P01, P02, P04, P07, P12bis, shown in Figure 1.3a), which represent the existing sediments already accumulated at the bottom of the basin. The sediment characteristics analysed during field campaign of 04 July 2014 was used as CFD inputs in this investigation, shown in Table 3.1. Three groups of particles with defined sizes (D10, D50, D90) were injected separately for each point.

Table 3.1. Sediments characteristics of different sampling points (CFD inputs)

	P01	P02	P04	P07	P12bis
D10 (µm)	18	13	11	13	193
D50 (µm)	139	89	61	71	535
D90 (µm)	804	679	305	308	1095
Density (kg/m^3)	2290	2225	2326	2311	2636

D10: sieving size with 10% of particle mass passing through.

The boundary condition based on the BTKE developed by Yan et al. (2014) was applied as the method enables to identify the preferential sediment deposition zone comparing to the observed ones. Indeed, despite the lack of representation of detailed process, such as dynamic entrainment, aggregation, consolidation, particle collision, BSS and BTKE are considered as appropriate boundary conditions to determine the sediments' deposition and resuspension (e.g. Dufresne, 2008; Stovin and Saul, 1994; Vosswinkel et al., 2012). BTKE-based results demonstrate good fits regarding sediment spatial distribution in DRB (Yan et al., 2014). The local TKE defined by Equation 3.2 is calculated by means of Ansys Fluent software.

$$k = \frac{1}{2}(\overline{(u')^2} + \overline{(v')^2} + \overline{(w')^2}) \quad \text{Equation 3.2}$$

where k is the local TKE, u', v', w' are velocity fluctuations.

The particle would resuspend when the local TKE is higher than the computed threshold, and would settle at the bottom otherwise. The BTKE threshold is described in Equation 3.3.

$$K_P = \xi v_s{}^2 \quad \text{Equation 3.3}$$

where ξ is a coefficient (here equals to 1.0) that accounts for particle properties and v_s is the settling velocity calculated through Equation 3.4 proposed by Julien (2010):

$$v_s = \frac{8\vartheta_m}{d}[(1 + 0.0139D^{*3})^{0.5} - 1] \quad \text{Equation 3.4}$$

where v_s is the particle settling velocity, ϑ_m is the kinematic viscosity of water (m^2/s), d is the particle diameter, D^* is the dimensionless particle diameter.

Table 3.2. Calculated BTKE thresholds from measured and calculated settling velocity

BTKE threshold calculated using Vs from		p01	p02	p04	p07	p12bis
10%v/v	Julien (2010)	3.62E-08	1.07E-09	1.49E-09	1.07E-09	6.83E-05
	VICAS	4.08E-09	5.06E-08	-	5.19E-08	1.30E-07
	Difference	3.21E-08	-4.96E-08	-	-5.08E-08	6.82E-05
50%v/v	Julien (2010)	1.32E-04	5.91E-06	2.01E-07	9.29E-06	4.26E-03
	VICAS	4.44E-07	4.94E-06	2.50E-07	4.00E-06	1.09E-05
	Difference	1.31E-04	9.73E-07	-4.87E-08	5.29E-06	4.25E-03
90%v/v	Julien (2010)	1.89E-03	2.65E-03	8.68E-04	8.51E-04	1.01E-02
	VICAS	1.51E-05	1.07E-04	1.88E-05	7.56E-05	1.45E-04
	Difference	1.87E-03	2.54E-03	8.49E-04	7.76E-04	9.98E-03

The calculated BTKE thresholds used in CFD model are illustrated in Table 3.2. In addition, particles' settling velocity distribution was also measured and BTKE threshold was calculated from measured settling velocity using Equation 3.3. In this case, it is assumed that finer particles settle slower, i.e. 10% of particle volume has a size inferior to d10 settles with settling velocity inferior to v10. The comparison of the BTKE thresholds calculated from these two datasets of settling velocities are illustrated in Table 3.2. Almost all BTKE thresholds used for CFD

modelling are higher than measured results, which leads to an overestimation of sediments sedimentation percentages. For further investigations, the BTKE threshold calculation method proposed by Isenmann et al., (2017) could be used to reduce this deviation.

The effect of turbulent flow field on the dispersion of particles was taken into consideration by using a stochastic method based on the discrete random walk model (DRWM) (Ansys, 2011). The DRWM includes the effect of instantaneous turbulent velocity fluctuations on the particle trajectories through the use of stochastic methods by eddies defined by a Gaussian distributed random velocity fluctuation u', v', w' in Equation 3.5, where ζ is a normal distributed random number and k is the turbulent kinetic energy.

$$u' = v' = w' = \zeta\sqrt{\frac{2k}{3}} \qquad \text{Equation 3.5}$$

In the DRWM, the fluctuating velocity components are discrete piecewise constant functions of time. Prediction of particle dispersion is based on the concept of the integral time scale T, defined in Equation 3.6.

$$T = \int_0^{\infty} \frac{u_p'(t)u_p'(t-\tau)}{\overline{u_p'^2}} d\tau \qquad \text{Equation 3.6}$$

For small particles that move with the fluid, the integral time becomes the fluid Lagrangian integral time T_L, approximated as follows:

$$T_L = C_L\frac{k}{\varepsilon} \qquad \text{Equation 3.7}$$

where C_L is the Lagrangian time scale constant to be determined as it is not well known, k is the turbulent kinetic energy and ε is the turbulent dissipation rate. C_L = 0.15, 1 and 2 were tested in this investigation.

3.2.2. Determination of the amount of resuspended and remobilized particles

During storm events, the accumulated sediments could (i) stay immobile, (ii) resuspend and then settle elsewhere, or (iii) resuspend and then escape the basin. In CFD model, three status were recorded during each simulation: settled, escaped and incomplete (i.e. particles remained in the water column when the simulation reaches its maximum numbers of calculation steps). In order to associate the recorded particle status to real estimation status, reference time (RT) defined by Equation 3.8 is recorded for each particle.

$$RT = T_E - T_I \qquad \text{Equation 3.8}$$

Where T_E corresponds to the timestamp when particle is recorded to be escaped, settled or incomplete at the end of calculation, T_I is the initial time.

Figure 3.2 illustrates the correspondence of recorded particle status by model and real estimation status. Computed ART (Average Residence Time spent by fluid particles, i.e. particles that have the same density as water) in DRB is between 4 and 5h. Therefore, the escaped particles are defined as the particles escaped from the system with RT < 5h. The particles with status incomplete and escaped with RT > 5h are assumed to be able to settle at the end of a storm event. The settled particles are divided into two cases: those which didn't resuspend since its initial status and those resuspended and finally settled. The particles with RT < 1s are considered to be static. The resuspended particles are gathered in three groups: decanted particles with RT > 1s, escaped particles with RT > 5h and incomplete. Percentage of the escaped and resuspended particles among the injected ones were used to quantify the resuspension and remobilization rate in the DRB. The locations and physical characteristics (density and diameter) were recorded when the particle settles at the bottom or escapes from the basin.

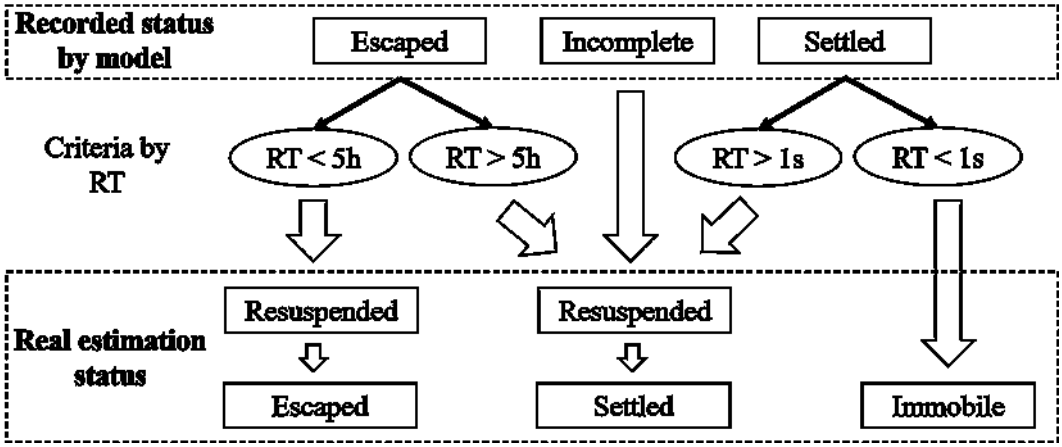

RT: Reference Time

Figure 3.2. Correspondence of recorded particle status by model and real estimation status

3.3. Results and discussions

3.3.1. Particle moving pattern with mean flow rate

Simulation with mean flow rate (Q = 0.35 m^3/s) under steady state conditions was firstly realized. The sediment transport was then simulated with DPM in an uncoupled way on the basis of flow simulation. About 40 000 inert particles were injected from each point with a velocity value of zero.

Results show that the coarse particles (D90) from all points stay immobile, as well as all the particles injected from P12bis whatever the particle size is. It is reasonable as the particles at P12bis have more important densities (see Table 3.1), which makes them more difficult to be suspended by the flow. In addition, in this area of the basin, the velocity is low and a big recirculation occurs, trapping all sediments close to the local pit (used as a local small settling tank). On the other hand, the percentages of suspended particles for the rest cases reaches 100% except for those of the median size particles (D50) from P01, which are 3.25%, 4.02%, 4.02% when C_L equals 0.15, 1 and 2, respectively. The reason for this phenomena could be that the median particle size at P01 is larger than the others (except P12bis).

Figure 3.3 reveals the percentages of escaped particle under three different conditions: (i) different injection areas, (ii) different particle size, (iii) different C_L. As expected, the fine particles (D10) are proved to escape more easily than the median particles (D50). The percentage of particles resuspended from P04 and P07 are relatively higher than those from P02 and P01, which can be accurately explained by their location on the main flow path (Yan, 2013). P04 and P07 (refers to ⑤ and ⑦ in Figure 1.4a) are located at the end of the flow pathway, and therefore the sediments are fine and escape more easily from the system. Although P02 (② in Figure 1.4a) is near orifice 2, the particles are more likely to be transported to downstream as shown in yellow in Figure 1.4a. Besides, P01 (③ in Figure 1.4a) is in the upstream section of the flow pathway and far away from the orifices, the sediments are consequently less likely to escape. As far as C_L is concerned, the fine particles have more tendency to escape when C_L equals 1. However, more median particles from P04 escape when C_L equals 2.

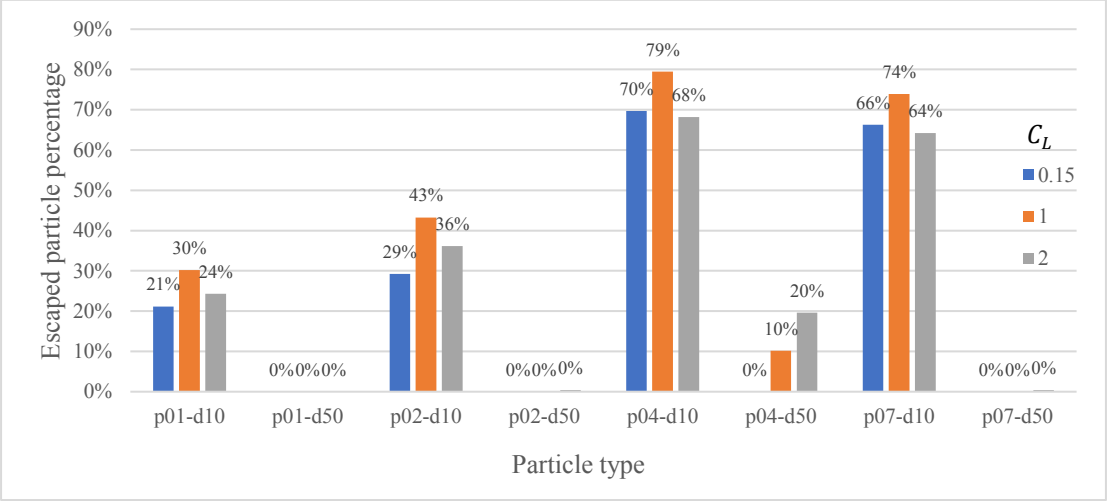

Figure 3.3. Escaped particle percentage with different (i) injection points, (ii) particle size, (iii) C_L (Q = 0.35 m^3/s)

Figure 3.5 illustrates the spatial distribution of particle depositions after resuspension and settling steps. Fine particles injected from P01, P02, P04 and P07, as well as median particles from P04, remained incomplete when the simulation terminated (RT > 5h). This means that these particles tend to stay in the resuspension state and will likely settle at the end of rain event. Thence, only median particles from P01, P02 and P07 are displayed in Figure 3.5 and results show that sediment dispersion is more obvious with a greater C_L. Overall, sediments from P01 tend to settle nearby right after resuspension (RT < 6min), while sediments from P02 and P07 are more likely to be transported to elsewhere in the basin. Sediments from P02 tend to follow the flow pathway marked with yellow arrow in Figure 1.4, compared to those following green or orange arrows. RT related to particles near ⑦ and ⑨ is therefore longer than that associated to particles settled at the centre of the basin. On the other hand, sediments from the P07 have the tendency to follow the flow pathway in orange and settle nearby, although a small part joins the pathway in yellow and settles in the centre when C_L = 1 and 2. Results with C_L = 2 show a great consistence with the observations and results obtained by Yan et al. (2014). Hence, C_L = 2 is applied for all additional simulations.

3.3.2. Particle moving pattern under different flow rates

In addition to the mean flow rate, two other flow rates (Q = 0.25 and 0.45 m^3/s) were also investigated. About 20 000 inert particles were injected from each point with a velocity value equals to zero, and particles of different size (D10, D50, D90) were injected separately. Only C_L = 2 was studied in this case.

Results demonstrate that sediments with a diameter of D90 from all locations and those with a diameter of D50 from P12bis remain immobile whatever the inflow rate is. However, sediments from P12bis with a diameter D10 resuspend when Q = 0.45 m^3/s and stay immobile when Q = 0.25 and 0.35 m^3/s. The percentages of resuspended particles from P01 with a diameter of D50 are 1.83%, 4.02%, 6.66% when Q = 0.25, 0.35 and 0.45 m^3/s, respectively. Only 11.18% of sediments from P07 with particles size of D50 remobilize and all the other particles resuspend completely.

The percentages of escaped particles according to various inflow rate conditions are presented in Figure 3.4. Generally, more particles escape when the inflow rate increases, except for P04. As far as P01 and P02 are concerned, the differences of escaped fine particle percentages among 3 different inflow rates vary from 9 to 17%. However, the differences are more significant for P07, representing 27-44%. Meanwhile, 12% of coarse particles injected from P07 escape when Q equals 0.45 m^3/s. The reason for this phenomena could be that P07 situates at the end of flow pathway near orifice 1, hence conveyed sediments are relatively fine and escape easily through orifice 1, particularly when inflow rates are high. As for P04, the percentages of escaped

particles (fine and median) decrease along with the augmentation of inflow rate, which is reasonable regarding its location near the gutter where sediments are mobilized even for low flow rate and low water level. In addition, most sediments from P04 follow the flow pathway in yellow or green (in Figure 1.4) and escape through the orifices, some of the particles may continue to follow the pathway in yellow and remain in the circulation, which happens more easily with a higher flow rate.

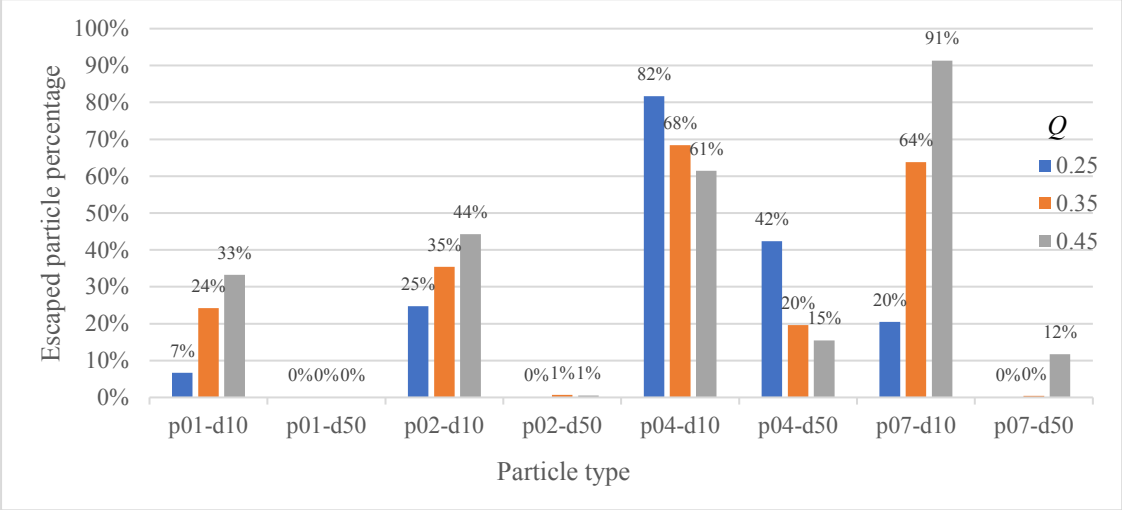

Figure 3.4. Escaped particle percentage with different inlet flow rates (C_L = 2)

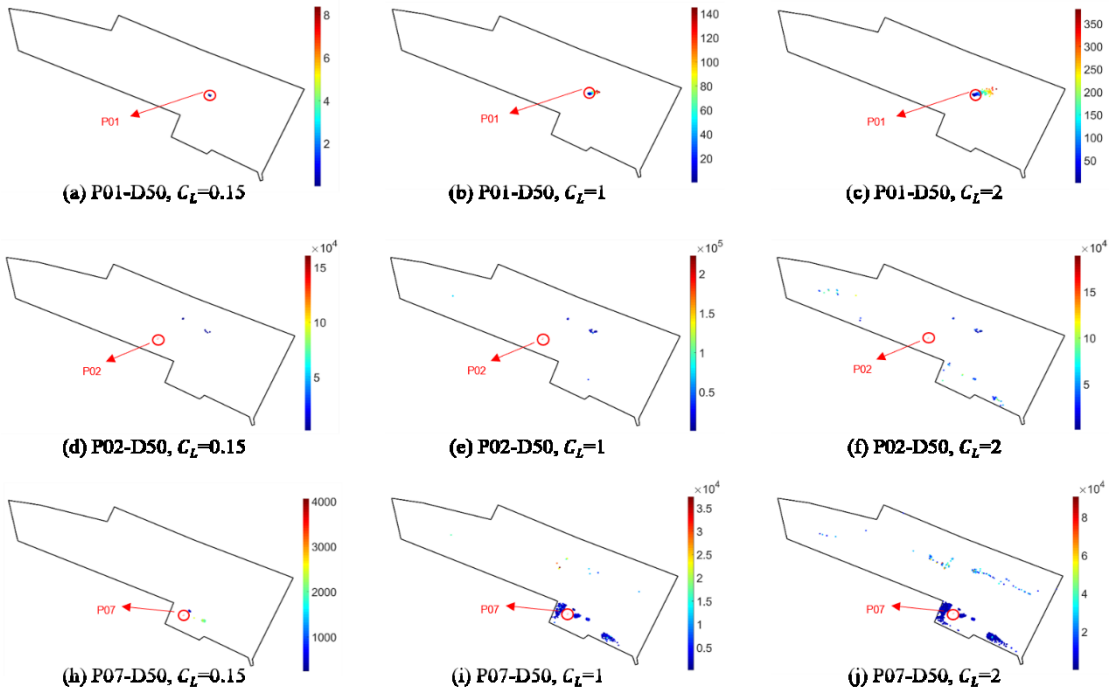

Note: The colour bar means particle residence time in the system (s).

Figure 3.5. Particle distribution with different (i) injection points, (ii) particle size, (iii) C_L (Q = 0.35 m^3/s)

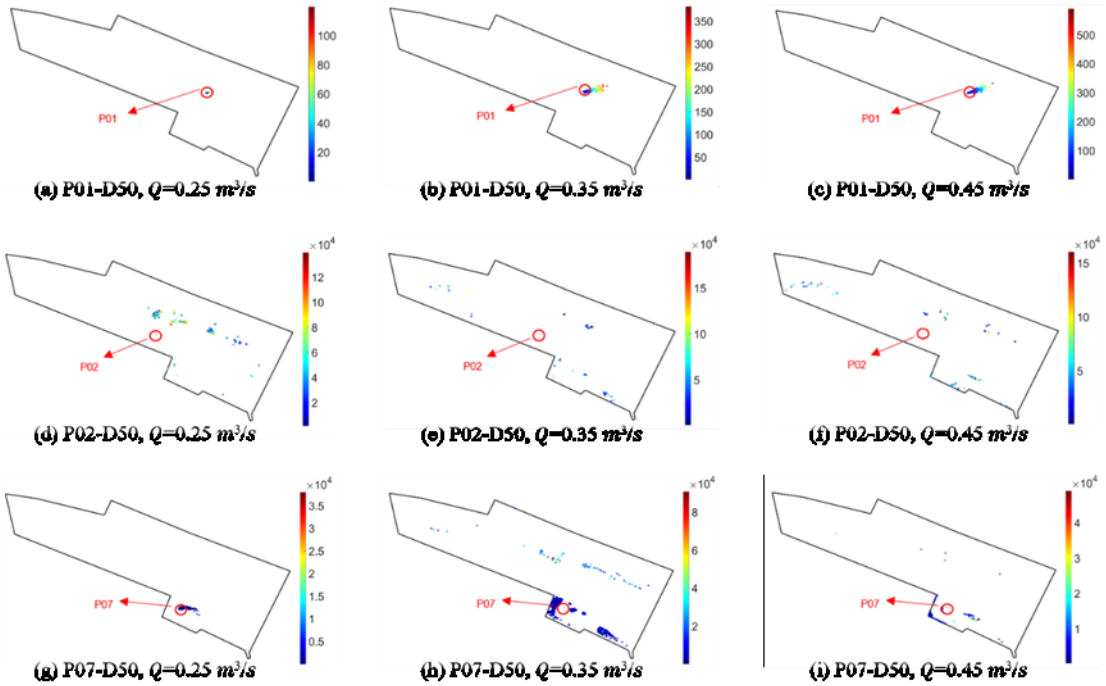

Note: The colour bar means particle residence time in the system (s).

Figure 3.6. Particle distribution with different inlet flow rates (C_L = 2)

Figure 3.6 compares the sediment deposition distribution of suspended particles under different inflow rates. In general, as expected, sediments have more tendency to be transported elsewhere or escape with a higher rate. It is observed that particles from P01 disperse more widely with a higher flow rate. In the case of P02, there are more depositions when Q = 0.25 and 0.45 m^3/s. Particles are carried farther by the inflow with higher rate, and more likely to settle nearby with a lower inflow rate. P07 shows similarities with P02, where sediments settle near P07 or farther when Q equals 0.25, 0.35 m^3/s, respectively. However, there are less depositions when Q reaches 0.45m^3/s since 12% of sediments escape through the orifice, as shown in Figure 3.4.

3.4. Chapter conclusions

In this chapter, the remobilization of already settled sediments in DRB is simulated based on an evaluated CFD hydrodynamic model (in Chapter 2). The percentages of resuspended and escaped sediments are quantified. As expected, the sediments which contain the finer particles are found to have more tendency to resuspend and to be transported towards the outlet, while the coarser particles remains immobile. P12bis is a specific point (near local pit designed for trapping coarse particles and hydrocarbon) where sediments of all sizes stay immobile given their high density. Normally, sediments are more easily to be washed away and escape the basin with a higher inflow rate except for P04 where sediments resuspend even for low flow rate and low water level given its location near the gutter and might continue to stay in the main

recirculation under strong flow conditions. Overall, sediments from P04 and P07 are more likely to escape the basin, which is consistent with the fact that these two locations situated at the end of particle transport pathway where fine sediments settle. Hence, these two locations should be the preferential zones for sediment cleansing according to the level of the contamination of sediments accumulated at these points. Further investigations on the value of C_L should be considered to strengthen the results and conclusions.

Chapter 4. Prediction of the distribution of trace metal contamination in DRB

This chapter presents methodology and results on the prediction of the distribution of trace metal contamination through (i) the investigation of the correlation between metal contents and settling velocity of sediments and (ii) the coupling of the derived correlation and solid transport model (based on the evaluated and tested model in Chapters 2 and 3). The published work related to this chapter is "Zhu, X., Chatain, V., Gautier, M., Blanc-Biscarat, D., Delolme, C., Dumont, N., ... & Lipeme Kouyi, G. (2019). Combination of Lagrangian Discrete Phase Model and sediment physico-chemical characteristics for the prediction of the distribution of trace metal contamination in a stormwater detention basin. Science of The Total Environment, 134263. https://doi.org/10.1016/j.scitotenv.2019.134263".

4.1. Introduction

Given the contamination of accumulated sediments in stormwater detention basin and its danger to superficial or underground aquatic environments toward which the stored stormwater are rejected, it is essential to understand the transport mechanism of these chemical pollutants in stormwater detention basins for the purpose of (i) a better design to promote pollutant sedimentation and improve treatment efficiency, as well as (ii) the determination of highly contaminated deposition zones that require specific treatment and intervention.

A thorough geochemical characterization of settled sediments can be used to determine the contamination distribution in stormwater detention basins. (Jang et al., 2010; Tedoldi et al., 2017). However, a large number of samples are needed, and their collection and characterization are expensive and time-consuming. Numerical models, on the other hand, are an effective and low-cost approach to predict the distribution of contamination. A chemical model was proposed by Vezzaro et al. (2010) to simulate the removal of micropollutants in such basins based on relevant removal processes, such as settling, volatilization, sorption, biodegradation and abiotic degradation. This model, however, fails under complex hydrodynamic conditions in basins (Sebastian et al., 2014c) as the interactions between hydrodynamics and physico-chemical characteristics are ignored. The combination of Discrete Phase Model (DPM) and the correlation between physical and chemical characteristics can be an appropriate alternative. Indeed, the simulation of particle transport provides a quick, convenient and low-cost way to characterise particle movement and predict preferential deposition zones of the particles and their associated pollutants. Such an approach permits alternative basin geometries to be compared, facilitating the design process. For example, a

DPM implemented in computational fluid dynamics (CFD) package allows particle transport mechanisms in stormwater detention basins to be simulated, with particle physical characteristics used as model inputs (Adamsson et al., 2003; Yan et al., 2014). Finally, the transport mechanisms of pollutants can be simulated by implementing the correlation between particle physical and chemical characteristics using outputs of DPM simulations or other solid transport model results.

Trace metals are considered as priority stormwater chemical pollutants related to urban activities. The decision No. 2455/2001/EC issued by the European Parliament and Council listed 33 priority substances, including Ni, Pb and their compounds. Zgheib et al. (2008) extended the list to 88 individual substances, including Cr and Cu. Iron, as a major earth element, plays a key role in the geochemistry of soils and sediments and is of great importance to many metals cycling processes (Taylor and Kauhauser, 2011). Iron oxides are also important for the sorption of trace metals (Bradl, 2004; Whitaker and Duckworth, 2018). As far as physical characteristics are concerned, settling velocity is an integrated property of particulate pollutants, as it is related to multiple characteristics such as diameter, density, shape and surface roughness (Loch, 2001). Several investigations are reported in the literature regarding both trace metal contents (Becouze-Lareure et al., 2019; Sébastian et al., 2014a) and particles' settling velocities in stormwater detention basins (Torres et al., 2007; Yan et al., 2014). However, to the best of our knowledge, little is known concerning the relationship between metal contents, particularly Fe, and settling velocity in urban stormwater detention components. Bentzen and Larsen (2009) investigated such relationship in a wet detention pond of road runoff, where high Cd, Cr, Zn and Ni contents were found associated with low settling velocities while the tendency for Cu and Pb was unclear. However, the conclusions were empirically drawn without quantitative analyses. Torres et al. (2007) found a significant correlation among median settling velocity (V50) and contents of Cd, Cu, Pb and Zn in a stormwater detention basin, but metal contents with respect to different fractions of settling velocities were not considered. Overall, a thorough analysis of the correlation between metal contents and settling velocity and the importance of Fe have not been considered in previous work.

The objective of this chapter is to predict the spatial distribution of trace metal contamination through (i) the investigation of the correlation between metal contents (major element: Fe and some trace metals: Cr, Cu, Ni and Pb) in trapped sediments and their settling velocity in a stormwater detention basin, and (ii) the implementation of such correlations in a solid transport model, taking into considerations the interactions between hydrodynamics and particle physico-chemical characteristics.

4.2. Methods and materials

4.2.1. Presentation of campaigns

Five campaigns were conducted during rain events in 2017 (from spring to winter). Nineteen sediment samples from 6 sampling points were collected and characterized (indicated in Figure 4.1). The main characteristics of the sampled rain events and their corresponding hydraulic parameters in the detention basin are presented in Table 4.1.

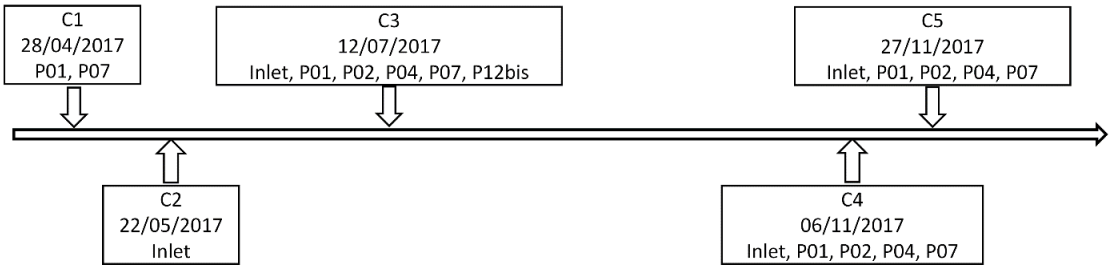

Figure 4.1. Campaign timeline and sampling points for each campaign

Table 4.1. Characteristics of the sampled rain events and corresponding hydraulic parameters in DRB

Campaign date of year 2017	C1 28/04	C2 22/05	C3 12/07	C4 06/11	C5 27/11
Rainfall characteristics					
Rain Duration (hour:min)	19:22	08:14	03:02	18:26	16:28
Total Depth (mm)	26.5	17.5	10.5	30.9	11.2
Mean Intensity ($mm \cdot h^{-1}$)	1.4	2.1	3.4	1.7	0.7
Max intensity ($mm \cdot h^{-1}$)	6	7.5	58.2	11.7	6.9
ADWP (days)	23	4	8	12	11
DRB hydraulic parameters					
Mean inflow rate (m^3/s)	0.21	0.31	0.24	0.31	0.11
Max inflow rate (m^3/s)	0.76	0.81	1.27	1.08	0.77
Max water level (m)	0.51	0.54	0.39	0.69	0.50

ADWP: antecedent dry weather period

4.2.2. Physical and chemical characterizations and determination of their correlation

In this study, particle-size distribution, settling velocity distribution and metal contents in sediments were analysed, according to the standards and protocols listed in Table 4.2.

Table 4.2. Standard and protocols for physical and chemical analyses

Analysis	Method	Standard
Particle-size distribution	Mastersizer 2000 laser diffraction granulometer	NF ISO 13320-1 (2000)
Settling velocity distribution	VICAS protocol (Chebbo et al, 2009)	
Metal content	ICP-OES	NF EN ISO 11885 (1998)

The VICAS protocol (a French acronym for Effluent Settling Velocity, Chebbo et al., 2009) is applied to measure settling velocity distribution. It is based on the principle of homogeneous suspension, where the solids are uniformly distributed over the entire sedimentation height. The measurement is realised with a plexiglas sedimentation column in the laboratory. The settled solids at a set of 10 predefined time points (t = 1, 2, 4, 8, 16, 32min, 1, 2, 4, > 24h) are manually collected at the bottom of the sedimentation column in aluminium receptacles. The evolution of accumulated mass of settled particles over time is then determined by measuring the mass in each receptacle, which yields the settling velocity distribution curve. Meanwhile, the average settling velocity in each receptacle defined in Equation 4.1 is used to investigate the correlation between metal contents and settling velocity:

$$Vs = \frac{H}{t} \qquad \text{Equation 4.1}$$

where Vs denotes particle settling velocity (mm/s), H is water height in the sedimentation column (mm) and t is the time point (s) when the receptacle with collected particles is removed.

Metal contents in particles are then analysed with ICP-OES (inductively coupled plasma optical emission spectrometry) method. The total suspended solids (TSS) are filtered through glass fibre filters (0.45 µm) and dried at 105 °C (French standard NF EN 872, 2005). Mineralization is then applied in order to extract soluble elements from particles with aqua regia (NF EN 16174, 2012). The obtained solution is finally diluted to 50 ml, filtered at 0.45 µm and analysed with ICP-OES equipment. For each element, the limit of detection (LOD) is calculated from the calibration. The limit of quantification (LOQ) is considered to be 3.3 times of LOD. In our study, as a precaution, only the values larger than 3 times of LOQ were considered as quantifiable.

Figure 4.2 shows the methodology of physical and chemical characterizations. Two groups of data (physical and chemical characteristics) were gathered from the collected samples, in order to, respectively, (i) obtain overall physical and chemical characterization of samples and associated global relationships and (ii) reveal in particular the correlation between metal contents and settling velocity, as well as its significance. The first group (Data of group I) consists of particle-size distribution, settling velocity distribution and metal contents (Fe, Cr, Cu, Ni and Pb) of 19 sub-samples (deriving from the 19 original samples). The second group (Data of group II) consists of settling velocities and metal contents (Fe, Cr, Cu, Ni and Pb) of 190 sub-samples under the VICAS protocol. For each of the 19 samples, 10 sub-samples, i.e. receptacles of particles removed from the bottom of experimental column at all the 10 predefined time points t, have different settling velocities (described by Equation 4.1). For each receptacle, metal contents in collected sediments are measured.

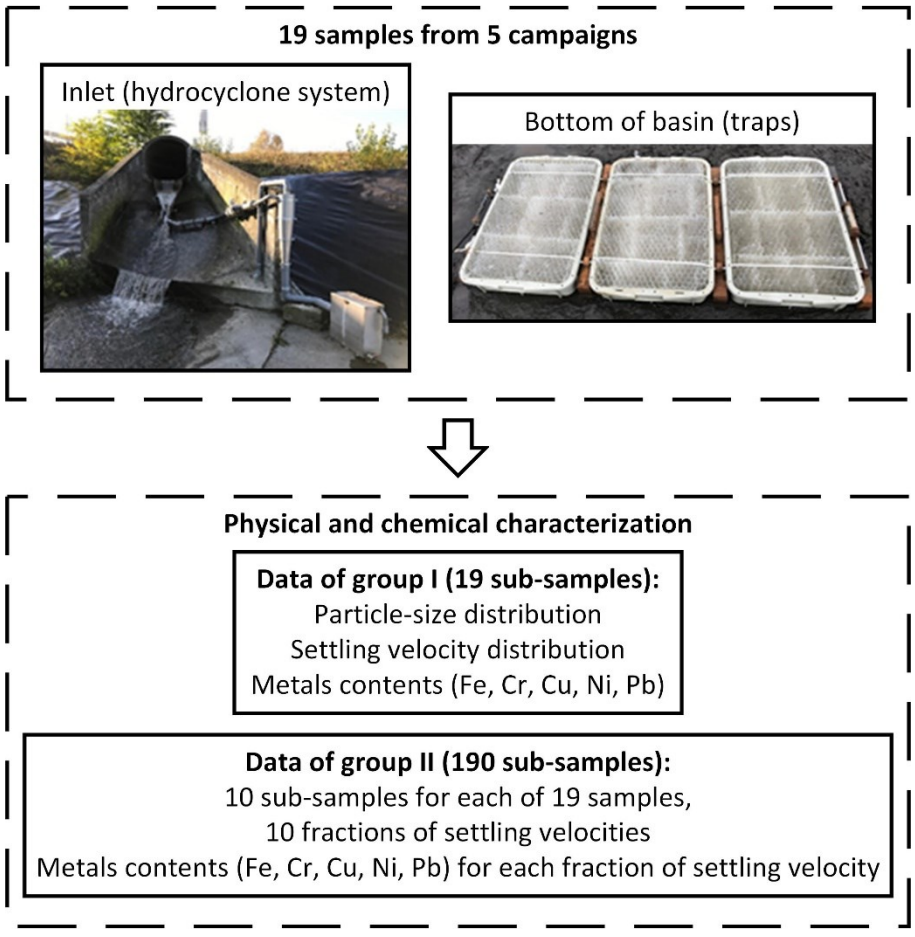

Figure 4.2. Methodology of physical and chemical characterization

Several statistics have been computed, including: (i) principal components of physical and chemical characteristics of group I via PCA (Principal Component Analysis), (ii) correlation

between metal contents and settling velocity based on the data of group II and test of significance, and (iii) correlation matrix for all metals accounting for data of group II. In this study, Spearman's rank correlation coefficient is applied as the settling velocities are not normally distributed according to the Shapiro-Wilk test (Shapiro and Wilk, 1965) and a monotonic relationship is observed between metal contents and settling velocity. Significance tests of correlation coefficient are also carried out by comparing p-value to a significance threshold (denoted as α, equal to 0.05 by default). Bonferroni correction (Dunnett, 1955) is applied to reduce false positive (Type I) errors when multi-comparisons are applied. In order to set FWER (Family-wise error rate) lower than α, it rejects the null hypothesis with p-value as follows:

$$p - value \leq \frac{\alpha}{m} \qquad \text{Equation 4.2}$$

where m is the total number of null hypotheses.

4.3. Results

4.3.1. Physical and chemical characteristics from data of group I

Physical and chemical characteristics are illustrated in Table 4.3. More details can be found in Table A1-A3 in Appendix B. In general, settling velocity varies with campaign and site, consistent with previous work (e.g. Torres et al., 2007). The samples collected from the inlet show the most significant temporal variability, with median settling velocity ranging from 1.9 to 11.6 m/h. Trapped particles from P01 have higher settling velocities than those from the other sampling sites at the bottom of DRB. Indeed, the location P01 is near the inlet where heavy particles settle rapidly, as demonstrated e.g. by Jacopin et al. (1999).

As illustrated in Table 4.3, Fe contents are at least 36 times higher than Cu contents and up to 200 times higher than the other trace metal contents (Cr, Ni and Pb). As for trace metals, Cu, Ni and Pb contents exceed the target values of Dutch standards (DTIV, 2000). Cu contents, as well as Pb contents in some cases, surpass even the intervention threshold. It is noticed that Fe contents at the inlet are lower (average 16.9 g/kg DM) than those observed in the basin (average 20.7-23.9 g/kg DM), in opposition to trace metals. Besides, samples collected from the inlet show a significant temporal variability, with a coefficient of variation of approximately 50%.

Figure 4.3 shows PCA results of all physical and chemical variables (particle size, settling velocity and metal contents). Principal component 1 (PC1) explains 48.9% of variance, while PC2 explains 22.9%. Overall, settling velocities are highly related among themselves (V20, V50 and V80). The same conclusion can be drawn for particle sizes (D10, D50 and D90). The

relationship among different metals, as well as that between metal contents and settling velocities or sizes, is unclear. Temporal variability is observed as expected. Event C3 is a storm of high rain intensity and maximum inlet flow rate but low total depth and rain duration. Event C4 is a rain event of the highest total depth and maximum water level in DRB. This may lead to strong variation of spatial distribution of sediments due to shear stress (Adamsson et al., 2003) or turbulence in DRB (Sechet and Le Guennec, 1999). Significant temporal variability is particularly observed for particles intercepted by the hydrocyclone device at the inlet of the basin. Among particles trapped at the bottom of DRB, those at P02 seem to be different from particles observed at other sites, characterized by their low settling velocities and high metal contents, regardless of the campaign. In fact, particles with high settling velocities tend to settle near the inlet (P01), while P02 is in the main recirculation zone with long residence time which enables particles to settle progressively (Zhu and Lipeme Kouyi, 2019).

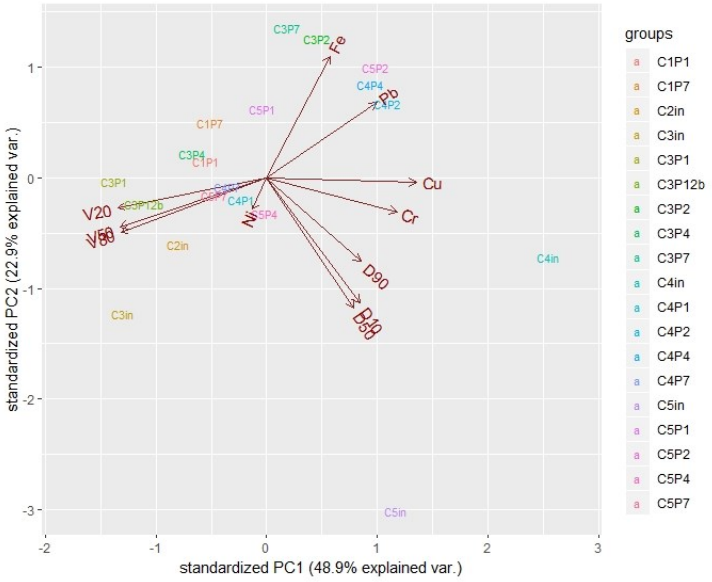

Figure 4.3. Principal component analysis (PCA) of physical and chemical characteristics based on the data of group I

Table 4.3. Physical and chemical characteristics of trapped sediments

Sample		D50 (μm)	V50 (m/h)	Fe contents (g/kg)	Trace metal contents (mg/kg)			
					Cr	Cu	Ni	Pb
C1	P01	69.2	7.0	nm	74.3	360.1	56.7	98.8
	P07	54.5	6.6	nm	78.3	325.7	54.1	114.3
C2	inlet	55.6	6.7	13.5	96.5	222.0	237.7	99.8
C3	inlet	313.5	11.6	18.2	71.5	242.3	85.2	114.1
	P01	52.9	9.6	20.4	73.5	233.5	74.6	105.7
	P02	37.7	3.4	nm	nm	nm	nm	nm
	P04	45.3	6.9	nm	nm	nm	nm	nm
	P07	45.5	4.1	27.5	93.1	278.8	93.9	137.1
	P12bis	78.3	7.5	15.4	62.7	226.8	70.5	95.8
	mean	95.5	7.2	20.4	75.2	245.4	81.1	113.2
	stdv	107.7	3.2	5.2	12.8	23.1	10.6	17.6
C4	inlet	Nm	1.9	21.0	154.3	584.4	93.8	200.6
	P01	144.6	5.9	18.7	76.3	308.7	58.1	96.7
	P02	199.3	2.9	25.6	96.4	457.4	68.7	136.6
	P04	129.4	2.6	24.4	80.5	428.2	61.9	140.7
	P07	79.8	6.7	17.9	89.6	355.3	63.1	111.5
	mean	138.3	4.0	21.5	99.4	426.8	69.1	137.2
	stdv	49.2	2.2	3.4	31.7	105.9	14.3	39.8
C5	inlet	870.5	4.3	14.9	110.4	429.0	80.4	69.7
	P01	78.5	6.0	24.7	94.9	349.2	65.7	115.7
	P02	100.2	2.1	22.2	89.1	378.3	72.7	167.2
	P04	433.3	5.4	21.1	65.8	258.1	59.2	112.3
	P07	109.8	5.7	16.6	66.3	275.0	42.7	88.9
	mean	318.5	4.7	19.9	85.3	337.9	64.1	110.8
	stdv	341.6	1.6	4.0	19.2	71.4	14.4	36.6
inlet	mean	413.2	6.1	16.9	108.2	369.4	124.3	121.1
	stdv	416.5	4.2	3.4	34.7	170.9	75.8	56.2
P01	mean	86.3	7.1	21.3	79.7	312.9	63.8	104.2
	stdv	40.3	1.7	3.1	10.1	57.3	8.2	8.6
P02	mean	112.4	2.8	23.9	92.8	417.8	70.7	151.9
	stdv	81.5	0.6	2.4	5.1	55.9	2.9	21.6
P04	mean	202.7	5.0	22.7	73.2	343.2	60.5	126.5
	stdv	204.1	2.2	2.4	10.4	120.3	1.9	20.1
P07	mean	72.4	5.8	20.7	81.8	308.7	63.5	113.0
	stdv	28.9	1.2	6.0	12.1	38.7	22.0	19.7

D50: median particle size, V50: median settling velocity, nm: not measured, stdv: standard deviation

4.3.2. Correlation between metal contents and settling velocity based on data of group II

All the results from different campaigns (C1-C5) and sampling points (inlet, P01, P02, P04, P07 and P12bis) are presented in Figure 4.4 (a-e) to analyse the correlation between metal contents and settling velocity. Figure 4.4 (f-j) are boxplots of different metals contents with respect to settling velocity. In general, results show that contents of the metals in settled sediments are relatively stable, with values varying within ranges of 15-35 g/kg, 20-120, 200-650, 20-150 and 50-250 mg/kg DM for Fe, Cr, Cu, Ni and Pb, respectively, except for a few outliers. [Fe] and [Pb] have significant correlations with log(Vs) after Bonferroni correction, especially in the case of [Fe], with a correlation coefficient equal to -0.52. Higher [Fe] and [Pb] are related to lower settling velocity. The best fit of their correlations are illustrated in Figure 4.4a and e and can be defined by the equation shown at the upper-right side. [Cu] tends to decrease slightly with the increasing of Vs, in opposite to [Cr]. Indeed, previous works suggest that Fe contents are relatively stable, while Cu can be variable in stormwater environment given its affinity with organic matter (Camponelli et al., 2010). No obvious correlation is observed between [Ni] and Vs. The dispersion around the regression line (marked as red dashed lines for 95% confidence interval) is related to spatio-temporal variabilities of metal contents and settling velocity distributions, physico-chemical processes and characteristics, as well as uncertainties on sampling and analytical measurements (Torres and Bertrand-Krajewski., 2008; Sébastian et al., 2015). The physico-chemical analyses conducted by Becouze-Lareure et al. (2018) show a high organic matter content for the trapped sediments in DRB. This may lead to changes in the physico-chemical conditions in the sediments, which could affect the solubility and availability of certain trace metals. These different processes and assumptions have already been observed in various investigations focusing on urban sediments, such as those from rivers (Chapman et al., 1998) and from reservoirs (Frémion et al., 2016; Frémion et al., 2017). Torres et al. (2007) also showed the spatial and temporal variability of settling velocity of DRB sediments.

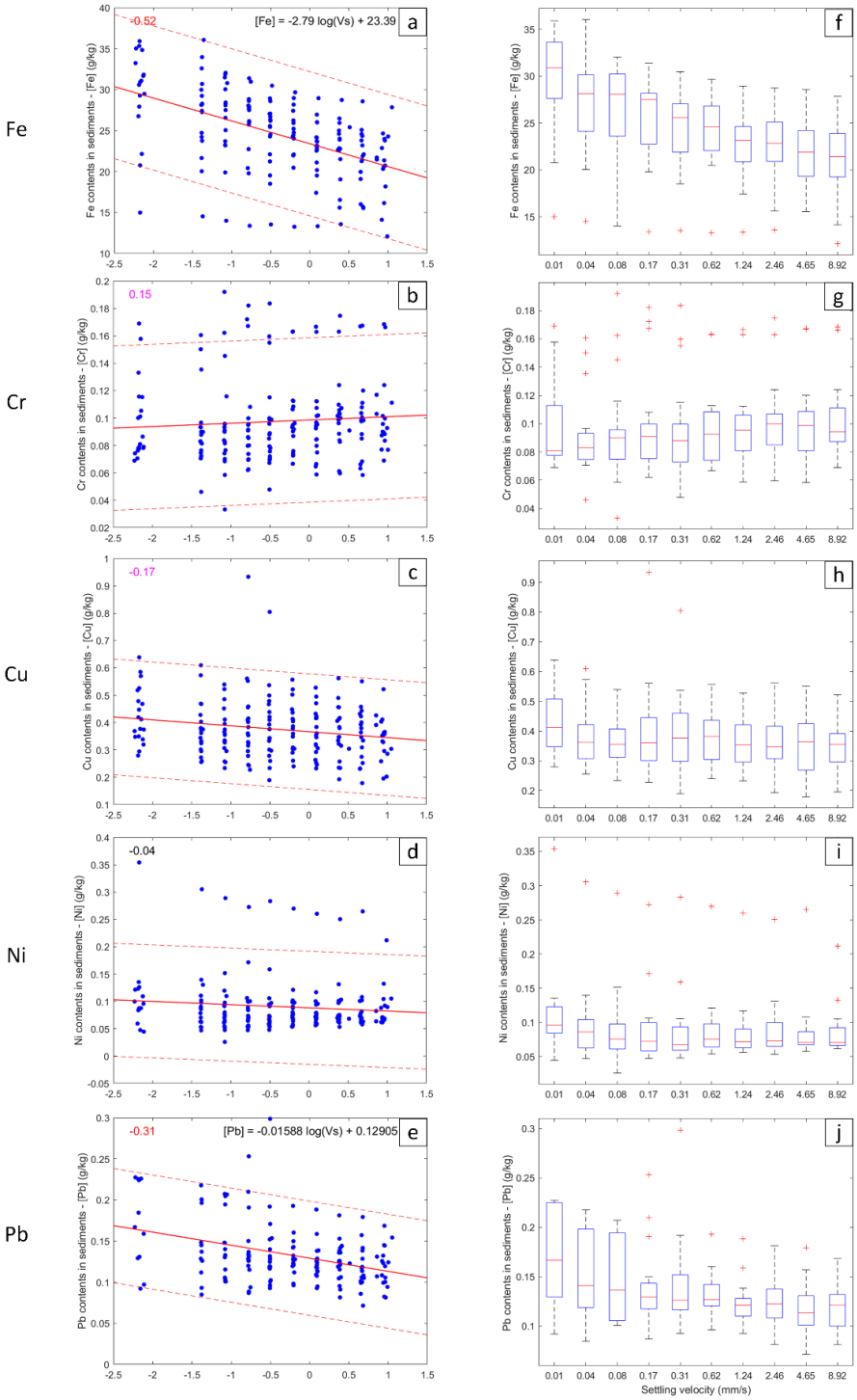

Parameters in (a-e)	Explications
Correlation coefficient	Left-upper side in red (p -value < 0.05/190 according to Eq. 2 with Bonferroni correction) when the correlation is significant; in magenta when p-value < 0.05.
Correlation equation	Right-upper side when the correlation coefficient is significant.
Correlation best fit	Least-squares error minimization, illustrated by red solid lines ———
95% confidence interval	Illustrated by red dashed lines – – –

Figure 4.4. (a-e) Correlation between metal contents [M] in g/kg DM and settling velocity (Vs) in mm/s based on data of group II; (f-j) Boxplot of different [M] with respect to each Vs.

4.3.3. Correlation matrix for different metals based on data of group II

The correlation matrix among different metals contents is also calculated (shown in Figure 4.5). Results show that almost all the studied metals have significant correlations with each other except for Cr versus Fe and Ni versus Pb. Fe and Pb are the most related metals, with a correlation coefficient of 0.61.

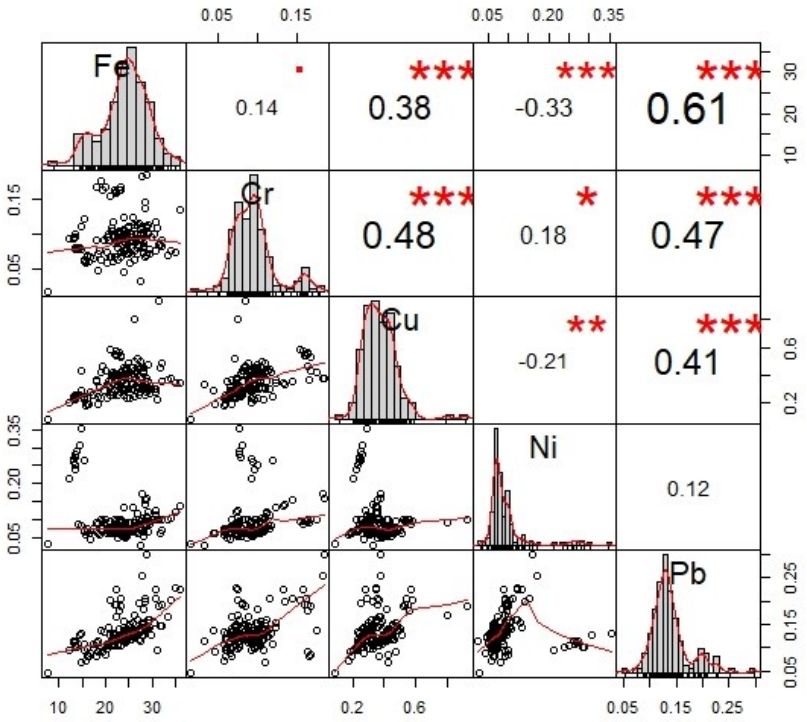

Figure 4.5. Correlation matrix of different trace metals contents in trapped particles: the distribution of each variable is listed on the diagonal. The bivariate scatter plots with their linear fits are displayed below the diagonal. The upper triangle contains the correlation coefficients and their significance levels. Each significance level is associated to a symbol: p-values of 0.001, 0.01, 0.05, 0.1 correspond to symbols of ***, **, * and ▪, respectively.

4.3.4. Stability and variability of the correlation

The stability and variability of the correlation has also been investigated. Figure 4.6 (a-e) illustrates the temporal and spatial variabilities of metal contents with respect to settling velocities. Results show that [Fe] from inlet is lower than those in basin, while trace metals concentrations are more significant at the inlet, which are related to the original samples. Figure 4.6 (f-j) illustrates averaged metal contents and their coefficients of variation (COV). Results show that [Fe] is quite stable in both space and time, with COV less than 30% except for a few outliers (30% is used to determine the significance of variability according to Couto et al., 2013).

[Cr] and [Cu] are relatively stable in space and in time, respectively. On the other hand, [Ni] shows an obvious spatial and temporal variability, while [Cr] is campaign-dependent (half of the COV are superior to 30%). Indeed, previous works show that Fe contents are relatively stable and Cu can be variable in stormwater environment given its affinity with organic matter (Camponelli et al., 2010). In addition, the variations of metal contents with respect to different settling velocities have been analysed for each campaign and each location (presented in Figure A1-A5 in Appendix C). The majority of the metals illustrate decreasing concentrations along with the augmentation of settling velocity. Fe content has the strongest relationship with settling velocity, with significant negative correlation coefficient (absolute value > 0.68), followed by Pb and Cu. As for Cr and Ni, their relationship with settling velocity is unclear. Overall, the correlation between Fe content and settling velocity is the most significant and stable, followed by Pb and Cu.

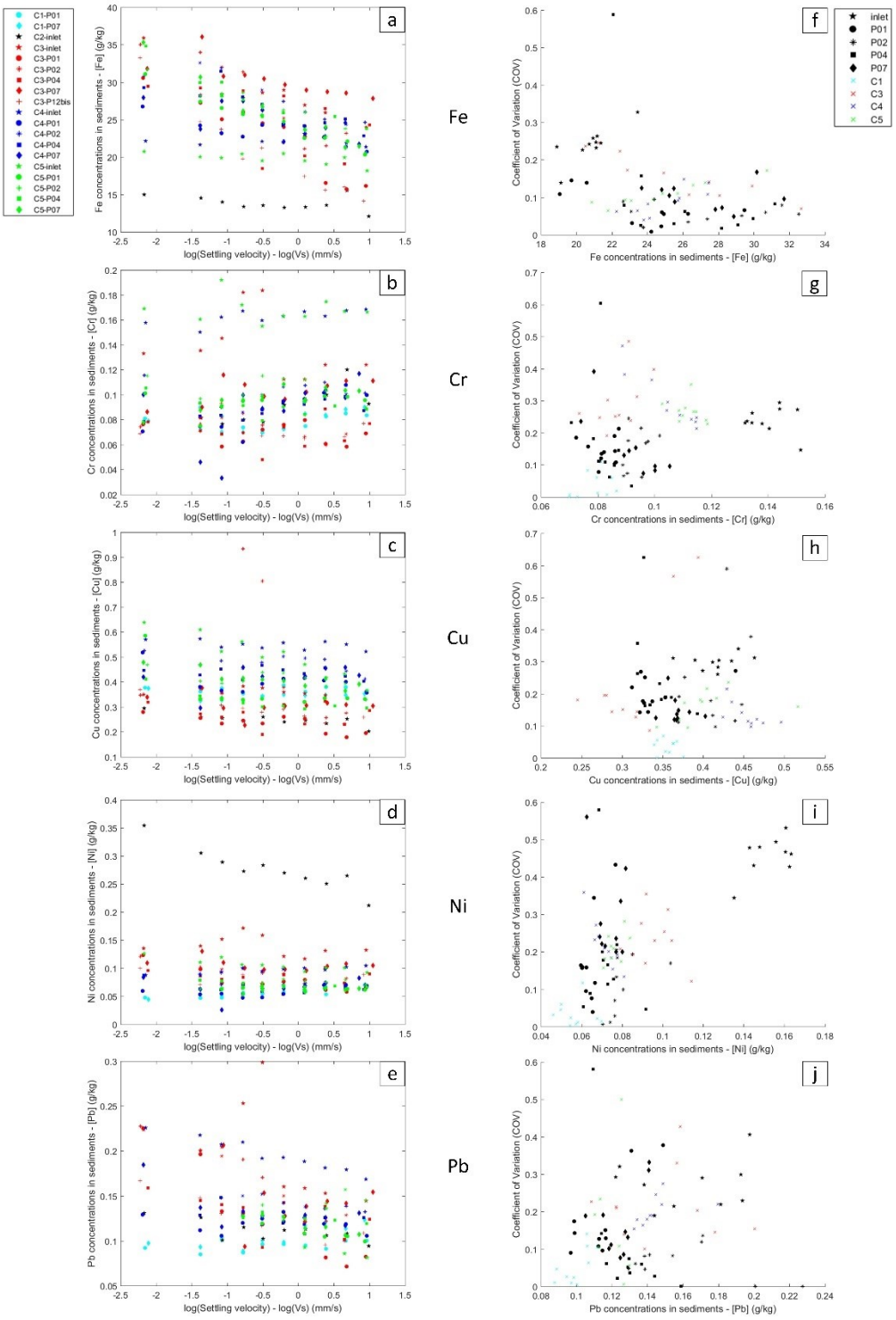

Figure 4.6. (a-e) Distribution of concentrations of metals [M] and settling velocities (Vs): values from different campaigns are depicted by a set of colours, different markers are employed to discriminate locations, (f-j) Averaged metals concentrations (x-axis) and their coefficients of variation (y-axis): For particles of the same Vs, [M] are averaged among all locations per campaign (marked as crosses and distinguished by colours), and among all campaigns per location (coloured in black and distinguished by markers).

4.3.5. Prediction of the distribution of trace metal contamination

Given the significant correlations of Fe and Pb contents with settling velocity, the derived correlations (equation in Figure 4.4) were applied on DPM outputs to simulate the spatial distribution of Fe and Pb contents in DRB. Figure 4.7 illustrates the comparison of the measured and simulated distribution of Fe and Pb contents at the base of DRB. The simulated [Fe] at P01, P02, P04 and P07 are consistent with the measurements obtained from group I, where P07 and P02 have the highest [Fe] in sediments. P07 shows a significant variation in [Fe]. Indeed, P07 is situated at the end of pathway, where sediments tend to be resuspend, as previous work has suggested (Zhu et al., 2017). In addition, P07 is near an orifice, which may lead to maximum flow shear and velocities around this site and through the orifice, increasing variability due to dispersion of sediments (e.g. interaction between burst and bedload transport, see e.g. Sechet and Le Guennec, 1999). Simulated [Pb] in DRB is around 129 mg/kg DM, which is not consistent with the measurements due to temporal variability. However, the results are consistent when comparing the simulated Fe contents distribution with the measured Pb contents at different sampling points. Indeed, significant positive correlation between Fe and Pb is revealed in Figure 4.5. Hence, it is interesting to use Fe as an indicator to predict other metals contents distribution. Uncertainties with 95% confidence interval of ± 8.8 g/kg and ± 69.4 mg/kg for Fe and Pb, respectively, are observed. In DRB, P02 and P07 are highly contaminated by Pb according to the analyses obtained, not only throughout this study, but also in many investigations carried over the last 10 years. For example, Becouze-Laureure et al. (2016) show that the areas farther from the inlet are more contaminated and that P02 presents highly contaminated sediments. The sediments at P02 and P07 settle slowly, with a mean settling velocity of around 2 mm/s, explained by the two locations being remote from the inlet.

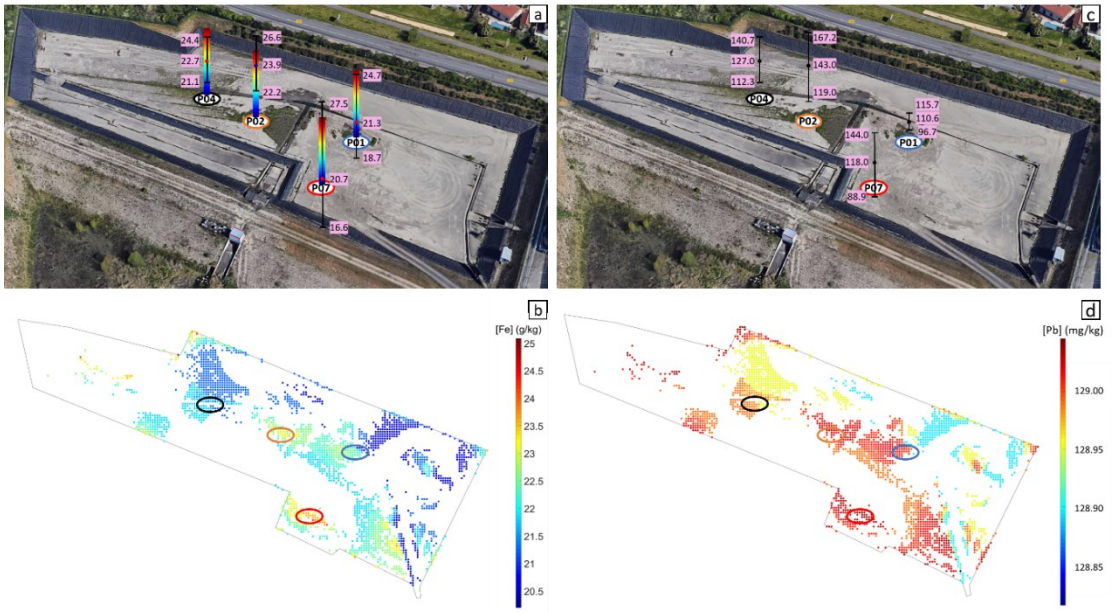

	[Fe] (g/kg DM)	[Pb] (mg/kg DM)
Measured [M] at P01, P02, P04 and P07: minimum, averaged and maximum values are plotted, respectively.	a (data of C3-C5 in group I)	c (data of C3-C5 in group I and previous campaign data by Becouze-Laureure et al. (2018))
Simulated median [M] spatial distribution at the bottom of DRB	b: uncertainty of ± 8.8 g/kg (95% confidence interval)	d: uncertainty of ± 69.4 mg/kg (95% confidence interval)

Figure 4.7. Comparison of measured and simulated Fe and Pb contents distribution: P01, P02, P04, P07 locations are coloured in blue, orange, black and red, respectively.

4.4. Discussions

4.4.1. Use of Fe as indicator of pollution and for the prediction of contamination distribution

In this study, [Fe] in trapped sediments is strongly related to settling velocity and this relationship is relatively stable from one site to another and from one event to another. In addition, significant correlations between Fe and trace metals are observed (Figure 4.5). Other studies have also observed positive correlations between Fe and Cr, Cu, Pb, Ni and Zn in highway stormwater runoff (Kayhanian et al., 2007). Drapeau et al. (2017) revealed a close link among Al, Fe and Si, as well as linear regression between Fe and Cu, Zn, P, S, Si and organic matter in a stormwater infiltration basin. Given the significant correlation between Fe and certain pollutants (here Pb and Cu), the simulated Fe content distribution can then be utilised to understand or to explain the distribution of other particulate pollutants that have affinities with Fe. Besides, iron isotopes have been widely used as tracers to analyse biochemical processes (e.g. metal transport, microbial redox reactions and transformation of organic matter-ferrihydrite coprecipitates), and track sources and other components such as suspended Fe-organic carbon aggregates (Gould et al., 2008; Ingri et al., 2018; Owens et al., 2012; Tishchenko et al., 2015). In DRB, P07 and P02 present the highest maximum values of [Fe] and are also

highly contaminated areas given the significant positive correlation between Fe and certain trace metals. Hence, P07 and P02 should be the preferential zones for cleaning.

4.4.2. Use of settling velocity for stormwater detention basin sediments management

Most studies on the correlation between particle physical and chemical characteristics in stormwater detention basins focus on the relationship between particle size (e.g. Kayhanian, 2012; Tuccillo, 2006) or sediment density (El-Mufleh et al., 2014) and trace metal contents. However, settling velocity should be emphasized given its relationship with other physical characteristics (Loch, 2001). It has been widely applied in urban stormwater management and its importance has been demonstrated (Ciccarello et al., 2012; Yun et al., 2010). Settling velocity is also a key element, when combined with the residence time, for the sizing of stormwater detention basins.

The design and management of stormwater detention basins not only need knowledge of hydrodynamic behaviour, but also an understanding of the spatial distribution of highly contaminated sediments. Various modelling approaches (e.g. CFD) can be used to address the understanding of the velocity field and the spatial distribution of sediment in stormwater detention basins (Adamsson et al., 2003). Given that the particulate fraction of certain metals and PAHs in stormwater from industrial catchments is above 60 % and 80 %, respectively (Becouze-Lareure et al., 2019) and most other pollutants are conveyed in particulate phase (Ashley et al., 2004), the investigation of the correlation between metal contents in sediments and settling velocity may support the coupling between chemical and physical aspects. The final simulation results help to predict pollutants deposition and determine the priority cleaning zone in stormwater detention basins. They may also be used as a support for the design of stormwater detention basins using trapping or removal efficient as targeted criteria.

4.4.3. Relationship between sediments physical and chemical characteristics

The significant correlation between metal contents in sediments and their settling velocity is a key finding of this study. Badin et al. (2008) suggested that organic matter in urban stormwater sediments is related to grain size. Bernardin-Souibgui et al. (2018) found that Nocardia counts are positively linked to volatile organic matter. Wiest et al. (2018) revealed that BPA is associated with fine particles. Concerning the physical characteristics, we can analyse particle-size distribution, density and shape related to each fraction of settling velocity to understand their links with chemical characteristics. Given the strong correlation of Fe content with settling velocity, it is interesting to investigate more thoroughly the oxidation states, isotopes of Fe and the related physical, chemical and biological processes, such as sorption and precipitation

(Taylor and Kauhauser, 2011). Besides, other pollutants such as PAHs, organic matter and some pathogenic bacteria can be investigated to see if they are related to metals or settling velocity.

4.4.4. Sediment management based on targeted dredging strategy

The methodology proposed in this chapter can be applied in any other stormwater detention or retention basin (dry or wet) constructed on a catchment (industrial, urban or periurban) in order to compare and evaluate deriving results against the obtained correlation in this study. This methodology also informs the intervention and treatment of sediments with a focus on the highly contaminated area. In general, the intervention criteria could be determined by comparing the metals contents to the Dutch target and intervention values (DTIV, 2000) and taking into account site specificities. The outcomes of this paper suggest that targeted dredging may be a good alternative for sediment management. In the case of DRB, P02 and P07 are highly contaminated and should be treated promptly. In theory, these contaminated sediments could be stored in places where less recirculation and sediment resuspension phenomenon occur (e.g. the upper-left side of DRB). Indeed, Becouze-Laureure et al. (2018) showed that the ecotoxicity level decreases over time and sediments should thus be left *in situ* before being discharged to a dedicated resource recovery plant or a separation device. Sediments from these most problematic zones could then be separated by means of screening and attrition (Petavy et al., 2009). As the focus is only placed on the problematic areas, less sediments need to be extracted and can be directly treated *in situ*. Such an approach could substantially reduce cost related to sediments transportation, treatment, and reuse.

4.5. Chapter conclusions

Better understanding of the spatial distribution of trace metal contamination in stormwater detention basins is vital to better manage accumulated sediments and better design such facilities, taking into account the interactions between hydrodynamics and sediment physico-chemical characteristics. This chapter investigated the locations of highly contaminated sediments with trace metals in a settling and detention basin by coupling a solid transport model with the relationships of sediment physico-chemical characteristics (correlation between Fe, Cr, Cu, Ni, Pb contents and settling velocity). Based on a large dataset, Fe and Pb contents have a significant correlation with settling velocity, followed by Cu and Cr. The observed significant correlation between Fe content and settling velocity remained stable for all campaigns and sampling sites. An equation describing this correlation is coupled with simulated spatial distribution of sediments to predict Fe content distribution. Obtained results are consistent with in situ measurements. Accounting for hydrodynamic behaviour (streamlines exhibiting recirculations, flow shear and turbulence characteristics), particles carrying Fe could then be tracked and used as an indicator to comprehensively identify trace metal contamination areas

(e.g. deposition and resuspension zones). This may help to determine the priority cleansing zone in detention basins and better design the stormwater detention basin by taking into consideration all these correlations as well as hydrodynamic parameters in sediments transport equations.

Conclusions and perspectives

Key conclusions

The research is carried out under the framework of the field observatory for urban water management (or OTHU in French). The experimental site is DRB, a stormwater detention basin which has been under monitoring and investigating for more than 20 years.

Stormwater detention basins are key components of BMPs for urban stormwater management. However, the accumulated sediments in these basins are contaminated with pollutants, such as trace metals, PAHs and some pathogenic bacteria. These accumulated deposits could be washed away and carried towards the downstream water system. The understanding of the hydrodynamic behaviour, sediments settling and resuspension is of great importance to better manage stormwater detention basins. This PhD work is designed to address scientific questions and contribute to increase knowledge on the operation of stormwater detention basins and the fate of accumulated sediments through three aspects:

- LSPIV experimental measurements of free surface velocity field for better understanding of the hydrodynamic behaviour and prediction of deposition zones.
- Modelling of sedimentation and resuspension of accumulated contaminated sediments and determination of the particle remobilization rate and the priority cleansing zone where sediments could be easily washed away and escape the basin.
- Prediction of highly contaminated zones which need specific treatments by investigating the correlation between metal contents and settling velocity and combing such correlation with sediments transport models.

In order to characterize sediments from the inlet of DRB, a new device – LW-HTS is firstly designed in this PhD work. The HTS separates sediments from stormwater thanks to the centrifugal force generated by its own geometry. It is designed according to the different in-situ limits (e.g. maximum site dimensions and maximum weight of the HTS) and the design principles reported in literature. The HTS is connected to LWS (at the upstream) to serve together as a new sediment sampling device and the efficiency is assessed through experiments and CFD modelling. As expected, LW-HTS has a better trapping performance for coarser particles and nearly 100% of particles passing through LWS were trapped in HTS. The LW-HTS is then used for sediment sampling at the inlet of DRB and for inlet sediments characterization.

To address the need of understanding of hydrodynamic behaviour through an experimental measurement method, LSPIV is applied in this PhD work. The flow patterns are key elements

for sediment transport and the LSPIV technique helps to measure free surface velocity field through the combination of camera and image treatment algorithms. The method is firstly evaluated by comparing its results with those obtained by Acoustic Doppler Velocimeter (ADV) at pilot scale. Then, the technique is applied to better understand the main flow field and explain spatial sediment distribution within DRB. Results illustrate two main flow patterns, which are consistent with observations and preliminary simulated results, i.e. water comes from the upper-right corner and moves towards the lower-left part. In some cases, a swirl is created at the centre, while in some other cases, flow continues to move leftward; flow moves from lower-right corner towards upper-left part. Low velocities and swirls that probably lead to sediment settling are observed at the centre of the basin. The LSPIV measurements are consistent with observations and CFD simulation results.

Based on the evaluated CFD hydrodynamic model, simulations of the resuspension and sedimentation of accumulated sediments are carried out. This part of work is important as accumulated deposits are contaminated and may be resuspended depending on hydrodynamic conditions and transported elsewhere within the basin or towards the outlet. The percentages of resuspended and escaped sediments for different inflow conditions are quantified, respectively. As expected, results show that fine particles (D10 of less than 20 μm) have more tendency to resuspend and be transported towards the outlet. Particles from P04 and P07 are more likely to escape than the others, which is consistent with the fact that these two locations situated at the end of particle transport pathway where fine sediments settle. Hence, these two locations should be the preferential zones for sediment cleansing.

Finally, this PhD work aims to predict contamination distribution in DRB to better manage the accumulated sediments through (i) the investigation of correlation between Fe, Cr, Cu, Ni, Pb contents in sediments and settling velocity and (ii) the combination of the derived correlation and solid transport models. Based on a large dataset (209 groups of samples, 5 campaigns, 6 sampling points including both inlet and basin), significant correlations are found between Fe and Pb contents and settling velocity, followed by Cu and Cr. An equation describing the correlation between Fe content and settling velocity is obtained and enables to predict Fe content distribution in DRB. Fe could be considered as a good indicator of the trace metal contamination of sediments accumulated in stormwater detention basins given the strong correlation between Fe and trace metals revealed both in this study and in the literature (e.g. Drapeau et al., 2017; Torres et al., 2007). In DRB, P07 and P02 are found to be highly contaminated, which should be the priority cleansing zone and specific treatments are needed. The obtained results can finally help for basin design by promoting pollution removal through settling processes and for basin management by removing firstly the identified highly contaminated sediments.

Overall, results show that P02, P04, P07 represent areas where sediments may be highly contaminated and could be easily washed away and escape the basin. These areas should be the priority treatment zone, e.g. we could lay out these contaminated sediments at the upper-left side of DRB where less recirculation and sediment resuspension phenomenon occur or even somewhere else near the basin. Indeed, Becouze-Laureure et al. (2018) shows that the ecotoxicity level decreases according to time and sediments should thus be left *in situ* before being discharged to a dedicated resource recovery plant or a separation device. For example, micropollutants in sediments could then be separated by means of screening and attrition (Petavy et al., 2009). Using Fe as indicator and CFD or other modelling approach seem appropriate to accurately locate highly contaminated zones that need specific management. As the focus is only placed on the problematic areas, less amounts of sediments are then needed to be extracted and can be directly treated *in situ*. Hence, this new management strategy leads to reducing cost related to sediments transportation, treatment, and reuse.

Perspectives

LSPIV application and improvements: LSPIV is proved to be capable of measuring free surface velocity field in stormwater detention basins. The applied methodology, including camera recording, image orthorectification, image treatments could be applied in any basins. In addition to the current application, several improvements could be taken into consideration. More cameras could be installed to cover a larger area and compensate the drawback of lower resolution for remote zones. We could also use artificial particles as tracers to better identify the tracers for image treatments and increase the accuracy for the calculation of velocity field. Moreover, wind effects could also be taken into consideration by measuring the wind condition *in situ* and integrating the measurement results into the calculation of free surface velocity field.

CFD modelling of sedimentation and resuspension of particulate pollutants: Sediments spatial distribution seem to be impacted by C_L (Lagrangian time scale constant) value in DRWM (discrete random walk model) as already demonstrated by Dufresne et al. (2009) or Yan et al. (2014). Indeed, additional investigation are needed to strengthen the choice of C_L value in DPM approach. For example, Javaherchi and Aliseda (2017) proposed a DRWM calibration methodology by modelling numerically the dispersion of particles using different values of C_L and compared against the theoretical prediction from Taylor's dispersion theory (Taylor, 1915).

Correlation between metal contents in sediments and settling velocity and its application: More campaigns and more sampling points could be performed to strengthen the derived correlation in this PhD work. In addition, the methodology to obtain the correspondence of metal contents and settling velocity could be applied to other OTHU basins to compare and evaluate deriving results against the obtained correlation in this study. Moreover, we could take more physical

and chemical parameters into consideration during additional campaigns in the future study. Concerning the physical characteristics, we could analyse particle-size distribution, density and form related to each fraction of settling velocity to analyse their links with chemical characteristics. Given the strong correlation of Fe content with settling velocity, it is interesting to investigate more thoroughly on the oxidation states, isotopes of Fe and the related physical, chemical and biological processes, such as sorption, precipitation (Taylor and Kauhauser, 2011). Besides, pollutants other than trace metals could be looked into to see if they are related to metals or settling velocity, such as:

- PAHs;
- organic matter: e.g. Badin et al. (2008) suggested that organic matter in urban stormwater sediments is related to grain size;
- some pathogenic bacteria: e.g. Bernardin-Souibgui et al. (2018) found that *Nocardia* counts are positively link to volatile organic matter;
- Bisphenol A: e.g. Wiest et al. (2018) revealed that BPA is associated to fine particles.

In addition, a new protocol is under development for settling velocity distribution measurements thanks to two turbidimeters (see Appendix D). It might be interesting to use this new system to investigate the relation between Fe content (using the derived correlation in this PhD work) and turbidity measurements.

References

Abarca, M., Guerra, P., Arce, G., Montecinos, M., Escauriaza, C., Coquery, M., & Pastén, P. (2017). Response of suspended sediment particle size distributions to changes in water chemistry at an Andean mountain stream confluence receiving arsenic rich acid drainage. Hydrological Processes, 31(2), 296-307.

Adamsson, Å., Stovin, V.R., and Bergdahl, L. (2003). Bed shear stress boundary condition for storage tank sedimentation. Journal of Environmental Engineering, 129(7), 651-657.

Adrian, R. J. (1991). Particle-imaging techniques for experimental fluid mechanics. Annual review of fluid mechanics, 23(1), 261-304.

Aguzzi, I. (2014). Analysis of a new protocol based on turbidimetry for measuring settling velocities, PIRD research project report, INSA Lyon

Andral, M. C., Roger, S., Montrejaud‐Vignoles, M., & Herremans, L. (1999). Particle size distribution and hydrodynamic characteristics of solid matter carried by runoff from motorways. Water Environment Research, 71(4), 398-407.

Ansys. (2011). Ansys version 14.0, Theory guide. Ansys. Inc., Canonsburg, PA.

Ashley, R. M., Bertrand-Krajewski, J. L., Hvitved-Jacobsen, T., & Verbanck, M. (Eds.). (2004). Solids in sewers. IWA Publishing.

Badin, A. L., Faure, P., Bedell, J. P., & Delolme, C. (2008). Distribution of organic pollutants and natural organic matter in urban storm water sediments as a function of grain size. Science of the total environment, 403(1-3), 178-187.

Barbosa, A.E., Fernandes, J.N., David, L. M. (2012). Key issues for sustainable urban stormwater management. Water Research, 46, 6787-6798.

Bardin, J. P., & Barraud, S. (2004). Aide au diagnostic et à la restructuration du bassin de rétention de Chassieu. Rapport INSA-Lyon–URGC Hydrologie Urbaine.

Bartholomä, A., & Flemming, B. W. (2007). Progressive grain-size sorting along an intertidal energy gradient. Sedimentary Geology, 202(3), 464-472.

Becouze-Lareure, C., Gonzalez-Merchan, C., Sébastian, C., Perrodin, Y., Barraud, S. and Lipeme Kouyi, G. (2014). Physical and Chemical Evolution of Sediments in Stormwater Detention Basin. 13th International Conference on Urban Drainage, Sarawak, Malaysia.

Becouze-Lareure, C., Lipeme Kouyi, G., Gonzalez-Merchan, C., Bazin, C., Sebastian, C., Barraud, S., & Perrodin, Y. (2018). Spatial and temporal dynamics of sediment ecotoxicity in urban stormwater retention basins: Methodological approach and application to a pilot site close to Lyon in France. Journal of Environmental Science and Health, Part A, 53(13), 1123-1130.

Bentzen, T. R., & Larsen, T. (2009). Heavy metal and PAH concentrations in highway runoff deposits fractionated on settling velocities. Journal of Environmental Engineering, 135(11), 1244-1247.

Bernardin-Souibgui, C., Barraud, S., Bourgeois, E., Aubin, J. B., Becouze-Lareure, C., Wiest, L., ... & Blaha, D. (2018). Incidence of hydrological, chemical, and physical constraints on bacterial pathogens, Nocardia cells, and fecal indicator bacteria trapped in an urban stormwater detention basin in Chassieu, France. Environmental Science and Pollution Research, 25(25), 24860-24881.

Bishop, C. A., Struger, J., Shirose, L. J., Dunn, L., & Campbell, G. D. (2000). Contamination and wildlife communities in stormwater detention ponds in Guelph and the Greater Toronto Area, Ontario, 1997 and 1998 Part II—Contamination and biological effects of contamination. Water Quality Research Journal, 35(3), 437-474.

Bradl, H. B. (2004). Adsorption of heavy metal ions on soils and soils constituents. Journal of colloid and interface science, 277(1), 1-18.

Camponelli, K. M., Lev, S. M., Snodgrass, J. W., Landa, E. R., & Casey, R. E. (2010). Chemical fractionation of Cu and Zn in stormwater, roadway dust and stormwater pond sediments. Environmental pollution, 158(6), 2143-2149.

Chai, T., & Draxler, R. R. (2014). Root mean square error (RMSE) or mean absolute error (MAE)?–Arguments against avoiding RMSE in the literature. Geoscientific model development, 7(3), 1247-1250.

Chapman, P. M., Wang, F., Janssen, C., Persoone, G., Allen, H. E. (1998). Ecotoxicology of Metals in Aquatic Sediments: Binding and Release, Bioavailability, Risk Assessment, and Remediation. Can. J. Fish. Aquat. Sci, 55, 2221–2243.

Chebbo, G., & Gromaire, M. C. (2009). ViCAs—An operating protocol to measure the distributions of suspended solid settling velocities within urban drainage samples. Journal of Environmental Engineering, 135(9), 768-775.

Choufi, L., Kettab, A., & Schleiss, A. J. (2014). Effet de la rugosité du fond d'un réservoir rectangulaire à faible profondeur sur le champ d'écoulement. La Houille Blanche, 5, 83-92.

Ciccarello, A., Bolognesi, A., Maglionico, M., & Artina, S. (2012). The role of settling velocity formulation in the determination of gully pot trapping efficiency: comparison between analytical and experimental data. Water Science and Technology, 65(1), 15-21.

Claro Barreto, A. (2014) Conception of a new sediment trap system and simulation of particles distribution in a settling basin. Mémoire de master MEGA, INSA de Lyon.

Claro Barreto, A., Lipeme Kouyi, G. and Vacherie, S. (2015). Utilisation du Leaping-Weir comme dispositive de piégeage de sédiments en temps de pluie et de mesure de faibles débits. Rencontres Universitaires de Génie Civil, Bayonne, France.

Coppola, L., Gustafsson, Ö., Andersson, P., Eglinton, T. I., Uchida, M., & Dickens, A. F. (2007). The importance of ultrafine particles as a control on the distribution of organic carbon in Washington Margin and Cascadia Basin sediments. Chemical geology, 243(1-2), 142-156.

Couto, M. F., Peternelli, L. A., & Barbosa, M. H. P. (2013). Classification of the coefficients of variation for sugarcane crops. Ciência rural, 43(6), 957-961.

Drapeau, C., Delolme, C., Chatain, V., Gautier, M., Blanc, D., Benzaazoua M., Lassabatere L. (2017). Spatial and temporal stability of major and trace element leaching in urban stormwater sediments. Open Journal of Soil Science, 7(11), 347-365.

DTIV, Dutch target and intervention values. ANNEXES Circular on target values and intervention values for soil remediation, 2000, 51 p.

Dufresne, M. (2008) La modélisation 3D du transport solide dans les bassins en assainissement : Du pilote expérimental à l'ouvrage réel, Doctoral dissertation, INSA de Lyon, Lyon, France.

Dufresne, M., Vazquez, J., Terfous, A., Ghenaim, A., & Poulet, J. B. (2009). Experimental investigation and CFD modelling of flow, sedimentation, and solids separation in a combined sewer detention tank. Computers & Fluids, 38(5), 1042-1049.

Dunnett, C. W. A multiple comparisons procedure for comparing several treatments with a control. Journal of the American Statistical Association. 1955, 50 (272): 1096–1121.

Dutta, P., Lehmann, C., Odedra, D., Singh, D., & Pohl, C. (2015). Tracking and quantifying developmental processes in C. elegans using open-source tools. Journal of visualized experiments: JoVE, (106).

El-Mufleh Al Husseini, A., Bechet, B., Gaudin, A., & Ruban, V. (2013). Trace metal fractionation as a mean to improve on the management of contaminated sediments from runoff water in infiltration basins. Environmental technology, 34(10), 1255-1266.

El-Mufleh, E., Béchet, B., Basile-Doelsch, I., Geffroy-Rodier, C., Gaudin, A., Ruban, V. (2014). Distribution of PAHs and trace metals in urban stormwater sediments: combination of density fractionation, mineralogy and microanalysis. Environmental Science and Pollution Research, 21, 9764–9776.

Ferziger, C. and Peric, M. (2002). Computational Methods for Fluid Dynamics. 3th edn, Springer-Verlag, Heidelberg.

Field, R., & Tafuri, A. N. (Eds.). (2006). The use of best management practices (BMPs) in urban watersheds. DEStech Publications, Inc.

Fincham, A. M., & Spedding, G. R. (1997). Low cost, high resolution DPIV for measurement of turbulent fluid flow. Experiments in Fluids, 23(6), 449-462.

Fleit, G., Baranya, S., Rüther, N., Bihs, H., Krámer, T., & Józsa, J. (2016). Investigation of the Effects of Ship Induced Waves on the Littoral Zone with Field Measurements and CFD Modeling. Water, 8(7), 300.

Frémion, F., Courtin-Nomade, A., Bordas, F., Lenain, J. F., Jugé, P., Kestens, T., & Mourier, B. (2016). Impact of sediments resuspension on metal solubilization and water quality during recurrent reservoir sluicing management. Science of the Total Environment, 562, 201-215.

Frémion, F., Mourier, B., Courtin-Nomade, A., Lenain, J. F., Annouri, A., Fondanèche, P., ... & Bordas, F. (2017). Key parameters influencing metallic element mobility associated with sediments in a daily-managed reservoir. Science of the Total Environment, 605, 666-676.

Fujita, I., & Komura, S. (1994). Application of video image analysis for measurements of river-surface flows. Proceedings of Hydraulic Engineering, 38, 733-738.

Fujita, I., Y. Muto, Y. Shimazu, R. Tsubaki, and S. Aya (2003). Velocity measurements around non-submerged and submerged spur dykes by means of large-scale particle image velocimetry. Proceedings of Hydraulic Engineering, 47, 943-948.

Fujita, I., Tsubaki, R., & Deguchi, T. (2007). PIV measurement of largescale river surface flow during flood by using a high resolution video camera from a helicopter, paper presented at Hydraulic Measurements and Experimental Methods. Am. Soc. of Civ. Eng., Lake Placid, NY.

Gasperi, J., Sebastian, C., Ruban, V., Delamain, M., Percot, S., Wiest, L., et al. (2014). Micropollutants in urban stormwater: occurrence, concentrations, and atmospheric contributions for a wide range of contaminants in three French catchments. Environmental Science and Pollution Research, 21, 5267-5281.

Gonzalez‐Merchan, G. (2012). Amélioration des connaissances sur le colmatage des systèmes d'infiltration d'eaux pluviales. Doctoral dissertation, INSA de Lyon, Lyon, France.

Gonzalez, R. C. & Wintz, P. (1987) Digital image processing. Addison-Wesley Publishing Company, Inc.

Goring, D. G., & Nikora, V. I. (2002). Despiking acoustic Doppler velocimeter data. Journal of Hydraulic Engineering, 128(1), 117-126.

Grizzard, T.J., Randall, C.W., Weand, B.L., and Ellis, K.L. (1986). The Effectiveness of Extended Detention Ponds for Urban Stormwater Pollution Management, Proceedings, EF/ASCE Conference on Urban Stormwater Quality, Impacts, and Enhancement Technology.

Happel, J., Brenner, H. (1983) Wall Effects on the Motion of a Single Particle. In: Low Reynolds number hydrodynamics. Mechanics of fluids and transport processes, vol 1. (pp. 286-357) Springer, Dordrecht

Hauet, A., Jodeau, M., Le Coz, J., Marchand, B., Moran, A. D., Le Boursicaud, R., & Dramais, G. (2014). Application of the LSPIV method for the measurement of velocity fields and flood discharges in reduced scale model and in rivers. HOUILLE BLANCHE-REVUE INTERNATIONALE DE L'EAU, (3), 16-22.

He, C., & Marsalek, J. (2013). Enhancing sedimentation and trapping sediment with a bottom grid structure. Journal of environmental engineering, 140(1), 21-29.

Hirt, C. W., & Nichols, B. D. (1981). Volume of fluid (VOF) method for the dynamics of free boundaries. Journal of computational physics, 39(1), 201-225.

Huang, H., Dabiri, D., & Gharib, M. (1997). On errors of digital particle image velocimetry. Measurement Science and Technology, 8(12), 1427.

Isenmann, G., Dufresne, M., Vazquez, J., & Mose, R. (2017). Bed turbulent kinetic energy boundary conditions for trapping efficiency and spatial distribution of sediments in basins. Water Science and Technology, 76(8), 2032-2043.

ISO, N. (2000). 13320-1. Particle size analysis: laser diffraction methods.

Jacopin, C., Bertrand-Krajewski, J. L., & Desbordes, M. (1999). Characterisation and settling of solids in an open, grassed, stormwater sewer network detention basin. Water Science and Technology, 39(2), 135-144.

Jang, Y. C., Jain, P., Tolaymat, T., Dubey, B., Singh, S., & Townsend, T. (2010). Characterization of roadway stormwater system residuals for reuse and disposal options. Science of the total environment, 408(8), 1878-1887.

Javaherchi, T., & Aliseda, A. (2017). The transport of suspended sediment in the wake of a marine hydrokinetic turbine: Simulations via a validated Discrete Random Walk (DRW) model. Ocean Engineering, 129, 529-537.

Julien, P.Y. (2010). Erosion and sedimentation. 2nd, Cambridge University Press, the Edinburgh Building, Cambridge CB2 8RU, UK.

Kayhanian, M., Suverkropp, C., Ruby, A., & Tsay, K. (2007). Characterization and prediction of highway runoff constituent event mean concentration. Journal of environmental management, 85(2), 279-295.

Kayhanian, M., McKenzie, E. R., Leatherbarrow, J. E., & Young, T. M. (2012). Characteristics of road sediment fractionated particles captured from paved surfaces, surface run-off and detention basins. Science of the total environment, 439, 172-186.

Kim, J. O., Choi, J., Lee, S., & Chung, J. (2016). Evaluation of hydrocyclone and post-treatment technologies for remediation of contaminated dredged sediments. Journal of environmental management, 166, 94-102.

Klepiszewski, K., Teufel, M., Seiffert, S., & Henry, E. (2011). Measurement of flow velocity profiles in tank structures using the prototype device OCM Pro LR. Water Science and Technology, 64(1), 263-270.

Konhauser, K. O., Kappler, A., & Roden, E. E. (2011). Iron in microbial metabolisms. Elements, 7(2), 89-93.

Launder, B.E. and Spalding, D.B. (1974). The numerical computation of turbulent flows. Computer Methods in Applied Mechanics and Engineering, 3(2), 269-289.

Lawrence, A. I, Marsalek, J, Ellis, J.B, Urbonas, B. (1996). Stormwater detention & BMPs. Journal of Hydraulic Research, 34(6), 799-813.

Lipeme Kouyi, G., Arias, L., Barraud, S., & Bertrand-Krajewski, J. L. (2010). CFD modelling of flows in a large stormwater detention and settling basin. NOVATECH 2010.

Lipeme Kouyi, G., Barraud, S., Becouze-Lareure, C., Blaha, D., Perrodin, Y., Wiest, L., ... & Bernardin-Souibgui, C. (2018). Caractérisation des sédiments d'un bassin de retenue-

décantation des eaux pluviales et éléments pour la gestion. Techniques Sciences Méthodes, (9), 65-75.

Lipeme Kouyi, G., Cren-Olivé, C., & Cournoyer, B. (2014a). Chemical, microbiological, and spatial characteristics and impacts of contaminants from urban catchments: CABRRES project. Environmental Science and Pollution Research, 21(8), pp 5263–5266.

Lipeme Kouyi, G., Østertoft, C., Yan, H. (2014b). CABRRES project: the influence of two large stormwater detention basins design on hydrodynamic and sediment distribution. 32èmes Rencontres Universitaires de Génie Civil – AUGC, 4-6 Juin, Orléans, 10 p.

Le Boursicaud, R., Pénard, L., Hauet, A., Thollet, F., & Le Coz, J. (2016). Gauging extreme floods on YouTube: application of LSPIV to home movies for the post-event determination of stream discharges. Hydrological Processes, 30(1), 90-105.

Le Coz, J., Jodeau, M., Hauet, A., Marchand, B., & Le Boursicaud, R. (2014). Image-based velocity and discharge measurements in field and laboratory river engineering studies using the free Fudaa-LSPIV-LSPIV software. In Proceedings of the International Conference on Fluvial Hydraulics, RIVER FLOW (pp. 1961-1967).

Lewis, Q. W., & Rhoads, B. L. (2015). Resolving two dimensional flow structure in rivers using large scale particle image velocimetry: An example from a stream confluence. Water Resources Research, 51(10), 7977-7994.

Lewis, Q. W., Lindroth, E. M., & Rhoads, B. L. (2018). Integrating unmanned aerial systems and LSPIV for rapid, cost-effective stream gauging. Journal of Hydrology, 560, 230-246.

Loch, R.J. (2001). Settling velocity- a new approach to assessing soil and sediment properties. Computers and electronics in agriculture, 31, 305-316

Loganathan, G.V., Watkins, E.W., and Kibler, D.F. (1994). Sizing storm-water detention basins for pollutant removal. Journal of Environmental Engineering, 120 (6), 1380-1399.

Maniquiz-Redillas, M.C., Geronimo, F.K.F., Kim, L.-H. (2014). Investigation on the effectiveness of pretreatment in stormwater management technologies. Journal of Environmental science, 26, 1824-1830.

Marsalek, J., Marsalek, P. M. (1997). Characteristics of sediments from a stormwater management pond. Water Science and Technology, 36, 117-122.

Maté Marín, A. , Rivière, N., & Lipeme Kouyi, G. (2018). DSM-flux: A new technology for reliable Combined Sewer Overflow discharge monitoring with low uncertainties. Journal of environmental management, 215, 273-282.

Meyer, A. M., Klein, C., Fünfrocken, E., Kautenburger, R., & Beck, H. P. (2019). Real-time monitoring of water quality to identify pollution pathways in small and middle scale rivers. Science of The Total Environment, 651, 2323-2333.

Molinaroli, E., Guerzoni, S., De Falco, G., Sarretta, A., Cucco, A., Como, S., ... & Magni, P. (2009). Relationships between hydrodynamic parameters and grain size in two contrasting transitional environments: the Lagoons of Venice and Cabras, Italy. Sedimentary Geology, 219(1-4), 196-207.

Morsi, S.A. & Alexander, A.J. (1972). An investigation of particle trajectories in two-phase flow systems. Journal of Fluid Mechanics, 55(02), 193-208.

Muste, M., Fujita, I., & Hauet, A. (2008). Large-scale particle image velocimetry for measurements in riverine environments. Water Resources Research, 44(4).

Muste, M., Ho, H. C., & Kim, D. (2011). Considerations on direct stream flow measurements using video imagery: Outlook and research needs. Journal of Hydro-environment Research, 5(4), 289-300.

Muste, M., Hauet, A., Fujita, I., Legout, C., & Ho, H. C. (2014). Capabilities of Large-scale Particle Image Velocimetry to characterize shallow free-surface flows. Advances in Water Resources, 70, 160-171.

NF EN 872. (2005). Water quality–Determination of suspended solids–Method by filtration through glass fiber filters.

NF EN 16174 (2012). Digestion of aqua regia soluble fractions of elements.

NF EN ISO 11885 (1998). Water quality - Determination of selected elements by inductively coupled plasma optical emission spectroscopy (ICP-OES)

Nortek. (2004). Vectrino velocimeter user guide, Rud, Norway.

Orszag, S. A., Yakhot, V., Flannery, W. S., Boysan, F., Choudhury, D., Maruzewski, J., & Patel, B. (1993). Renormalization group modeling and turbulence simulations. Near-wall turbulent flows, 1031-1046.

Park, N. S., Kim, S. S., & Jung, N. C. (2008). Remodeling a sedimentation basin outlet structure for improving performance. Environmental Engineering Science, 25(6), 887-894.

Persson, J. (2000). The hydraulic performance of ponds of various layouts. Urban Water J. 2(3), 243–250.Raffel, M., Willert, C. E., Wereley, S. T., & Kompenhans, J. (2007). Particle Image Velocimetry. Springer Berlin Heidelberg.

Petavy, F., Ruban, V., Conil, P., Viau, J. Y., & Auriol, J. C. (2009). Treatment and valorisation of stormwater sediments. Global Nest Journal, 11(2), 189-195.

Randall, C. W., Ellis, K., Grizzard, T. J. and Knocke, W. R. (1982). Urban Runoff Pollutant Trap by Sedimentation, Proceedings, EF/ASCE Conference on Stormwater Detention Facilities - Planning, Design, Operation, and Maintenance, Henniker, NH, 205-219.

Rosenkrantz, R. T., Pollino, C. A., Nugegoda, D., & Baun, A. (2008). Toxicity of water and sediment from stormwater retarding basins to Hydra hexactinella. Environmental pollution, 156(3), 922-927.

Schwab, D. J., Beletsky, D., DePinto, J., & Dolan, D. M. (2009). A hydrodynamic approach to modeling phosphorus distribution in Lake Erie. Journal of Great Lakes Research, 35(1), 50-60.

Sébastian, C. (2013) Bassin de retenue des eaux pluviales en milieu urbain : performance en matière de piégeage des micropolluants. Doctoral Dissertation, INSA de Lyon, Lyon, France.

Sébastian, C., Barraud, S., Gonzalez-Merchan, C., Perrodin, Y., & Visiedo, R. (2014a). Stormwater retention basin efficiency regarding micropollutant loads and ecotoxicity. Water Science and Technology, 69(5), 974-981.

Sébastian, C., Barraud, S., Ribun, S., Zoropogui, A., Blaha, D., Becouze-Lareure, C., et al. (2014b) Accumulated sediments in a detention basin: chemical and microbial hazard assessment linked to hydrological processes. Environmental Science and Pollution Research, 21, 5367-5378.

Sébastian, C., Becouze-Lareure, C., Kouyi, G. L., & Barraud, S. (2015). Event-based quantification of emerging pollutant removal for an open stormwater retention basin–Loads, efficiency and importance of uncertainties. Water Research, 72, 239-250.

Sechet, P. & Le Guennec B. (1999). The role of near wall turbulent structures on sediment transport. Water Research, 33 (17), 3646-3656

Shapiro, S. S. & Wilk, M. B. (1965). An analysis of variance test for normality (complete samples). Biometrika. 52 (3–4): 591–611. doi:10.1093/biomet/52.3-4.591. JSTOR 2333709. MR 0205384. p. 593

Shavit, U., Lowe, R. J., & Steinbuck, J. V. (2007). Intensity capping: a simple method to improve cross-correlation PIV results. Experiments in fluids, 42(2), 225-240.

Stovin, V. R. and Saul, A. J. (1994). Sedimentation in storage tank structures. Water Science and Technology, 29(1-2), 363-372.

Tauro, F., Piscopia, R., & Grimaldi, S. (2017). Streamflow Observations From Cameras: Large-Scale Particle Image Velocimetry or Particle Tracking Velocimetry?. Water Resources Research, 53(12), 10374-10394.

Taylor, G. (1915). Diffusion by continuous movements. eddy motion in the atmosphere. Philos. Trans., 1.

Taylor, K. G., & Konhauser, K. O. (2011). Iron in Earth surface systems: A major player in chemical and biological processes. Elements, 7(2), 83-88.

Thielicke, W. (2014). The Flapping Flight of Birds—Analysis and Application. Thesis, University of Groningen.

Thielicke, W., & Stamhuis, E. (2014). PIVlab–towards user-friendly, affordable and accurate digital particle image velocimetry in MATLAB. Journal of Open Research Software, 2(1).

Torres A, Hasler M, Bertrand-Krajewski JL. (2007). Spatial heterogeneity and inter-event variability of sediment settling distributions in a stormwater retention tank. Proceedings of 6th NOVATECH conference, Lyon, France.

Torres, A. (2008). Décantation des eaux pluviales dans un ouvrage réel de grande taille: éléments de réflexion pour le suivi et la modélisation. Thèse de Doctorat, INSA Lyon.

Torres, A., & Bertrand-Krajewski, J. L. (2008). Evaluation of uncertainties in settling velocities of particles in urban stormwater runoff. Water Science and Technology, 57(9), 1389-1396.

Torres, A., Lipeme Kouyi, G., Bertrand-Krajewski, J. L., Guilloux, J., Barraud, S., & Paquier, A. (2008). Modelling of hydrodynamics and solid transport in a large stormwater detention and settling basin. In 11 th International Conference on Urban Drainage.

Urbonas, B. (1994).Assessment of stormwater BMPs and their technology. Water Science and Technology, 29(1-2), 347-353.

Vallet, B., Lessard, P., & Vanrolleghem, P. A. (2016). A storm water basin model using settling velocity distribution. Journal of Environmental Engineering and Science, 11(4), 84-95.

Vanoni, V.A. (1975). Sedimentation Engineering, Manuals and Reports on Engineering Practice No. 54, American Society of Civil Engineers, New York.

Vesilind, P. A. and Jones, G. N., (1990) A reexamination of the batch thickening curve. – Research Journal of the Water Pollution Control Federation, 1990, vol 62, 7, pp 887-893

Vezzaro, L., Eriksson, E., Ledin, A., & Mikkelsen, P. S. (2010). Dynamic stormwater treatment unit model for micropollutants (STUMP) based on substance inherent properties. Water science and technology, 62(3), 622-629.

Vonk, J. E., Giosan, L., Blusztajn, J., Montlucon, D., Pannatier, E. G., McIntyre, C., ... & Eglinton, T. I. (2015). Spatial variations in geochemical characteristics of the modern Mackenzie Delta sedimentary system. Geochimica et Cosmochimica Acta, 171, 100-120.

Vosswinkel N., Lipeme Kouyi G., Ebbert S., Schnieders A., Maus C., Laily A.-G., Mohn R. and Uhl M.(2012). Influence of unsteady behaviour on the settling of solids in storm water tanks. Proceedings of the 9th Urban Drainage Modelling International Conference, 3rd - 7th September, Belgrade, Serbia, 14 p.

Wahl, T. L. (2002). Discussion of "Despiking Acoustic Doppler Velocimeter Data" by Derek G. Goring and Vladimir I. Nikora. Journal of Hydrology, 129(6), 484-487.

Walcker, N., Bertrand-Krajewski, J. L., Vacherie, S., Lepot, M., Castebrunet, H., Barraud, S., & Lipeme Kouyi, G. (2018). Une nouvelle station de mesure pour l'acquisition de séries chronologiques en hydrologie urbaine. Techniques Sciences Méthodes, (3), 55-64.

Westerweel, J., Dabiri, D., & Gharib, M. (1997). The effect of a discrete window offset on the accuracy of cross-correlation analysis of digital PIV recordings. Experiments in fluids, 23(1), 20-28.

Westerweel, J., & Scarano, F. (2005). Universal outlier detection for PIV data. Experiments in Fluids, 39(6), 1096–1100. doi:10.1007/s00348-005-0016-6

Whitaker, A., & Duckworth, O. (2018). Cu, Pb, and Zn Sorption to Biogenic Iron (Oxyhydr) Oxides Formed in Circumneutral Environments. Soil Systems, 2(2), 18.

Wik, A., Lycken, J., & Dave, G. (2008). Sediment quality assessment of road runoff detention systems in Sweden and the potential contribution of tire wear. Water, air, and soil pollution, 194(1-4), 301-314.

Wiest, L., Baudot, R., Lafay, F., Bonjour, E., Becouze-Lareure, C., Aubin, J. B., ... & Vulliet, E. (2018). Priority substances in accumulated sediments in a stormwater detention basin from an industrial area. Environmental Pollution, 243, 1669-1678.

Yan, H. (2013). Experiments and 3D modelling of hydrodynamics, sediment transport, settling and resuspension under unsteady conditions in an urban stormwater detention basin. Doctoral Dissertation, INSA de Lyon, Lyon, France.

Yan, H., Lipeme Kouyi, G., Gonzalez-Merchan, C., Becouze-Lareure, C., Sebastian, C., Barraud, S., & Bertrand-Krajewski, J. L. (2014). Computational fluid dynamics modelling of flow and particulate contaminants sedimentation in an urban stormwater detention and settling basin. Environmental Science and Pollution Research, 21(8), 5347-5356.

Yang, J., Chen, Y., Kontis, K., & Li, Y. (2016). Wind tunnel experiments of novel wing configurations for design and customisation in an industry 4.0 environment. In Software, Knowledge, Information Management & Applications (SKIMA), 10th International Conference on (pp. 92-97). IEEE.

Yun, Y., Park, H., Kim, L., & Ko, S. (2010). Size distributions and settling velocities of suspended particles from road and highway. KSCE Journal of Civil Engineering, 14(4), 481-488.

Zgheib, S., Moilleron, R., & Chebbo, G. (2008). Screening of priority pollutants in urban stormwater: innovative methodology. Water Pollution IX, 111, 235-244.

Zgheib, S., Moilleron, R., Saad, M., Chebbo, G. (2011) Partition of pollution between dissolved and particulate phases: What about emerging substances in urban stormwater catchments? Water Research, 45, 913-925.

Zgheib, S., Moilleron, R., Chebbo, G. (2012) Priority pollutants in urban stormwater: Part 1 – Case of separate storm sewers. Water Research, 46(20), 6683-6692.

Zhu, X., Claro Barreto, A., Lipeme Kouyi, G. (2016). Design and performance evaluation of Hydrocyclone and Lamella Settler for Urban Stormwater Sediments. 8th international conference on Sewer Processes and Networks – SPN8, Rotterdam, Netherlands, 31 Aug.-2 Sept.

Zhu, X., Lipeme Kouyi, G., Becouze-Lareure, C, Barraud, S, Bertrand-Krajewski, J.-L. (2017). 3D numerical modelling of resuspension and remobilization of sediments in a stormwater detention basin. Aquaconsoil, Lyon, 26-30 june 2017.

Zhu, X., & Lipeme Kouyi, G. (2019). An analysis of LSPIV ‐ based surface velocity measurement techniques for stormwater detention basin management. Water Resources Research, 55(2), 888-903.

Appendix

Appendix A: Matlab code for Fe concentration distribution in DRB

```
clear all; close all; clc;

edge_xls = 'coordonees_edges_bassin.xls';
[number1,txt1,raw1] = xlsread(edge_xls, 'A1:B16');
edge = [number1;number1(1,:)];

txt = ['chassieu.txt'];
tmp = importdata(txt);
siz = 30;

figure(1)
plot(edge(:,1), edge(:,2), 'k');
hold on

v1 = zeros(203,121);
v2 = zeros(203,121);
v3 = zeros(203,121);

TS1 = tmp(:, 1:2);
Dia = tmp(:,4);

d =
[0.000015;0.000026;0.000038;0.000050;0.000064;0.000082;0.000106;0.000146;0.
000241;0.000920];
Fe1 = [9.31E-11; 4.68E-10; 1.42E-09; 3.18E-09; 6.53E-09; 1.35E-08; 2.86E-
08; 7.26E-08; 3.17E-07; 1.72E-05];
m1 = [3.71101E-12; 1.93258E-11; 6.03349E-11; 1.37445E-10; 2.88242E-10;
6.06261E-10; 1.30959E-09; 3.42197E-09; 1.53911E-08; 8.56212E-07];
Fe = zeros(size(Dia));
m = zeros(size(Dia));
for k = 1:10
    p = Dia==d(k);
    Fe(p) = Fe1(k);
    m(p) = m1(k);
end

x = floor(TS1(:,1));
y = floor(TS1(:,2));
```

```
x1 = x - 872;
y1 = y - 157;
for str = 1:size(x,1)
    v1(x1(str),y1(str))= v1(x1(str),y1(str))+ Fe(str);
    v2(x1(str),y1(str))= v2(x1(str),y1(str))+ m(str);
end
mask = v2~=0;
v3(mask) = v1(mask)./v2(mask);

idx = find(mask);
L = v3(idx);
[x2,y2] = ind2sub([203,121],idx);
x3 = x2+873-0.5;
y3 = y2+158-0.5;

scatter(x3, y3, siz,(L), 'filled');

colormap(jet)
colorbar()
axis equal;
axis([865 1080 155 280]);
set(gcf, 'Position', get(0, 'Screensize'))
set(gcf,'PaperPositionMode','auto')
h=colorbar;
set(h,'fontsize',40);
set(get(h,'Title'),'String','[Fe] (g/kg)')
xt = get(gca, 'XTick');
set(gca, 'FontSize', 40)
axis off
saveas(gcf, ['[Fe] distribution.png'])
savefig(gcf,['[Fe] distribution'])
hold off
```

Appendix B: Physical and chemical characteristics of sediments

Table A1. Sediments particle-size and settling velocity distribution

Sample		Particle-size (μm)			Settling velocity (m/h)		
		D10	D50	D90	V20	V50	V80
C1	P01	9.9± 1.6	69.2 ± 13.2	501.9 ± 252.3	1.9 ± 0.0	7.0 ± 0.1	21.7 ± 0.6
	P07	9.5 ± 1.1	54.5 ± 5.2	206.4 ± 37.6	1.9 ± 0.0	6.6 ± 0.1	20.0 ± 0.6
C2	inlet	11.1 ± 1.4	55.6 ± 5.3	312.9 ± 59.1	1.8 ± 0.2	6.7 ± 0.2	20.2 ± 0.8
C3	inlet	24.2 ± 6.7	313.5 ± 222.8	1365.8 ± 36.1	3.2 ± 0.4	11.6 ± 0.7	32.8 ± 1.0
	P01	9.1 ± 2.0	52.9 ± 13.6	308.5 ± 274.9	2.9 ± 0.3	9.6 ± 0.6	28.9 ± 1.0
	P02	6.3 ± 0.6	37.7 ± 5.4	260.9 ± 171.0	1.0 ± 0.2	3.4 ± 0.2	9.9 ± 0.6
	P04	7.4 ± 2.0	45.3 ± 19.8	493.5 ± 448.5	1.9 ± 0.2	6.9 ± 0.2	22.2 ± 0.9
	P07	8.2 ± 1.1	45.5 ± 7.3	200.9 ± 79.6	1.3 ± 0.4	4.1 ± 0.4	12.4 ± 1.0
	P12bis	12.5 ± 1.3	78.3 ± 6.7	402.3 ± 52.4	2.1 ± 0.1	7.5 ± 0.1	23.3 ± 0.6
C4	inlet	nm	nm	nm	0.5 ± 0.1	1.9 ± 0.2	6.1 ± 0.4
	P01	23.7 ± 3.0	144.6 ± 28.8	1077.0 ± 84.8	1.6 ± 0.1	5.9 ± 0.2	16.9 ± 0.9
	P02	20.0 ± 3.9	199.3 ± 157.7	1282.7 ± 93.4	0.9 ± 0.3	2.9 ± 0.4	8.1 ± 0.4
	P04	18.8 ± 5.8	129.4 ± 211.5	1224.0 ± 129.0	0.8 ± 0.2	2.6 ± 0.4	7.7 ± 0.4
	P07	17.3 ± 2.0	79.8 ± 9.0	641.5 ± 157.2	1.9 ± 0.1	6.7 ± 0.1	20.8 ± 0.7
C5	inlet	370.9 ± 17.2	870.5 ± 13.8	1473.1 ± 14.7	0.9 ± 0.5	4.3 ± 0.8	14.7 ± 1.0
	P01	16.5 ± 1.6	78.5 ± 7.5	520.2 ± 81.0	1.7 ± 0.1	6.0 ± 0.1	17.3 ± 0.7
	P02	18.8 ± 4.1	100.2 ± 33.7	944.4 ± 254.7	0.6 ± 0.1	2.1 ± 0.2	6.9 ± 0.3
	P04	28.6 ± 3.6	433.3 ± 113.5	1268.2 ± 70.7	1.5 ± 0.1	5.4 ± 0.2	15.3 ± 0.3
	P07	20.7 ± 2.0	109.8 ± 11.4	870.0 ± 90.0	1.6 ± 0.1	5.7 ± 0.2	16.2 ± 0.3

D10: sieving size with 10% of particle mass passing through.

V10: 10% of particle volume has a settling velocity inferior to V10.

Uncertainty of particle-size analyses: coefficient of variation among triplicate measurements.

Uncertainty of settling velocity measurements: evaluated by Monte Carlo simulations and the law of propagation of uncertainties (Torres and Bertrand-Krajewski, 2008).

Table A2. Metal contents measured directly in dried sediments

Sample		Metal contents of dried sediments								
		Major elements (g/kg)			Trace metals (mg/kg)					
		Al	Ca	Fe	Cd	Cr	Cu	Ni	Pb	Zn
C1	P01	11.5 ± 0.6	61.2 ± 3.1	21.3 ± 1.1	1.6 ± 0.2	79.6 ± 4.0	359.8 ± 18.0	81.0 ± 4.1	90.4 ± 4.5	2379.0 ± 118.9
	P07	12.7 ± 0.6	66.5 ± 3.3	24.5 ± 1.2	1.5 ± 0.1	86.9 ± 4.3	336.7 ± 16.8	61.1 ± 3.1	96.0 ± 4.8	2118.7 ± 105.9
C2	inlet	5.6 ± 0.3	189.3 ± 9.5	13.4 ± 0.7	1.1*	90.0 ± 4.5	298.2 ± 14.9	187.8 ± 9.4	79.5 ± 4.0	8156.0 ± 407.8
C3	inlet	11.7 ± 0.6	70.2 ± 3.5	26.4 ± 1.3	2.1*	132.9 ± 6.6	370.9 ± 18.5	137.7 ± 6.9	122.8 ± 6.1	3117.7 ± 155.9
	P01	14.8 ± 0.7	65.5 ± 3.3	26.9 ± 1.3	1.8*	94.9 ± 4.7	283.1 ± 14.2	93.4 ± 4.7	115.7 ± 5.8	2941.4 ± 147.1
	P02	15.3 ± 0.8	63.8 ± 3.2	26.7 ± 1.3	2.1 ± 0.2	78.3 ± 3.9	334.5 ± 16.7	86.3 ± 4.3	124.9 ± 6.2	2112.7 ± 105.6
	P04	15.8 ± 0.8	71.4 ± 3.6	27.1 ± 1.4	2.1 ± 0.2	78.1 ± 3.9	314.3 ± 15.7	90.3 ± 4.5	118.9 ± 5.9	2286.7 ± 114.3
	P07	14.0 ± 0.7	63.0 ± 3.1	25.5 ± 1.3	1.9 ± 0.2	97.5 ± 4.9	297.9 ± 14.9	87.0 ± 4.3	114.0 ± 5.7	2534.7 ± 126.7
	P12bis	12.1 ± 0.6	62.6 ± 3.1	23.3 ± 1.2	3.1 ± 0.3	88.8 ± 4.4	328.0 ± 16.4	96.4 ± 4.8	119.2 ± 6.0	2730.3 ± 136.5
C4	inlet	nm	nm	nm	nm	nm	nm	nm	nm	nm
	P01	10.1 ± 0.5	54.8 ± 2.7	19.0 ± 1.0	1.4 ± 0.1	82.5 ± 4.1	364.7 ± 18.2	55.4 ± 2.8	84.7 ± 4.2	2421.0 ± 121.1
	P02	9.8 ± 0.5	49.2 ± 2.5	15.8 ± 0.8	1.7 ± 0.2	68.8 ± 3.4	319.9 ± 16.0	44.4 ± 2.2	79.5 ± 4.0	1632.6 ± 81.6
	P04	13.3 ± 0.7	67.5 ± 3.4	22.0 ± 1.1	1.6 ± 0.2	74.0 ± 3.7	370.6 ± 18.5	47.4 ± 2.4	94.8 ± 4.7	1778.9 ± 88.9
	P07	12.2 ± 0.6	61.4 ± 3.1	22.4 ± 1.1	1.6 ± 0.2	93.7 ± 4.7	366.1 ± 18.3	66.3 ± 3.3	102.0 ± 5.1	2286.2 ± 114.3
C5	inlet	5.6 ± 0.3	93.2 ± 4.7	12.3 ± 0.6	0.9*	59.8 ± 3.0	165.1 ± 8.3	34.4 ± 1.7	39.7 ± 2.0	1029.9 ± 51.5
	P01	11.8 ± 0.6	56.0 ± 2.8	21.4 ± 1.1	1.4 ± 0.1	91.3 ± 4.6	321.2 ± 16.1	59.6 ± 3.0	95.4 ± 4.8	2124.7 ± 106.2
	P02	14.6 ± 0.7	49.0 ± 2.5	25.0 ± 1.3	1.8 ± 0.2	90.0 ± 4.5	360.1 ± 18.0	59.9 ± 3.0	110.6 ± 5.5	2183.9 ± 109.2
	P04	12.0 ± 0.6	49.8 ± 2.5	20.0 ± 1.0	1.4 ± 0.1	66.6 ± 3.3	238.4 ± 11.9	50.8 ± 2.5	87.4 ± 4.4	1732.8 ± 86.6
	P07	12.0 ± 0.6	56.0 ± 2.8	21.6 ± 1.1	1.7 ± 0.2	98.8 ± 4.9	403.1 ± 20.2	63.5 ± 3.2	103.0 ± 5.2	2557.7 ± 127.9

*not quantifiable, nm: not measured

Table A3. Metal contents measured directly in sediments after TSS filtration procedure (French standard NF EN 872, 2005)

Sample		Metal contents of sediments after TSS filtration procedure				
		Major element (g/kg)	Trace metals (mg/kg)			
		Fe	Cr	Cu	Ni	Pb
C1	P01	nm	74.3 ± 3.7	360.1 ± 18.0	56.7 ± 2.8	98.8 ± 4.9
	P07	nm	78.3 ± 3.9	325.7 ± 16.3	54.1 ± 2.7	114.3 ± 5.77
C2	inlet	13.5 ± 0.7	96.5 ± 4.8	222.0 ± 11.1	237.7 ± 11.9	99.8 ± 5.0
C3	inlet	18.2 ± 0.9	71.5 ± 3.6	242.3 ± 12.1	85.2 ± 4.3	114.1 ± 5.7
	P01	20.4 ± 1.0	73.5 ± 3.7	233.5 ± 11.7	74.6 ± 3.7	105.7 ± 5.3
	P02	nm	nm	nm	nm	nm
	P04	nm	nm	nm	nm	nm
	P07	27.5 ± 1.4	93.1 ± 4.7	278.8 ± 13.9	93.9 ± 4.7	137.1 ± 6.9
	P12bis	15.4 ± 0.8	62.7 ± 3.1	226.8 ± 11.3	70.5 ± 3.5	95.8 ± 4.8
C4	inlet	21.0 ± 1.1	154.3 ± 7.7	584.4 ± 29.2	93.8 ± 4.7	200.6 ± 10.0
	P01	18.7 ± 0.9	76.3 ± 3.8	308.7 ± 15.4	58.1 ± 2.9	96.7 ± 4.8
	P02	25.6 ± 1.3	96.4 ± 4.8	457.4 ± 22.9	68.7 ± 6.9	136.6 ± 6.8
	P04	24.4 ± 1.2	80.5 ± 4.0	428.2 ± 21.4	61.9 ± 3.1	140.7 ± 7.0
	P07	17.9 ± 0.9	89.6 ± 4.5	355.3 ± 17.8	63.1 ± 3.2	111.5 ± 5.6
C5	inlet	14.9 ± 0.7	110.4 ± 5.5	429.0 ± 21.5	80.4 ± 8.0	69.7*
	P01	24.7 ± 1.2	94.9 ± 4.7	349.2 ± 17.5	65.7 ± 3.3	115.7 ± 5.8
	P02	22.2 ± 1.1	89.1 ± 8.9	378.3 ± 18.9	72.7 ± 7.3	167.2 ± 8.4
	P04	21.1 ± 1.1	65.8 ± 3.3	258.1 ± 12.9	59.2 ± 3.0	112.3 ± 5.6
	P07	16.6 ± 0.8	66.3 ± 3.3	275.0 ± 13.8	42.7 ± 4.3	88.9 ± 4.4

*not quantifiable, nm: not measured

Appendix C: Variability of the correlation between metal contents and settling velocity

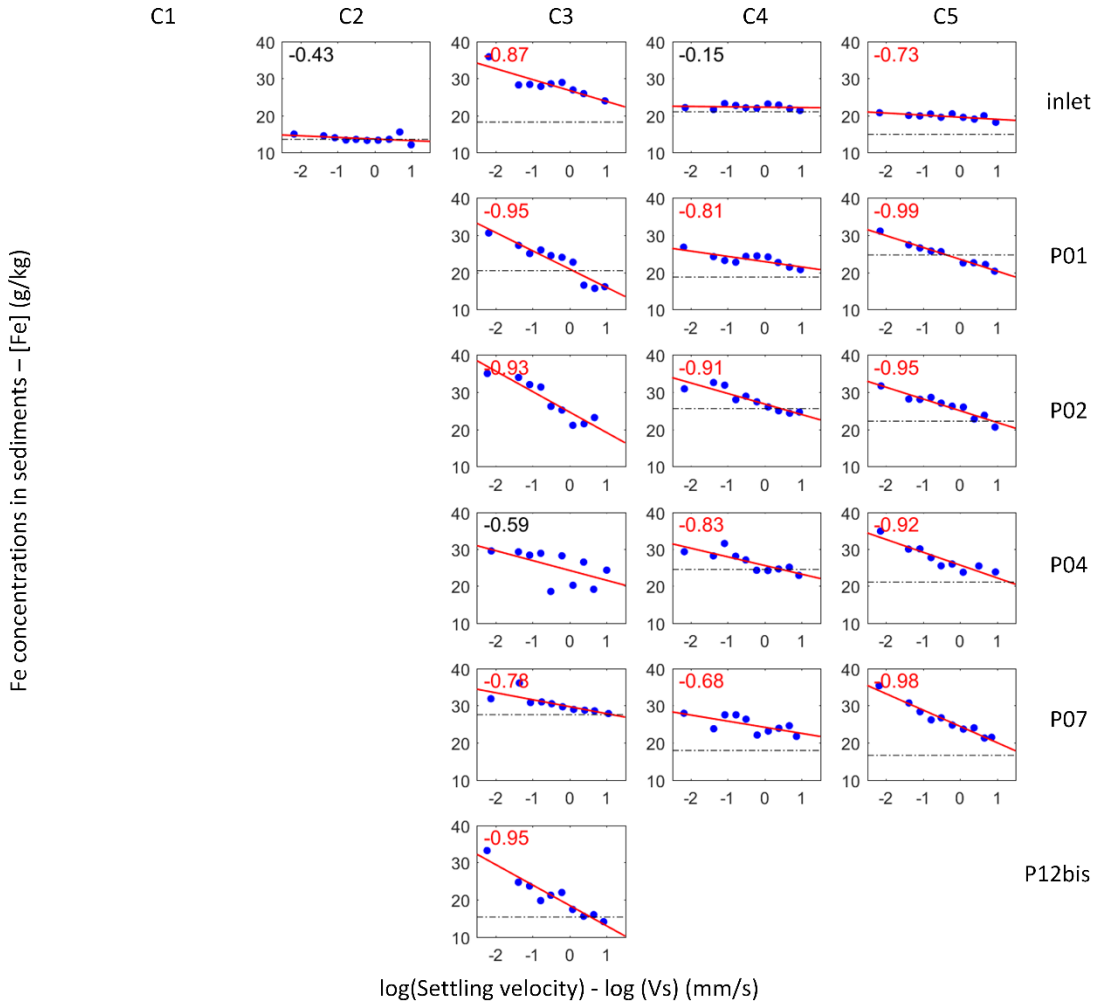

Figure A1. Spatial and temporal variability on the correlation between [Fe] and log(Vs)

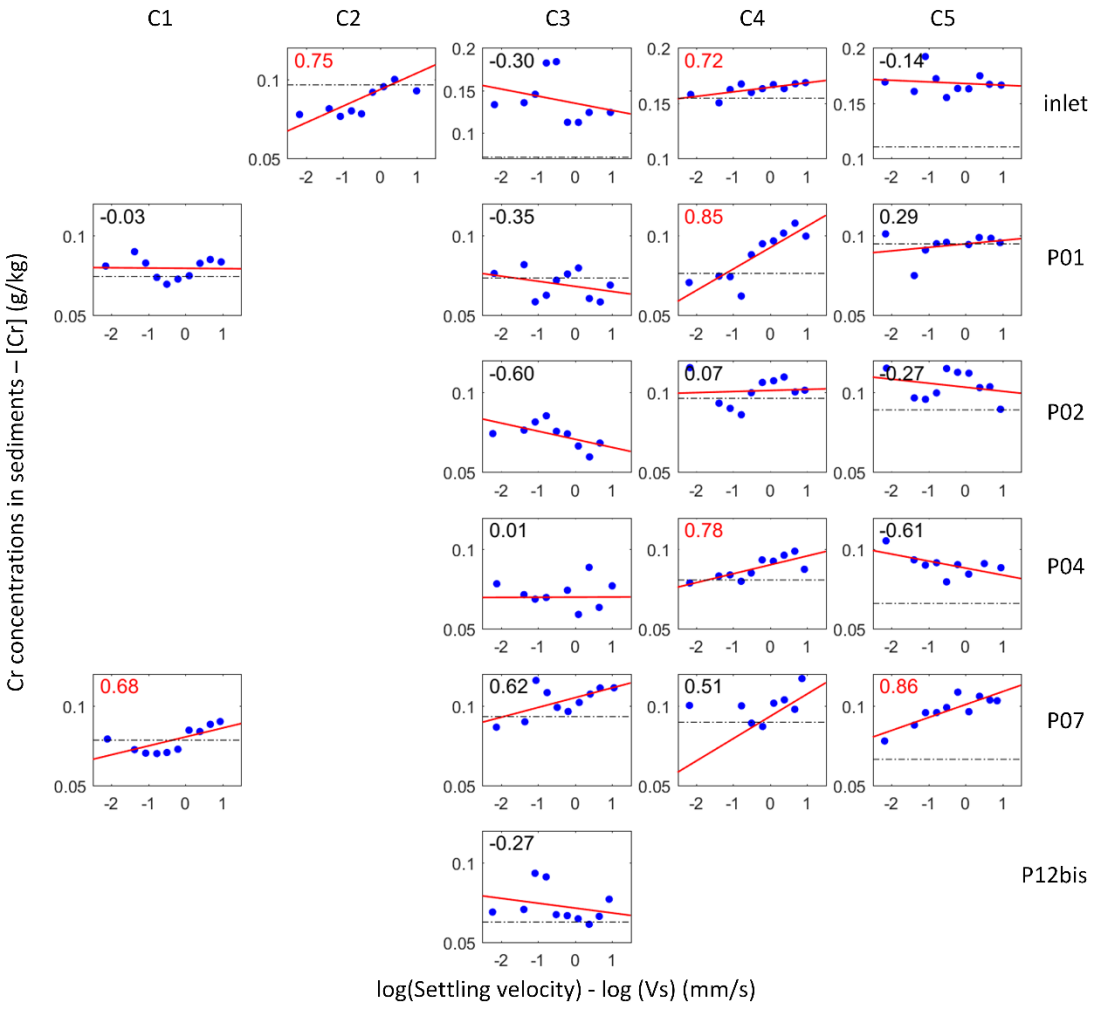

Figure A2. Spatial and temporal variability on the correlation between [Cr] and log(Vs)

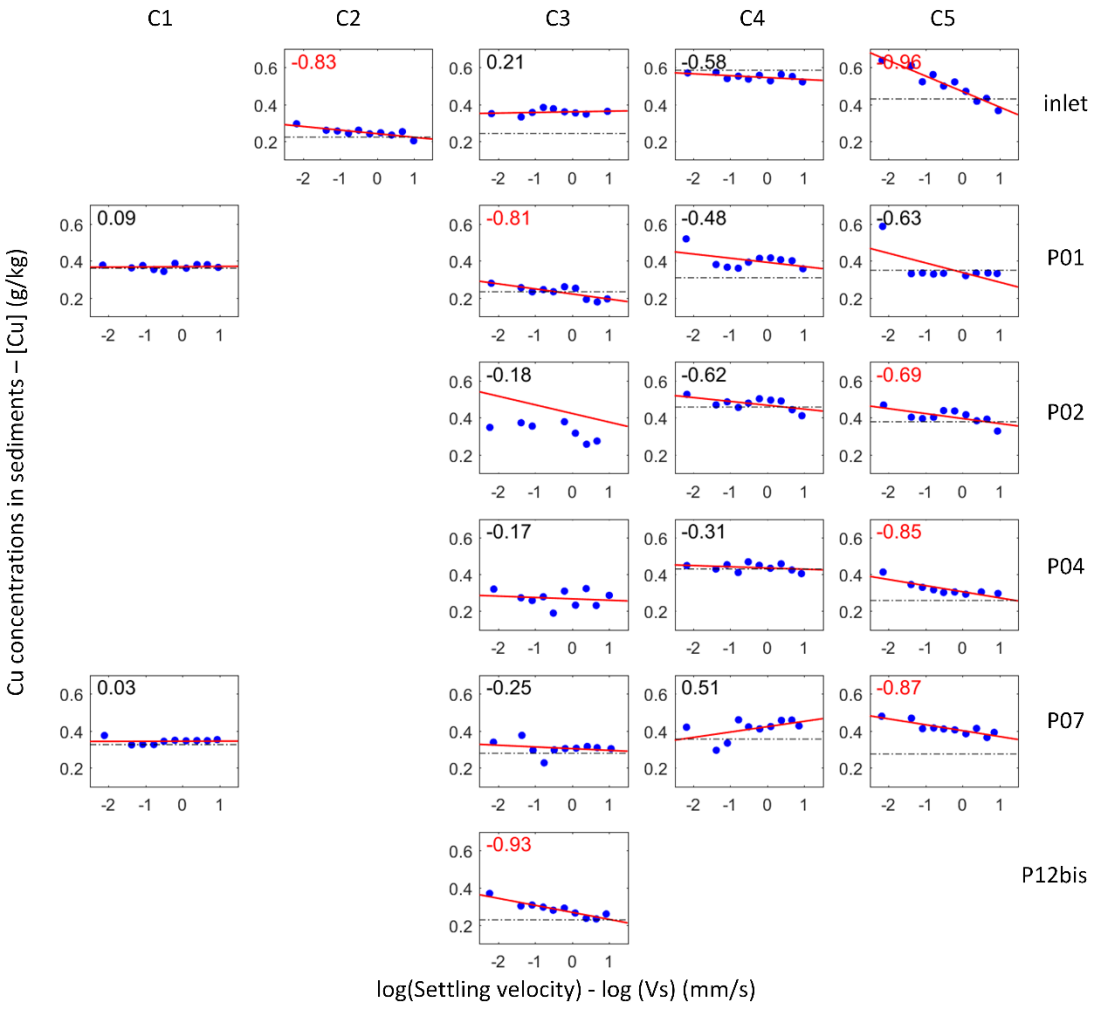

Figure A3. Spatial and temporal variability on the correlation between [Cu] and log(Vs)

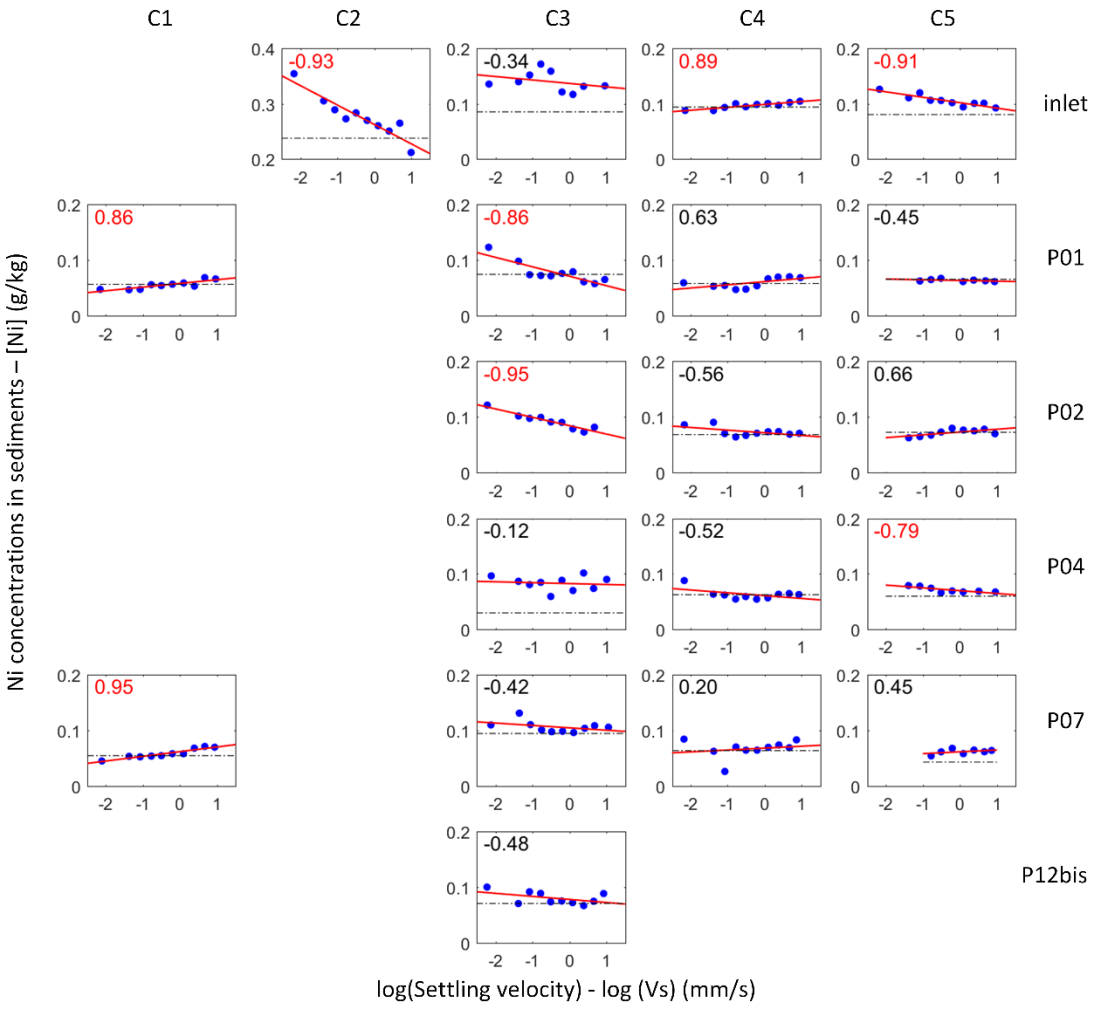

Figure A4. Spatial and temporal variability on the correlation between [Ni] and log(Vs)

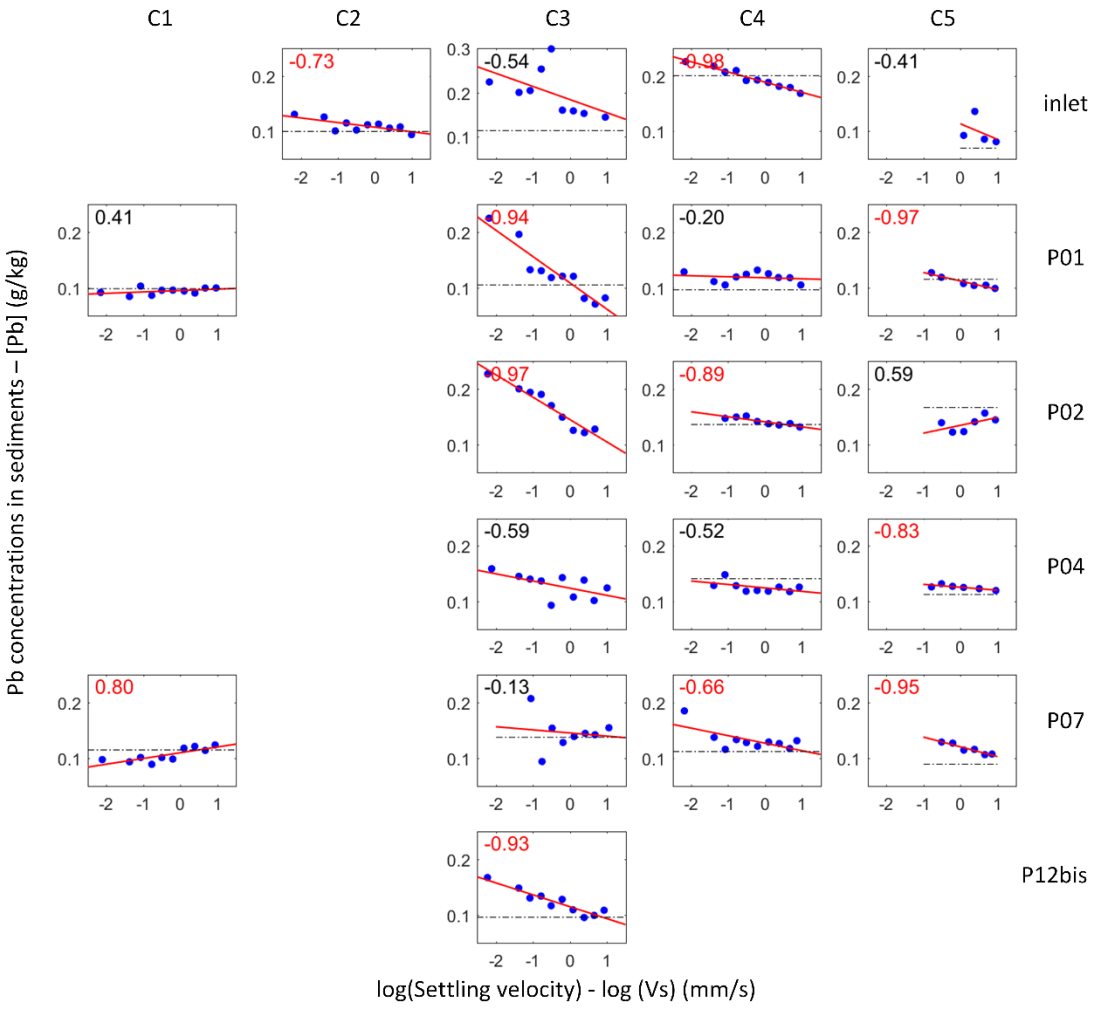

Figure A5. Spatial and temporal variability on the correlation between [Pb] and log(Vs)

Appendix D: New protocol for settling velocity distribution measurements

During my PhD work, I have participated in the development of a new protocol for settling velocity distribution measurements. Figure A6a illustrates the standard VICAS equipment for settling velocity distribution measurement proposed by Chebbo and Gromaire (2009). The principal measurement methodology is presented in section 2.3.2.1. This traditional VICAS measurements require practiced, attentive and accurate manipulation by the operator as we need to carefully introduce the aluminium plates for sample collection at the bottom of the column. This avoids turbulence and resuspension of sediments from the tank. It can be also time-consuming as the operator needs to collect samples at each predefined time (1, 2, 4, 8, 16, 32 min and 1, 2, 4, >24 h) and realise TSS filtration for each sample.

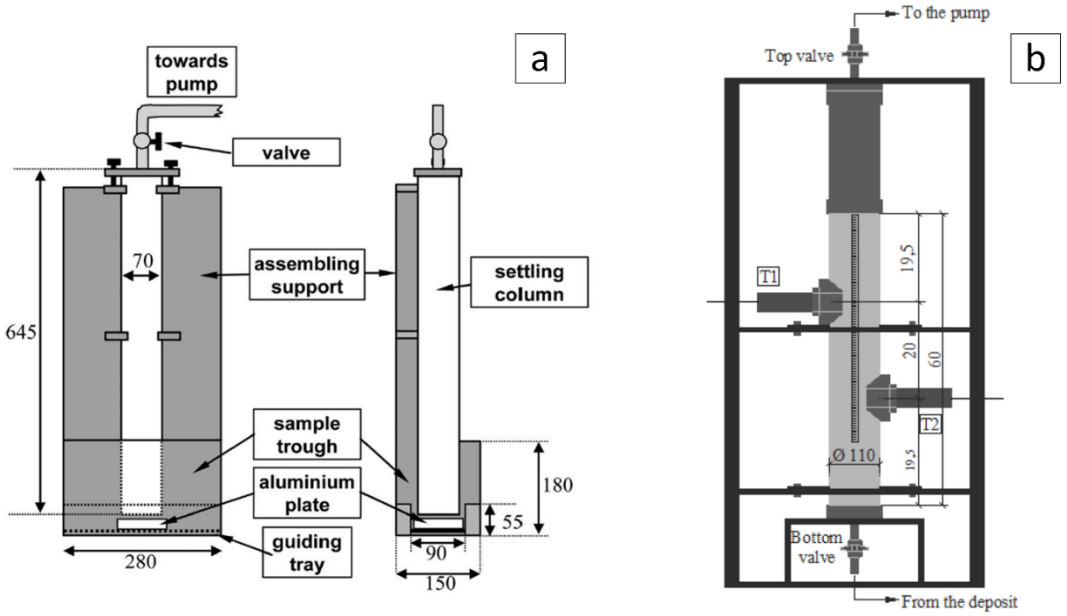

Figure A6. Scheme of VICAS equipements for settling velocity measurement: (a) standard French VICAS protocol (Chebbo and Gromaire, 2009), (b) new-proposed protocol based on turbidimetry (Aguzzi, 2014)

A new protocol based on two turbidimeters is then proposed to resolve the above problems. As shown in Figure A6b, instead of collecting samples at the bottom of column, this new protocol proposes a sealed column with two turbidimeters (T1 & T2) measuring turbidity at different heights continuously and transforms measurement results to particle settling velocity distribution (PSVD) curve. A numerical inversed model (see Matlab code below) has been established to obtain mass variation from a known PSVD based on the hypothesis that settling velocity varies with particle concentrations (Vesilind et Jones, 1990) described by Equation A1.

$$\frac{Vs(t)}{Vs_0} = \alpha\left(\frac{C(t)}{C_0}\right)^{\beta} \qquad \text{Equation A1}$$

where $Vs(t)$ represents particle settling velocity at time t (mm/s), Vs_0 is particle initial settling velocity (mm/s), $C(t)$ represents particle concentrations in the column at time t (mg/l), C_0 is initial particle concentration in the column (mg/l), α and β are calibration parameters, both equal to 1.

The numerical results are compared to the experimental results obtained by Aguzzi (2014) where a correlation between turbidity (*Turb*) and TSS concentrations (*TSS*) was applied and described by Equation A2. As illustrated in Figure A7, the numerical and experimental results consist at the level of T1. The new-proposed protocol needs further experiments and parameter estimation exercises and the validated protocol will help to facilitate PSVD measurements and reduce system error caused by manipulation.

$$TSS = -1.7559 + 2.6028 * Turb \qquad \text{Equation A2}$$

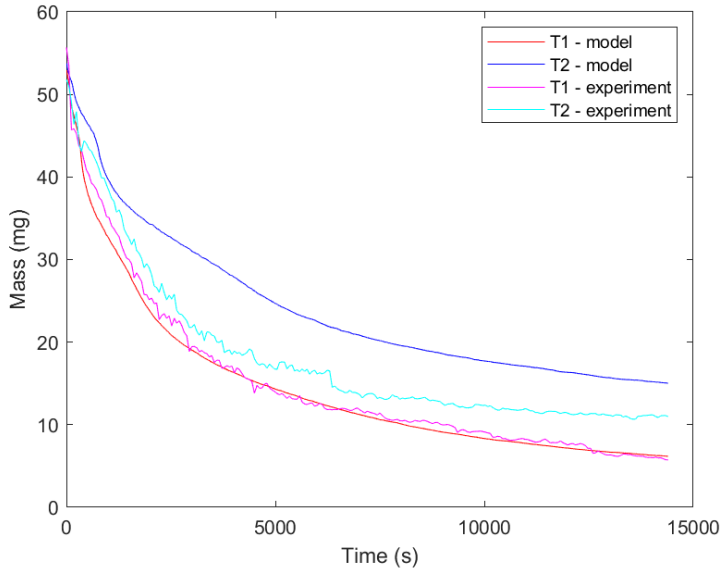

Figure A7. Comparison of mass variations obtained by numerical models and experiments

Matlab code for new-proposed VICAS protocol to obtain mass variation from known PSVD

```
clear all; close all; clc;

C = 1131.39;            %initial concentration [kg/m3]
np = 100000000;         %number of paticles
t = 10;                 %time interval [s]
page = 100000;          %divide np into many pages to accelerate
calculation
num_page = ceil(np/page);


z = 5;                  %thickness of turb [mm]
H = 600;                %colonne height [mm]
d = 110;                %colonne diameter [mm]
vol = pi*d^2/4*H*10^-6; %colonne volume [m3]
mp = C*vol/np;          %mass per particle [kg]
TS = floor(14400/t);    %time step
alpha = 1;
beta = 1;

%define paticle initial settling velocity and position
v = load('settling_curve.csv');
X = [0;v(:,1)];
Y = [0;v(:,2)];
a = rand(np,1);
V0 = interp1(Y,X,a,'spline','extrap');
P = H*rand(np,1);

Turb = zeros(TS,2);
S = zeros(np,1);
Turb1 = zeros(np,1);
Turb2 = zeros(np,1);

%Ts = 1
P = P + V0*t;
S = P > H;
S1 = sum(S);
Turb1 = P>=195-z/2 & P<=195+z/2;
Turb(1,1) = sum(Turb1);
Turb2 = P>=395-z/2 & P<=395+z/2;
Turb(1,2) = sum(Turb2);
V = V0*alpha*((np-S1)/np)^beta;
```

```
for i = 1:TS                    %i: timestamp
   for j = 1:num_page           %j: page
       V0_sub = V0((j-1)*page+1:j*page);
       P_sub = P((j-1)*page+1:j*page);
       V_sub = V((j-1)*page+1:j*page);

       P_sub = P_sub + V_sub*t;
       S_sub = P_sub > H;
       Turb1_sub = P_sub>=195-z/2 & P_sub<=195+z/2;
       Turb2_sub = P_sub>=395-z/2 & P_sub<=395+z/2;
       V_sub = V0_sub*alpha*((np-S1)/np)^beta;

       P((j-1)*page+1:j*page) = P_sub;
       V((j-1)*page+1:j*page) = V_sub;
       S((j-1)*page+1:j*page) = S_sub;
       Turb1((j-1)*page+1:j*page) = Turb1_sub;
       Turb2((j-1)*page+1:j*page) = Turb2_sub;
   end
   S1 = sum(S);
   Turb(i,1) = sum(Turb1);
   Turb(i,2) = sum(Turb2);
end

Turbmass = zeros(TS,3);
for i = 1:TS
    Turbmass(i,1) = t*i;
    Turbmass(i,2) = Turb(i,1)*mp;  %[kg]
    Turbmass(i,3) = Turb(i,2)*mp;
end

save(['Turbmass_model.mat'],'Turbmass');

load('turbmass_exp.mat');

fig = figure(1);
plot(Turbmass(:,1),Turbmass(:,2),'r',Turbmass(:,1),Turbmass(:,3),'b',turbma
ss_exp(:,1),turbmass_exp(:,2),'m',turbmass_exp(:,1),turbmass_exp(:,3),'c')
legend('T1 - model','T2 - model', 'T1 - experiment','T2 - experiment')
xlabel ('Time (s)')
ylabel ('Mass (mg)')
```

Présentation des résultats majeurs de la thèse – Résumé étendu exigé pour une thèse rédigée en anglais

La contamination des eaux pluviales urbaines est avérée depuis plusieurs années. On sait par exemple que les métaux, les Hydrocarbures Aromatiques Polycycliques - HAP, et certaines bactéries pathogènes sont véhiculés sous forme majoritairement particulaire dans les eaux pluviales urbaines. L'apparition de plusieurs contraintes règlementaires (en particulier la Directive Cadre Européenne sur l'Eau - DCE) et la perception des risques écotoxicologiques poussent plusieurs collectivités à mettre en place des techniques dites alternatives pour la gestion de ces eaux contaminées. L'une de ces techniques consiste à stocker l'eau pendant un certain temps afin de permettre une dépollution par décantation. Ces ouvrages sont appelés bassins de retenue-décantation des eaux pluviales. Les bassins de retenue-décantation ont trois fonctions principales : stocker les eaux pluviales pour éviter les inondations à l'aval, favoriser la décantation, éviter la remise en suspension et la remobilisation des polluants décantés vers l'aval. Les dépôts ainsi constitués représentent des zones de contamination importante. Ces ouvrages sont des écosystèmes à part entière avec un habitat faunique très riche et un risque très élevé de contamination des milieux aquatiques superficiels ou souterrains vers lesquels les eaux transitant par ces systèmes sont rejetées. En outre, ces ouvrages nécessitent un entretien et une gestion particulière, impliquant des expositions des techniciens lors d'opérations diverses (curages). Il est donc indispensable de maîtriser les mécanismes à la base du comportement hydrodynamique de ses ouvrages, de caractériser les contaminants présents dans le dépôt et de prédire la distribution des contaminants dans le but de mieux concevoir et gérer de manière durable les sédiments accumulés au sein de ces ouvrages.

L'ouvrage étudié dans le cadre de cette thèse est le bassin de retenue-décantation Django Reinhardt (BDR) situé à Chassieu et connecté à un bassin d'infiltration. C'est un ouvrage étudié dans le cadre de l'observatoire de terrain en hydrologie urbaine (OTHU). La thèse comprend principalement 3 objectifs :

- Mesures expérimentales du champ de vitesse au niveau de la surface libre du bassin à l'aide de la méthode LSPIV (Large-Scale particle image velocimetry, en anglais) pour une meilleure compréhension du comportement hydrodynamique et la prédiction des zones de dépôt.
- Modélisation de la décantation et de la remise en suspension des sédiments contaminés accumulés et détermination des zones où les sédiments pourraient facilement être lessivés et transférés vers le bassin d'infiltration à l'aval.

- Détermination des zones du bassin où les sédiments sont les plus contaminés grâce à l'intégration de la relation entre la vitesse de chute et les teneurs en métaux dans les modèles de transport solide.

Afin de caractériser les polluants particulaires à l'entrée du BDR, un nouveau dispositif composé d'un leaping-weir et d'un hydrocyclone (LW- HTS) a été conçu. Le LW-HTS opère une séparation solide-liquide dans les eaux pluviales grâce à la force centrifuge générée par le mouvement rotatif de l'eau du fait d'une entrée tangentielle au niveau de l'hydrocyclone. Le dispositif LW-HTS a de bonnes performances de piégeage pour les particules les plus grossières et que près de 100% des particules entrant au niveau du leaping-weir sont piégées dans la boîte de piégeage de HTS. Le LW-HTS est ensuite utilisé pour l'échantillonnage de sédiments à l'entrée de BDR et les caractéristiques (granulométrie notamment) des sédiments semblent comparables à celles des particules piégées dans le bassin.

Concernant l'analyse du comportement hydrodynamique du BDR à l'aide de la LSPIV, la méthode est tout d'abord évaluée en comparant ses résultats avec ceux obtenus à l'aide du vélocimètre acoustique Doppler (ADV) à l'échelle pilote (utilisation du pilote DSM – dispositif de surveillance et de maîtrise des flux). La technique LSPIV a été ensuite appliquée pour mieux comprendre les directions principales (recirculations) des écoulements et pour expliquer la distribution spatiale des sédiments dans le BDR. Les résultats illustrent deux principaux comportements d'écoulement, cohérents par rapport aux observations et aux résultats numériques préliminaires, à savoir: (i) mouvement du coin supérieur droit (entrée du bassin) vers la partie aval gauche. Dans certains cas, une recirculation est créée au centre, tandis que dans d'autres cas, le flux continue de se déplacer vers la gauche; (ii) Le flux se déplace du coin inférieur droit vers la partie supérieure gauche. La sensibilité de différents paramètres de traitement d'image est testée pour obtenir des résultats plus robustes lors de l'application de LSPIV. On observe également au centre du bassin des vitesses faibles et des recirculations, dont une zone de recirculation centrale, qui pourraient rallonger le temps de séjour et entrainer la sédimentation. Les mesures de champ de vitesse de surface basées sur LSPIV peuvent être utilisées pour évaluer des modèles numériques et pour prédire les zones de dépôt de sédiments.

Sur la base du modèle hydrodynamique évalué, des simulations de la remise en suspension des sédiments en place et de leur décantation sont réalisées. Cette partie du travail est importante car les dépôts accumulés sont contaminés et peuvent être remis en suspension en fonction des conditions hydrodynamiques et transportés ailleurs dans le bassin ou vers la sortie. Les pourcentages de sédiments remis en suspension et ceux qui s'échappent du bassin pour différentes conditions de flux sont quantifiés. Comme attendu, les résultats montrent que les particules fines ont plus tendance à se remettre en suspension et à être transférées vers la sortie.

Les particules accumulées aux points P04 et P07 sont plus susceptibles de se remobiliser par rapport aux sédiments situés à d'autres endroits du bassin, ce qui est cohérent avec le fait que ces deux points sont situés à la fin de trajectoire de particules. Ainsi les points concernés devraient être les zones préférentielles à curer.

Étant donné que les dépôts contaminés peuvent avoir une influence sur la qualité des eaux superficielles et souterraines à l'aval, les mécanismes de transport des polluants et la répartition spatiale de la contamination dans le bassin sont traités dans cette thèse. La corrélation entre les teneurs en Fe, Cr, Cu, Ni, Pb dans les sédiments et la vitesse de chute est tout d'abord établie. Sur la base d'un vaste ensemble de données (209 groupes d'échantillons, 5 campagnes, 6 points d'échantillonnage comprenant l'entrée et le bassin), les teneurs en Fe et en Pb ont une corrélation très significative avec la vitesse de chute, suivies des teneurs en Cu et Cr. Comme attendu, les variabilités spatio-temporelles sont observées pour les vitesses de chute et pour les teneurs en métaux. Une équation décrivant la corrélation entre la teneur en Fe et la vitesse de chute est obtenue et permet de prédire la distribution spatiale des teneurs en Fe dans BDR. Compte tenu de sa forte relation avec les métaux lourds, le Fe peut être considéré comme un bon indicateur de la contamination des sédiments en certains polluants métalliques piégés. La Figure A8 montre la distribution spatiale de la teneur en Fe dans le BDR. P07 et P02 sont fortement contaminés, ce qui devrait être les zones nécessitant des traitements spécifiques. Les résultats obtenus sont utiles et peuvent aider à mieux concevoir ces ouvrages de retenue-décantation et à mieux gérer les sédiments accumulés.

En conclusion, les résultats montrent que P02, P04, P07 représentent des zones où les sédiments sont fortement contaminés et pourraient facilement être emportés et s'échapper du bassin. Ces zones doivent être la zone de traitement prioritaire. Par exemple, nous pourrions déposer ces sédiments contaminés dans la partie supérieure gauche de DRB, où il y a moins de recirculation et de remise en suspension des sédiments. En effet, Becouze-Laureure et al. (2018) montre que le niveau d'écotoxicité diminue avec le temps et que les sédiments doivent donc être laissés *in situ* avant d'être rejetés au centre de traitement. L'utilisation du Fe comme indicateur et de la modélisation CFD ou d'une autre approche de modélisation semble appropriée pour localiser les zones hautement contaminées nécessitant une gestion spécifique. Par conséquent, moins de quantités de sédiments seront extraites et pourraient être gérées directement *in situ*. Cette nouvelle stratégie de gestion contribue également à une réduction des coûts liés au transport, au traitement et à la valorisation des sédiments.

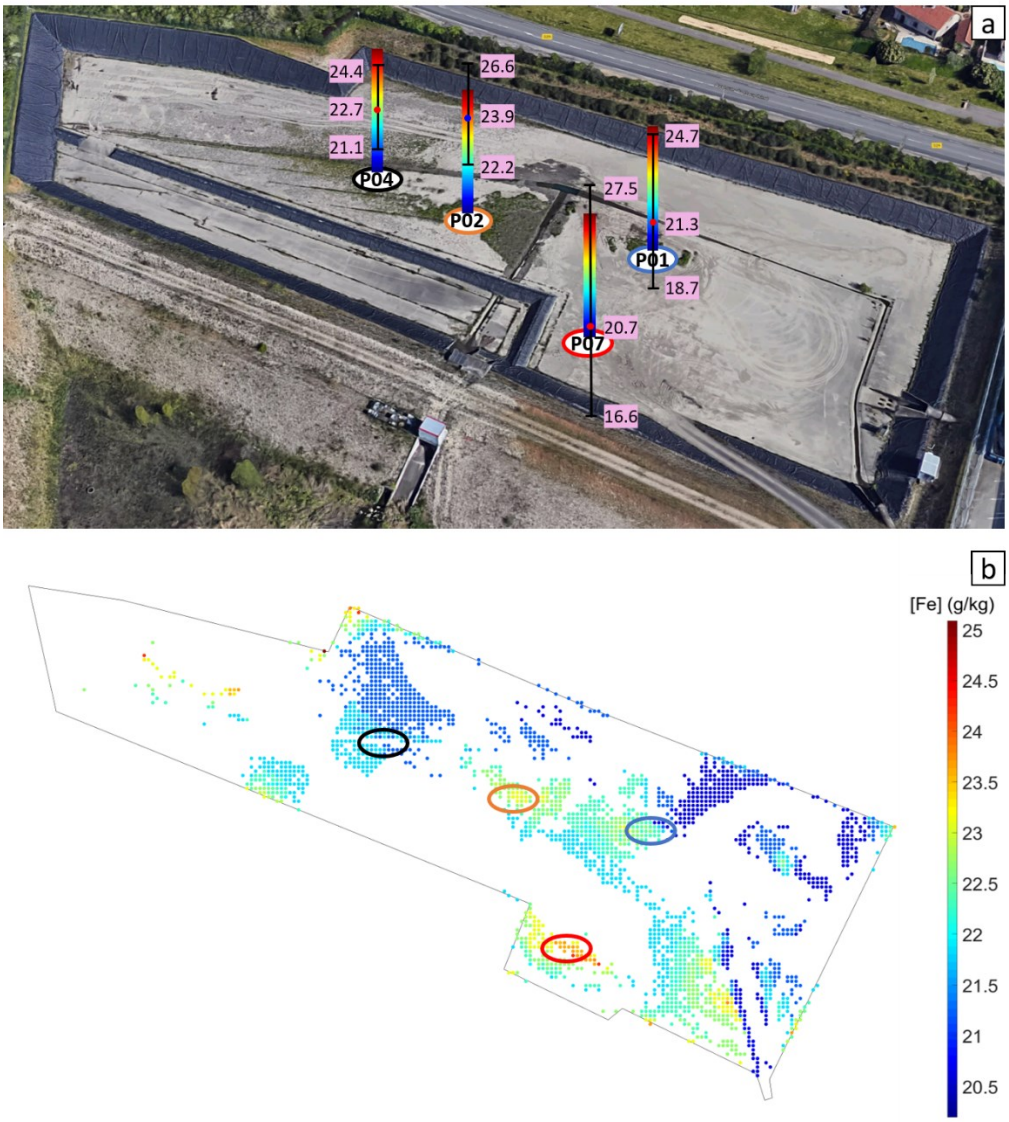

Figure A8. (a) Measured [Fe] (Fe content in sediment in g/kg DM) at P01, P02, P04, P07 obtained from data of C3-C5 in group I: minimum, averaged and maximum values are plotted, respectively, (b) [Fe] distribution at the bottom of DRB applying the obtained correlation between [Fe] and settling velocity (equation in Figure 4.4). P01, P02, P04, P07 locations are coloured in blue, orange, black and red, respectively.

Publications during the thesis

Published, submitted and prepared papers

Zhu, X., Lipeme Kouyi, G. (2019). An analysis of LSPIV□based surface velocity measurement techniques for stormwater detention basin management. Water Resources Research, 55(2), 888-903. https://doi.org/10.1029/2018WR023813

Zhu, X., Chatain, V., Gautier, M., Blanc-Biscarat, D., Delolme, C., Dumont, N., ... & Lipeme Kouyi, G. (2019). Combination of Lagrangian Discrete Phase Model and sediment physico-chemical characteristics for the prediction of the distribution of trace metal contamination in a stormwater detention basin. Science of The Total Environment, 134263. https://doi.org/10.1016/j.scitotenv.2019.134263

International and national conferences

Zhu X., Claro Barreto A., Lipeme Kouyi G. (2016). Design and performance evaluation of Hydrocyclone and Lamella Settler for Urban Stormwater Sediments. 8th international conference on Sewer Processes and Networks – SPN8, Rotterdam, Netherlands, 31 Aug.-2 Sept.

Zhu X., Lipeme Kouyi G. (2016). Expérimentations et modélisation de l'hydrodynamique et du transport de sédiments dans un bassin de retenue-décantation des eaux pluviales. 7eme Journées Doctorales de l'Hydrologie Urbaines, Nantes, 11-12 octobre 2016.

Zhu X., Lipeme Kouyi G., Becouze-Lareure C, Barraud S, Bertrand-Krajewski J.-L. (2017). 3D numerical modelling of resuspension and remobilization of sediments in a stormwater detention basin. Aquaconsoil, Lyon, 26-30 june 2017.

Zhu X., Miguet S., Lipeme Kouyi G. (2017). Application of Large Scale Particle Image Velocimetry to measure surface velocity field in a stormwater detention basin and to validate CFD model. ICUD, Prague, 10-15 September 2017.

Haboub K., Zhu X., Maruéjouls T., Bertrand-Krajewski J-L., Vanrolleghem P.A. (2019). A new approach of measuring TSS settling velocity based on turbidity measurements. 9th International Conference on Sewer Processes & Networks - SPN9, Aalborg, Denmark, 27-30 August. (accepted)

Other international communications

Zhu X., Lipeme Kouyi G. (2017). Use of free surface velocity measurements in a stormwater detention basin to validate CFD model, 23rd EJSW – Monitoring urban drainage systems, Chichillianne, 15-20 May 2017.

FOLIO ADMINISTRATIF

THESE DE L'UNIVERSITE DE LYON OPEREE AU SEIN DE L'INSA LYON

NOM : ZHU DATE de SOUTENANCE : 26/06/2019

(avec précision du nom de jeune fille, le cas échéant)

Prénoms : Xiaoxiao

TITRE : INFLUENCE OF HYDRODYNAMICS AND CORRELATION OF METAL CONTENTS WITH SETTLING VELOCITIES ON CONTAMINATION DISTRIBUTION IN A STORMWATER DETENTION BASIN

NATURE : Doctorat Numéro d'ordre : 2019LYSEI035

Ecole doctorale : Ecole Doctorale ED162 MECANIQUE, ENERGETIQUE, GENIE CIVIL, ACOUSTIQUE

Spécialité : Génie Civil

RESUME :

Les bassins de retenue-décantation ont trois fonctions principales : stocker les eaux pluviales pour éviter les inondations, favoriser la décantation des polluants particulaires, éviter la remise en suspension et la remobilisation des polluants décantés vers l'aval. La conception et la gestion de telles installations nécessitent de connaître les caractéristiques hydrodynamiques, celles des sédiments et de pouvoir prédire les zones où les dépôts sont fortement contaminés.

L'objectif principal de la thèse est d'identifier les zones où les teneurs en polluants sont élevées au niveau des sédiments des bassins de retenue-décantation. Le site d'étude est le bassin de rétention des eaux pluviales de Django Reinhardt (BDR), qui est un bassin sec à l'exutoire d'un bassin versant industriel. Ce bassin a fait l'objet de plusieurs études dans le cadre de de l'Observatoire de Terrain en Hydrologie Urbaine (OTHU).

Dans un premier temps, les mesures de vitesses de surface par LSPIV (Large-Scale Particle Image Velocimetry) ont permis de mieux comprendre l'hydrodynamique au sein de l'ouvrage. Ces mesures ont été exploitées pour évaluer les modèles CFD (Computational Fluid Dynamics). A notre connaissance, c'est la première fois que cette technique de mesure est appliquée au cas des ouvrages de gestion des eaux pluviales. Les résultats montrent que les modèles CFD identifient la principale zone de recirculation qui favorise la décantation. Ces modèles évalués ont ensuite été employés pour simuler le transport de polluants particulaires, leur sédimentation et leur remise en suspension. L'exploitation des résultats de ces simulations a permis d'indiquer les points où les sédiments sont remis en suspension et transférés vers le bassin d'infiltration à l'aval et de prédire les zones d'accumulation en métaux. Les résultats obtenus montrent également que les teneurs en fer dans les sédiments sont fortement corrélées aux vitesses de chute. Le fer pourrait être un bon indicateur du niveau de contamination des sédiments en certains métaux lourds.

Les résultats de cette thèse contribuent à améliorer les règles de conception des bassins de retenue-décantation des eaux pluviales et les stratégies de gestion des sédiments associés.

MOTS-CLÉS : Décantation, eaux pluviales, sédiments, métaux, remise en suspension, vitesse de chute, hydrodynamique

Laboratoire (s) de recherche : Déchets Eaux Environnement Pollution (DEEP)

Directeur de thèse: Gislain LIPEME KOUYI

Président de jury : Benjamin DEWALS

Composition du jury : Véronique RUBAN, Philippe SECHET, Jean-Luc BERTRAND-KRAJEWSKI, Denise BLANC-BISCARAT, Jérôme LE COZ, Francois CLEMENS, Benjamin DEWALS, Gislain LIPEME KOUYI